UNIVERSIDADE DA BEIRA INTERIOR
Engenharia

CFD Analysis of the Combustion of Bio-Derived Fuels in the CFM56-3 Combustor

Jonas Miguel Pires de Oliveira

Dissertação para a obtenção do Grau de Mestre em
Engenharia Aeronáutica
(Ciclo de estudos integrado)

Orientador: Prof. Doutor Francisco Miguel Ribeiro Proença Brójo

Covilhã, fevereiro de 2016

Dedication

To my beloved parents, João de Oliveira and Jacqueline de Oliveira whom without I would never be where I am now. Thank you for everything!

To my brothers, Steven and Christopher to whom I wish only the best for their future.

For my family, whose affection and encouragement were my source of inspiration.

"The best way to predict your future is to create it"

Abraham Lincoln

Acknowledgements

A big thank you to my family who supported me unconditionally throughout these five years away from home. My love for you is beyond words!

There are not enough words to thank my supervisor, Professor Francisco Brójo, whom was always there to ensure that I was following the right path. Professor, you basically provided me everything that was needed to perform this study, starting with the negotiations with TAP; suggesting the scanning of the combustor; and lending your personal computer, in which the scanning of the model was held, and also in which most of the simulations were performed. I am forever grateful for the kind patience and encouragement which you always demonstrated, being key factors to making me prepare this project.

My deepest thanks to TAP for providing the combustor, which was the foundation of this work; and a special thanks to Eng. Joana Palmeiro for hosting our visit to TAP, and for also providing important information for the development of this study.

I would also like to acknowledge Olga Skvortsova, a member of Artec support team, for all of her kind advices to solve some persistent problems that rose during the scanning phase.

I am profoundly grateful to CODI, and more especially Jennifer Faustino, for enabling that this hole project of reverse engineering could gain life, as they performed a 3D print of the model combustor and offered it to UBI. Moreover, thank you João Correia for first suggesting this, and for ensuring that all was done so that this could be performed.

A big thank you to my dear friend Robert Gonçalves, for not only being of good company during the first half of the preparation of this project, providing moments of laughter and comfort, but for also providing important tips during the CFD analysis; he was also responsible for my introduction to LaTeX, which proved really useful in organizing this document.

I would like to thank Eng. Pedro Santos for reviewing this document, but above all, for being a good friend.

And last but not least, I wish to thank all of my friends from my hometown and those made in my academic life, especially Bryan, Jorge, Elvis, Ricardo, Alexandre, Francisco, Pedro and Gilberto, whom are truly a huge part of my life.

Resumo

Uma simulação CFD é realizada numa câmara de combustão do motor CFM56-3, usando como combustíveis Jet-A e uma mistura de biocombustíveis a 100%. É pretendido avaliar a viabilidade destes biocombustíveis num ponto de vista da combustão, ao analisar as emissões e a energia extraída quando estes combustíveis são injetados, a fim de que estes biocombustíveis possam ser considerados como uma possibilidade de futuros combustíveis para a aviação comercial. Os três biocombustíveis que foram considerados para este estudo, são extraídos de sementes da planta *jatropha*, de *algas* e de *girassol*. Devido à confidencialidade que reina entre as empresas de manufatura de turbinas a gás, é muito difícil obter o *blueprint* de qualquer parte de uma turbina a gás, e a câmara de combustão em estudo não foi exceção. Felizmente a TAP gentilmente cedeu uma câmara de combustão ainda em serviço, na qual foi possível realizar um scan 3D, com recurso ao scanner pertencente à UBI, denominado de *Spider* da *Artec Group*. A partir deste modelo 3D, um ficheiro STL pôde ser exportado, e depois importado para o *CATIA V5*, que por sua vez foi o *software* escolhido para efetuar o *CAD*. Todas as partes da câmara de combustão relevantes para o estudo são representadas, onde estão incluídos os *swirlers* primário e secundário, os injetores de combustível, os orificios para arrefecimento, as paredes e o *dome*; apenas um quarto da câmara de combustão é usado para o estudo numérico devido à simetria existente, e devido ao facto que dos 20 injectores de combustível presentes, existem 4 em que é injetado uma mistura mais rica. A malha numérica é criada com recurso ao *HELYX-OS*, e o *software* comercial *ANSYS Fluent 15.0* é usado para efetuar o estudo numérico. Devido à complexidade deste estudo, a atomização do combustível não é considerada. O modelo viscoso usado é o RSM; todas as entradas de ar, bem como os injetores de combustível são definidos como *mass-flow inlets*, e a saída da câmara de combustão é definida como um *pressure-outlet*. Os resultados finais estão razoalmente de acordo com os dados de referência apresentados pela ICAO, quando Jet-A é queimado, apresentando um erro no geral muito reduzido. Entre todos os combustíveis simulados, foi provado que aumentando a potência resultava num aumento de emissões NO_x e num decréscimo de $UHC's$; contudo um comportamento inesperado de uma redução de emissões CO com o aumento da potência, foi verificado. O biocombustível que apresentou os melhores resultados ao longo de todo o ciclo de potência da ICAO, com respeito às emissões NO_x, CO e UHC, foi o proveniente de *girassol*, uma vez que foi previsto valores de emissões inferiores, quando comparados com os restantes combustíveis. O biocombustível proveniente de *jatropha* foi o que apresentou uma maior redução de emissões CO_2, representando um decréscimo de 20% comparando com o de Jet-A, e a energia extraída representou um menor decréscimo de 6% quando comparado com o mesmo combustível. No geral pode ser concluído que os biocombustíveis estudados têm o potencial de substituir a querosene, e apesar de que um maior consumo é exigido aos biocombustíveis, de forma a produzir a mesma energia que Jet-A, uma redução significativa de emissões é prevista.

Palavras-chave

TAP; CFM56-3; Câmara de combustão; *CATIA V5*; *HELYX-OS*; CFD; *ANSYS Fluent*; Biocombustíveis; Emissões

Abstract

A CFD simulation of a CFM56-3 combustor burning Jet-A and a 100% blend of biofuels, is performed. It is intended to evaluate the viability of these biofuels in a combustion point of view, by analysing the emissions and the energy extracted when burning these through ICAO's LTO cycle, so that these biofuels can be considered as a future civil aviation fuel. The three biofuels considered for this study were extracted from *jatropha* seeds, *algae* and *sunflower*. Due to the confidentiality that exits among GTE manufacturers, it is very difficult to obtain the blueprint of any given part of a GTE, and the combustor in study was no exception. Fortunately TAP kindly provided an operational CFM56-3 combustor, and with the aid of a 3D scanner, named *Spider* from *Artec group*, which belongs to UBI, it was possible to create a 3D model of the combustor. From this 3D model, an STL file can be exported, and then imported into *CATIA V5*, which is the software chosen to perform the CAD. All of the relevant parts of the combustor is represented, which include the primary and secondary swirlers, fuel injectors, cooling holes, walls and the dome; only one quarter of the combustor was used for the numerical study due to the existing symmetry, and due to the fact that within the existing 20 fuel injectors, there are four of them that inject the fuel with a richer mixture. The numerical mesh is created using *HELYX-OS* and the commercial software *ANSYS Fluent 15.0* is used to perform the numerical study. Due to the complexity of this study, the atomization of the fuel was not considered. The viscous model used is the RSM; all of the air-inlets as well as the fuel injectors are defined as *mass-flow inlets*, and the exit of the combustor is defined as a *pressure-outlet*. The final results show reasonable agreement with the reference values presented by ICAO, when Jet-A is combusted, representing an error in general very low. Among all of the fuels simulated, it was proved that increasing the power produced higher NO_x and lower UHC; however an unexpected behaviour of CO emission decrease with a power increase, was predicted. The biofuel that presented the best performance in ICAO's LTO cycle regarding NO_x, CO and UHC emissions was *sunflower* biofuel, as these emissions were lower when compared to all of the fuels. *Jatropha* biofuel presented the highest CO_2 reduction, representing a 20% decrease from Jet-A, and the energy extracted represented a minimal decrease of 6% when compared to the same fuel. Overall, it can be concluded that the biofuels studied have the potential to replace kerosene, and despite more biofuel has to be burned to produce the same amount of energy as Jet-A, a significant reduction in emissions is predicted.

Keywords

TAP; CFM56-3; Annular combustor; *CATIA V5*; *HELYX-OS*; CFD; *ANSYS Fluent*; Biofuels; Emissions

Contents

List of Figures

List of Tables

List of Acronyms

AFR	Air to Fuel Ratio
App.	Appendix
ASTM	American Society of Testing and Materials
Bio-SPK	Bio-derived Synthetic Paraffinic Kerosene
BTU	British Thermo Unit
CAD	Computer-Aided Design
CC	Gas turbine Combustion Chamber
CEA	Chemical Equilibrium with Application
CFD	Computational Fluid Dynamics
CPU	Central Processing Unit
CZ	Combustion Zone
DLE	Dry Low Emissions
DLN	Dry Low No_x
DLR	Deutch Zentrum fur Luft-und Raumfahrt
DNS	Direct Numerical Simulation
EI	Emission Index
ERF	Explicit Relaxation Factor
EU	European Union
EV	Environmental Burner
EVM	Eddy Viscosity Model
FAME	Fatty Acid Methyl Ester
FAR	Fuel to Air Ratio
FGB	First Generation Biofuel
FSRFL	Fuel Stream Rich Flammability Limit
FT	Fischer-Tropsch
GE	General Electric
GHG	Green House Gas
GTC	Gas Turbine Combustor
GTE	Gas Turbine Engine
H	Hydrogen
HCN	Hydrogen Cyanide
HEFA	Hydroprocessed Esters and Fatty Acids
HHV	Higher Heating Value
HPC	High Pressure Compressor
HPT	High Pressure Turbine
ICAO	International Civil Aviation Organization
ICE	Internal Combustion Engine
IPCC	International Panel on Climate Change
KPPSMOKE	Kinetic Post-Processor
LES	Large Eddy Simulation
LHV	Lower Heating Value
LPC	Low Pressure Compressor
LPP	Lean Premixed-Pre vaporized

LPT	Low Pressure Turbine
LTO	Landing and Take-Off
MAC	Modern Annular Combustor
NASA	National Research Council of Canada
NCN	Cyanonaphthalene
NRC	National Research council of Canada
P&W	Pratt and Whittney
PDF	Probability Density Function
PLF	Pressure Loss Factor
PM	Particulate Matter
PN	Particulate Number
PPM	Part Per Million
PRESTO!	PREssure STaggering Option
PZ	Primary Zone
RAM	Random Access Memory
RANS	Reynolds-Averaged Navier-Stokes
RQL	Rich-Quench-Lean
RSM	Reynolds Stress Model
SAC	Single Annular Combustor
SEV	Sequential Environmental Burner
SFC	Specific Fuel Consumption
SGB	Second Generation Biofuel
SIMPLE	Semi-Implicit Method for Pressure Linked Equations
SME	Soy-Methyl-Ester
SN	Smoke Number
SPK	Synthetic Paraffinic Kerosene
STL	Stereo Lithography
TAP	Transportes Aéreos de Portugal
TAPS	Twin Annular Premixing Swirler
TTQ	Temperature Traverse Quality
UBI	Universidade da Beira Interior
UHC	Unburned Hydrocarbons
UNFCCC	United Nations Framework Convention on Climate Change
URF	Under Relaxation Factor
USA	United States of America
WLE	Wet Lean Emissions
WWII	World War Two

Nomenclature

$\frac{1}{2}v^2$	Mass specific system kinetic energy	$[J/kg]$
A	Area	$[m^2]$
C	Heat capacity	$[J/K]$
C_μ	k - ε model constant	$[0.09]$
c_p	Specific heat at constant pressure	$[J/kg.K]$
CO_2	Carbon dioxide	$[-]$
CO	Carbon monoxide	$[-]$
D_{sw}	Swirler diameter	$[mm]$
F	Engine thrust	$[kN]$
F_{00}	Engine take-off thrust	$[kN]$
G_m	Axial flux of angular momentum	$[-]$
G_t	Axial thrust	$[-]$
gz	Mass-specific system potential energy	$[J]$
H/C	Hydrogen to carbon ratio	$[-]$
m	Mass	$[kg]$
$\dot{m}$	Mass flow rate	$[kg/s]$
M	Molecular weight	$[kg/kmol]$
n	Number of moles in a gas	$[kmol]$
n_{fuel}	Moles of fuel combusted	$[kmol]$
n_{water}	Moles of water vaporized	$[kmol]$
N_2	Diatomic nitrogen	$[-]$
NO_x	Oxides of nitrogen	$[-]$
O_2	Oxygen	$[-]$
p	Pressure	$[Pa]$
p_{fund}	Fundamental pressure	$[Pa]$
Q	Heat transfer	$[W/m^2]$
q_{cv}	Heat transferred across the control surface from the surroundings to the control volume	$[W/m^2]$
R_{CO}	Carbon monoxide oxidation rate	$[mol\ m^{-3}s^{-1}]$
r_p	Pressure ratio p_2/p_1	$[-]$
R_μ	Universal gas constant	$[8315\ J/kmol.K]$
S_N	Swirl number	$[-]$
SG_{gas}	Specific gravity of gas with respect to air	$[MW\ gas/28.96]$
SN	Smoke number	$[-]$
SO_x	Oxides of sulphur	$[-]$
T	Temperature	$[K]$
t	Time	$[s]$
T_{ad}	Adiabatic flame temperature	$[K]$
$TSFC$	Trust Specific Fuel Consumption	$[g/kN]$
U	Compressor outlet velocity	$[m/s]$
v	Velocity	$[m/s]$
V	Volume	$[m^3]$
W_{cv}	Work done by the control volume	$[J]$
k	Kinetic energy per unit mass	$[m^2/s^2]$

u	velocity	$[m/s]$
n_l	Number of layers	$[-]$

Greek letters

γ	Mass fraction	$[kg/kg]$
δ_f	Final layer thickness	$[-]$
δ_s	Layer stretching	$[-]$
ε	Eddy viscosity	$[m^2/s]$
η_{joule}	Efficiency of the air-standard Brayton - Joule cycle	$[-]$
μ	Absolute viscosity	$[Pa.s]$
μ_T	Turbulent viscosity	$[Pa.s]$
π_{00}	Engine pressure ratio at take-off	$[-]$
ρ	Density	$[kg/m^3]$
σ	Stress tensor	$[Pa]$
τ	Sheer stress	$[Pa]$
ϕ	Equivalence ratio	$[-]$
	Scalar such as pressure, energy or species concentration	$[-]$
χ	Mole fraction	$[-]$

Subscripts

0	Engine inlet stage
1	Compressor inlet stage
2	Combustion chamber inlet stage
3	HPT inlet stage
4	LPT outlet stage
5	Engine exit stage
a	Air
c	Combustion chamber
f	fuel
i	Element/Molecule
	Inlet
ref	Reference state
	Reference data
o	Outlet
i,j	Coordinate directions

Chapter 1

Introduction

1.1 Motivation

In a world which the constant concern of global warming is an every day matter, the emissions that result from the combustion of fossil fuels are usually placed at the top as the main responsible for Greenhouse Gas (GHG)[1] emissions, which are appointed as the primary factor that leads to global warming. The aviation industry by itself is responsible for around 3% of the total European Union (EU) GHG emissions, but the problem is that aviation is the only direct source of emissions into the upper atmosphere and that these numbers are increasing fast, 87% since 1990 [1]. This increase is mainly because people are seeking more and more aviation as a transport due to their increasingly lower costs throughout the years, and its environmental costs being neglected. Just to clarify the magnitude of these environmental costs, a person flying from London to New York and back, generates roughly the same amount of emissions as an average person in the EU does by heating their home for a whole year [2]. By 2020, global aviation emissions are projected to be around 70% higher than in 2005, even if fuel efficiency improves by 2% a year. Yet, darker forecasts are made by the International Civil Aviation Organization (ICAO), which predicts that by 2050 these emissions could grow up to 300%-700% [3]. This increase in emissions drifts of course by the continuous increase of the demand of fuel, which in turn comes from the increase in the number of operational aircraft. In contrast, the resource of fossil fuel is depleting and will be finished in a near future. In fact, according to British Petroleum (BP) [4], known oil deposits will only last until 2068, if we carry on this consumption rate. Consequently, the price of jet fuel has been increased rapidly from $0.72/gallon (2002) to $2.98/gallon (2013) in 10 years [5]. Fossil fuel subsidies, which amounted to half a trillion US Dollars worldwide in 2011 [6], are effectively an incentive to pollute and as such are a major blocker to sustainable energy development.

Fortunately, we have the technology and practical solutions at hand to reduce the amount of heat-trapping emissions resultant by the continuous increase in traffic in the aviation industry. These solutions come in the form of protocols, improvements in aircraft structures/engines and alternative fuels. An example of a protocol that commits to reducing GHG emissions is the Kyoto Protocol. This protocol established that between 2008 and 2012, developed countries and countries in economic transition would have to reduce their GHG emissions by about 5% below their 1990 levels [7]. Overall, this protocol was a success. The 37 industrial nations that stuck with the protocol, after the United States of America (USA) pulled out in 2005, say they exceeded their promises, cutting their emissions during the agreed timeframe to an average of 16% below 1990 levels [8]. However, these major cuts came from non-rich industrialized countries witch where not the focus of this protocol and whose economy had collapsed after the fall of the Berlin wall, meaning that reductions would have happened anyway. In the meantime, emissions in the

[1] A GHG is a gas in an atmosphere that absorbs and emits radiation within the thermal infra-red range. This process is the fundamental cause of the greenhouse effect (global warming).

rest of the world have increased sharply thanks to rapid industrialization nations like China, which are not covered by the original deal.

Changes in the structure of aircraft have also been held in order to decrease fuel consumption, thus reducing the emissions of GHG. An example of this is the new design feature in the wing tips, blended winglets. In this design the wingtip sweeps upwards reducing drag witch consequently increases fuel efficiency. Modifications in the engines have also taken part in the quest to reduce GHG emission from civil aviation. The most significant change in the engine configuration was an increase in its bypass ratio[2]. This increased greatly the fuel efficiency in civil aviation when compared to its predecessor low-bypass engine, that was more compact but less fuel efficient and much more noisier [9]. The CFM56 engine is a successful example in the family of high-bypass engines.

Although changes like these did reduce the GHG emissions, they still present some problems. Modifications in aircraft components require a huge amount of money to take place; this is because these specific changed features has to be implemented in every single plane of the fleet, in order to achieve the desired reduction in GHG emissions. Another problem is the dependence in fossil fuels; these changes still do not resolve the fact that kerosene[3] will no longer be available in the near future, due to the disappearance of known oil deposits. So changing the fuel source is one of the few options that remain for the aviation industry to reduce its GHG emissions. Alternatives like solar, electric and hydrogen propelled aircraft are currently being researched, but are not expected to be implemented in the near future due to the aviation need for high power-to-weight ratio[4] and globally compatible infrastructure.

The seek of a renewable drop-in fuel[5] suitable for the aviation industry, comes as the best solution to resolve all the problems mentioned above. The environmental effects of any alternative fuel must be considered, this includes emissions from the engine and also life-cycle effects associated with the production and use of an alternative fuel [10]. Safe and reliable operations of the engine must not be compromised in any way. Biofuel[6] is a suitable choice which not only could significantly lower GHG emissions but it is also a renewable fuel. Since 2008, several flight tests have been performed to investigate the technology and safety, using biofuel [11]. The problem is that the major part of these tests were performed using blends of biofuel added to conventional jet fuel that, which consequently, did not remove the fossil fuel component. However, in 2012, the National Research Council of Canada (NRC) performed the first flight on a civil aircraft, using a 100% unblended biofuel obtained from the plant *Brassica Carinata*. Overall, this flight test was a success. Tests results show that this biofuel reduced emissions and provided a better fuel efficiency than petroleum aviation fuel [12].

Biomass derived from organisms, like switchgrass and waste, are the source of which future biofuels should be produced from. This is because, unlike biofuel produced after food crops,

[2]The bypass ratio defines the amount of air that bypasses the core of the engine, from the air that goes through the core. For a deeper insight in the bypass ratio concept, it is advised to check section 2.1.2.

[3]Kerosene is a combustible hydrocarbon liquid widely used to power jet engines of aircraft.

[4]Power-to-weight ratio is a measurement of actual performance of any engine or power source.

[5]A drop-in fuel is an alternative fuel that does not require adaptation of the fuel distribution network nor the engine fuel systems. It can be used without restrictions on aircraft or engine operability.

[6]Biofuels are energy sources made from living things, or the waste that living things produce, also known as biomass.

like soy been, biomass derived from non-food crops do not enter in conflict with food resources. If the production of biofuel did enter in conflict with food resources, then there would be a big problem to deal with in the future. This is due to the inevitable increase in the price of food, putting biofuels as a global responsible for the crises that would appear. Even still, some do present problems with the use of biomass to obtain biofuel. Biomass production under intensive monoculture systems can have negative impacts on biodiversity, including habitat loss, the expansion of evasive species, contamination from fertilizers/herbicides and air pollution resultant from the production process of biofuel [13]. The continuous demand of biofuel in the future would also inevitably result in a continuous increase of its price, similar to the price increase that is taking place with fossil fuel. To solve some of these problems, the author suggests that if each airliner could build their own environmental controlled infrastructures to produce their own biofuel, in areas which are less conducive to farming, e.g. cities, it would give airliners a steady supply of fuel which could reduce significantly the pricing factors and could mitigate the problem with habitat loss. This solution might not supply 100% of the fuel demands, but it certainly would be of benefit.

The main impact of trends and developments with the use of biofuels relative to combustor[7] design, will be felt in fuel-nozzle design for multifuel capability, and in fuel/air management for minimum soot[8] and gaseous emissions. These emissions include Oxides of Nitrogen (NO_x), Unburned Hydrocarbons (UHC), Carbon Monoxide (CO), Particulate Matter (PM) and Oxides of Sulphur (SO_x)[9]. Although these pollutants do not contribute directly to global warming, they are hazardous to human health and therefore must be reduced. Carbon dioxide (CO_2) and water vapour (H_2O) are also products of the combustion process, but they are not regarded as pollutants because they are a natural consequence of the complete combustion of a hydrocarbon fuel. However, these two contribute to global warming and the only way to reduce them, is to burn less fuel [14].

The problem of controlling emissions is complicated because of the fact that Gas Turbine Engines (GTE) operate over a wide range of power and ambient conditions. Aircraft engines have two requirements; the first is for very high combustion efficiency at low power, this is due to the large amount of fuel burned during taxiing and ground manoeuvring, and the primary problem here is the reduction of UHC. At take-off power, climb and cruise the main concern are NO_x. ICAO sets standards on a worldwide basis, for both Landing and Take-off (LTO) cycles, and also for cruise at high altitude; the first is concerned with air quality in the regions surrounding airports, and the second with ozone depletion in the upper atmosphere [15].

Research and development of biofuel for the aviation industry promises a prospect and interesting work, however it also issues many challenges due to strict requirements of aviation fuel that are regulated by the American Society for Testing and Materials (ASTM). As these requirements are achieved, so as combustion products and the efficiency of these biofuels been correctly studied, the world takes a step closer to become less dependent of fossil fuels and mitigate global warming issues. This moment will come sooner than people think, and as the Saudi oil Minister Sheik Ahmed Zaki Yamani said in the 1970's, "The Stone Age did not end for lack of stone, and the oil age will end long before the world runs out of oil." [16].

[7] The combustor is the component of the gas turbine engine, in which combustion takes place.

[8] The term soot refers to impure carbon particles that result from the incomplete combustion of hydrocarbons.

[9] SO_x only appears in the emissions if there is any sulphur in the fuel.

1.2 Main Goals

The present work firstly focuses on the construction of an annular combustor of the CFM56-3 engine. A 3D scan was performed on a real sized combustor in order to extract all the measurements needed to conduct a Computer Assisted Design (CAD) with the commercial software *CATIA V5*. This geometry is then imported into a CFD software, *ANSYS Fluent*, to perform a numerical analyses in order to study the combustion of some biofuels, when injected into the combustor. The parameters analysed were the quantity of emitted pollutant, namely NO_x, CO and UHC, and the energy extracted from the combustion of these biofuels, throughout ICAO's LTO cycle. The aim is to verify if this biofuel could substitute completely conventional jet fuel, in a combustion point of view.

The selection criteria, adopted by the author, to choose which biofuels should be used in this study, where based on their sustainability characteristics and life-cycle assessment. The importance of these features are discussed in chapter 3. The biofuels sources chosen were extracted from *algae*, *sunflower* and *jatropha* seeds.

The final goal for this study, is to present a detailed guide for the CFD problem setup, in a way that any student or engineer could successfully perform a non-premixed combustion case, with *ANSYS Fluent*.

1.3 Task Overview

In the current chapter, the author expresses his motivation behind the development of this thesis. Here, the problems are presented, as well as the solutions that appeared to resolve these problems; why did these solutions not work, and what is the best solution to resolve the presented problems, following with the challenges associated with it. The objectives proposed for this thesis are also presented, focusing which parameters will be studied when a biofuel is used as the main fuel, in a GTE. An Historical review is presented in order to understand the problems and concerns that appeared throughout the time of combustors development. Finally, a bibliographic review is presented, focusing on other works related to the subject and pointing out their importance in this area.
This chapter was written with the intent that any person with minimal scientific knowledge could understand what is proposed for this work.

Chapter 2 introduces the principals behind a GTE. A close-up on the main requirements, types and configurations of the combustor are then presented along with some combustion fundamentals.

Chapter 3, the properties, composition and specifications of conventional jet fuel are analysed and then compared to the chosen biofuels.The reasons that led to the selection of these biofuels, are also mentioned in this chapter. The economical, sociological and ecological effects associated with the use of biofuels are analysed.

Chapter 4 starts by introducing the theory behind numerical modelling. The model construction, which includes the scanning process, the CAD design and the generation of the numerical mesh, is then explained in detail along with the problem set-up.

Chapter 5 presents the numerical results obtained from the CFD simulation. The results are then explained in detail and discussed throughout this chapter. Possible problems encountered in this work are also mentioned. To conclude this chapter, the conclusions resultant from the CFD simulation are presented along with future work proposals.

1.4 Historical Review

For the last two centuries, investigators made many attempts in order to find the best mobile capable of transforming the fuel energy into mechanical work, in a most simple way. Since then, the evolution of the GTE is directly related to the evolution process of the combustor, due to the importance of this in a GTE.

Sir Isaac Newton was the first to theorize, in the 18th century, that a rearward-channelled explosion would propel an aircraft forward at a great rate of speed, in other words, as the hot air blasts backwards through the nozzle, the plane moves forward. This theory was based on his third law of motion; for every action, there is an equal and opposite reaction. Since then, several attempts have been made in order to build a engine that would work on this principle. The first attempt was made by Henry Giffard in 1852, who developed a three-horse power steam engine to propel his airship. Although this flight was counted as a success, the airship lacked the power to navigate properly [17]. In 1894, Hiram Maxim also did not succeed to propel his triple biplane with a steam engine, in fact it only flew for a few seconds [18]. These flights failed due to the fact that these steam engines were powered by heated coal, making them too heavy for flight. The internal combustion reciprocating engine[10] then appeared along with the first flight of the Wright Bothers, in 1903, becoming the sole means to propel aircraft until late 1930s.

World War II contribution to jet engine development.

Military aircraft were propelled by an internal combustion piston engine, by the time the appearance of World War II (WWII) was imminent. The ability for these aircraft to accelerate during flight, in order to operate in combat situations, was limited to the size of its engine, the amount of energy in the fuel, and how quickly could the fuel be burned in the engine. Some of these problems became to complex to resolve, for example, one way to obtain more power from a piston engine is to increase the size of the engine, but as this is done, the engine will become heavier which will affect the aircraft agility, thus it is not desired in the military field. Problems regarding propulsive efficiency were also encountered; this declined as blade tips approached the speed of sound. All these problems motivated engineers to seek a new type of power plant, which would later be known as a gas turbine engine, commonly known as jet engine.

A British pilot named Frank Whittle, designed and patented the first turbo jet engine in 1930, but it was in Germany, by the hands of a physicist named Hans Von Ohain, that the first jet engine first flew in 1939 [19]. Whittle did not succeed in making the first turbo jet flight, because there were many problems regarding the combustor systems. The method adopted by Whittle to prepare the fuel for the combustion process, was to heat it above the boiling

[10]Also known as piston engine; is a heat engine that uses one or more reciprocating pistons to convert pressure into a rotating motion.

point of its heaviest hydrocarbon ingredient, in order to vaporize the fuel completely before the combustion process. The fuel was maintained at high pressures so that vaporization would not occur until it was injected into the combustor, through a nozzle that then reduced the fuel pressure to that of the combustion zone. With this design, Whittle encountered some difficulties relative to its vaporizing tubes, which were experiencing thermal cracking and coking up issues. Difficulties were also encountered in controlling the fuel flow rate. [14]

After many attempts on making a functional combustor, Whittle replaced the vaporizer tubes with a pressure-swirl atomizer and placed a large air swirler located at the upstream end of the liner, as shown in figure 1.1. The function of this last feature was to create a reversal toroidal flow, to recirculate a portion of the hot combustion products, providing a rapid mixing of fuel vapor, air and combustion products that was required to achieve high heat-release rates. Stub pipes were also implemented in order to supply the required amount of air, to complete the combustion process and to reduce the gas temperatures to an acceptable level for the turbine. This combustor was then implemented in the Power Jets W1 engine, which employed 10 separate tubular combustors in a reverse-flow arrangement, to permit a short shaft engine. This engine was used by Whittle to propel the first British turbojet-powered flight, in the evening of May 15, 1941 [14].

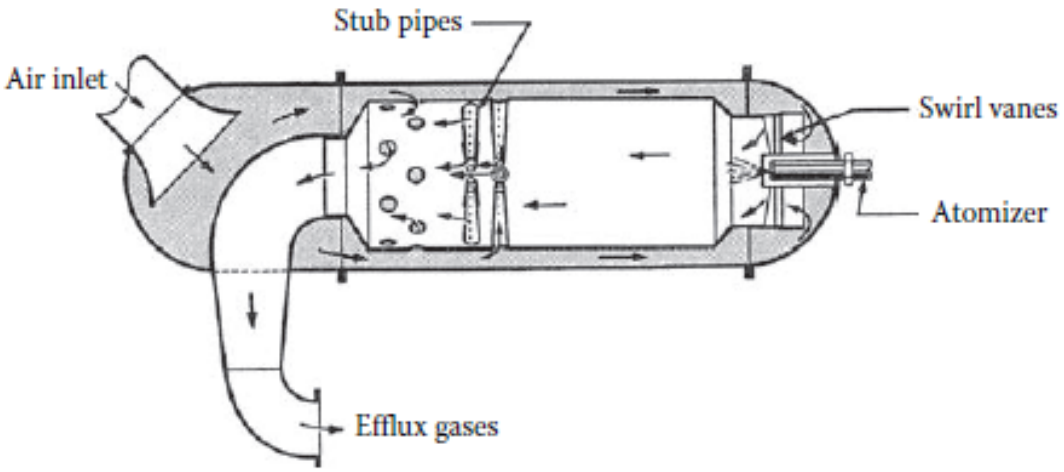

Figure 1.1: Reverse-flow atomizer combustor [14].

Later on, and still in Britain, the straight-through combustor was invented and implemented in the De Havilland Goblin engine, as well as the first annular combustor, which was employed on the Metrovick engine. The invention of this annular combustor came with the use of upstream fuel injectors, and the introduction of downstream dilution air; the upstream fuel injectors were claimed to have the fuel droplets at a higher residence time in the combustion zone, providing more time for fuel evaporation. The downstream dilution air served two purposes; firstly, air is introduced through a first row of scoops, supplying the needs of air to complete the combustion process, with the remaining of this air serving for dilution purposes; the second row of scopes was solely for dilution purposes. Low Pressure losses and low pattern factors[11] where achieved, but

[11]The pattern factor represents the outlet temperature of the combustor, and it should be at a uniform temperature at any given point within the outlet of the combustor.

the fact that this configuration made the engine too heavy, and that the scoops were subject to burnout because of their exposure to the high-velocity combustion gases, made them non feasible for aircraft applications. Upstream fuel injectors are also no longer used, because it is very difficult to eliminate entirely the problem of carbon deposition on the atomizer face.

The Jumo 004 and its contemporary BMW 003, where the only axial-flow[12] turbojet engines to go into production during WWII [20]. The Jumo 004 was developed by Anselm Franz, and employed six-can combustors. Franz was the first to recognize the superiority of an annular combustor design, but he opted for the can configuration because it would present less of a problem, and allow bench testing with a single can [21]. Three of these cans carried spark plugs, using interconnectors[13] to guarantee ignition in the remaining combustors. Each of these combustors were designed to burn diesel fuel, with fuel pressures of up to 5.2 MPa [14] from a pressure swirl atomizer. The approach held in the combustor design was to derive a flame chamber region in the combustor for primary combustion at close to stoichiometric ratio [21]. In order to obtain good mixture and a short flame length, the primary combustion air was introduced in the combustion chamber through helical slots to produce a swirl; the fuel was sprayed upstream into the primary combustion zone. A cutaway view of the combustor can is shown in figure 1.2.

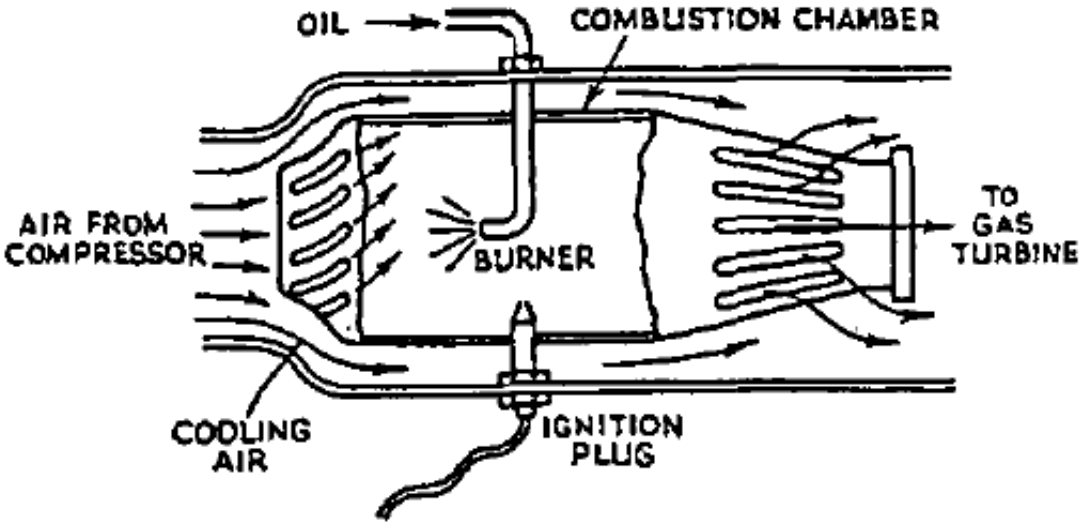

Figure 1.2: Jumo 004 tubular combustor [21].

The BMW 003 was the world's second successful axial-flow turbojet engine and the only one that was used during WWII. Although the development of this engine began before the Jumo 004, the BMW 003 went into production later due to development problems. This engine employed an annular combustor, which had 16 equispaced, downstream-spraying pressure atomizers. The fuel nozzles were surrounded by a baffle[14] and the primary combustion air flowed both through and around the nozzle. The required dilution air to complete combustion and lower the temperature of the combustion products, was obtained through 40 scoops attached to the outer liner.

[12] An axial-flow turbojet allows air to flow straight through the engine, thereby creating less resistance than the centrifugal-flow engines turbojet designs, by Hans von Ohain and Whittle.

[13] Interconnectors, also known as cross fire tubes; provide the mean to initiate combustion in the combustors, without spark plugs.

[14] A baffle consists usually of a plate, placed in the flow stream to create a region of low velocity and flow reversal, in order to improve flame stabilization.

This configuration resulted in a combustor which had a relatively low pressure loss, but also a high length/hight ratio, which led to a long engine. Initially, the average life span of these combustors were very low, about 25 hours [20]. This was due to the fact that these combustors were made from a mild sheet steel with an aluminium coating, which had a heat resistance below of the required value.

The slow development of the jet engine during WWII, was due to the confidentiality of inventions and developments that nations had during the war. The only nation to successfully introduce a combat jet plane during WWII, was Germany with the Messerschmitt Me-262, but they were introduced to late to be decisive.

The end of WWII and the technological explosion of jet engines

The surrender of Germany, in 1945, exposed inventions hidden during wartime, which made possible to solve some of the problems that Britain and Germany had with their jet engines. The engines pre WWII, were fuel inefficient, extremely pollutant, unreliable and noisy. With the junction of both technologies, these engines matured, and in less then 20 years they became the standard means of propulsion for civil aircraft [15].

General electric (GE), Rolls-Royce (RR) and Pratt & Whittney (P&W), were among the first to start developing an efficient jet engine for aircraft application, and lost no time in producing their own combustor designs. GE employed a reverse flow combustor on the J31 engine, which was whittle-derived; a straight-through version was then implemented on the J33, J35 and J47 [14]. P&W also held with the tubular combustor in the J57 jet engine, in the early 1950s. The J57 employed eight of these liners within an annular casing. Each of these combustors had a perforated tube, which went through its axial axis, and extended of up to a half the length of the combustor. As a consequence, this central tube made the tubular combustor act like an annular combustor, being supplied with fuel from six equispaced, pressure-swirl atomizers. [14]

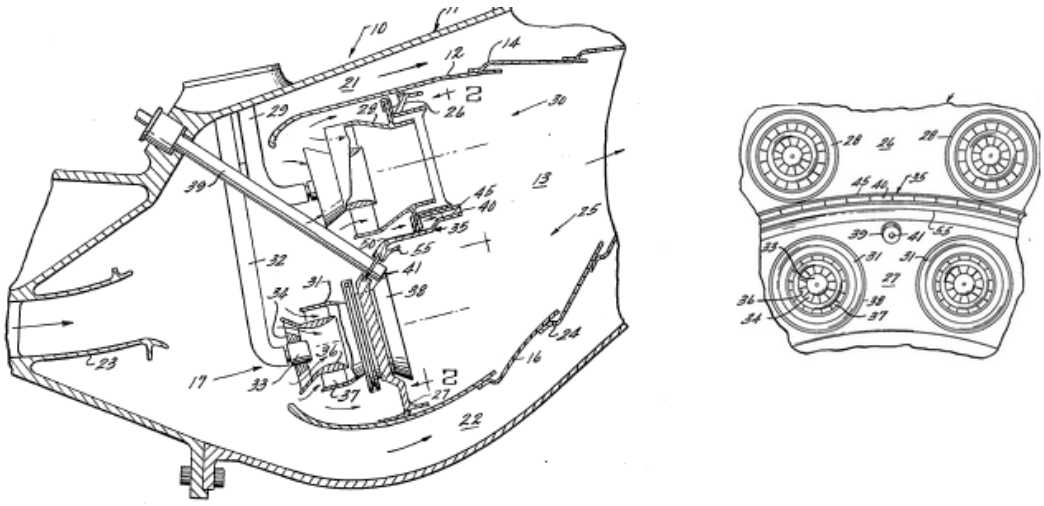

Figure 1.3: On the left of this figure, it is represented an axial cross-sectional view of a double annular combustor, and on the right, a front view of the injectors are displayed [22].

In the mid 1970s, the preoccupation of pollutant emissions resultant from aircraft operation led engineers to search for technological improvements on engine designs to reduce emissions and make the engine more fuel efficient. The quest to achieve low emission combustors has

led combustion engineers to develop staged combustion techniques, wherein a set of burners is used for low speed and low temperature conditions such as idle, and additional burners are used for high temperature operating conditions, such as take-off conditions. One particular concept of this staged combustor is the Double Annular Combustor (DAC), illustrated in figure 1.3, wherein the two stages are located concentrically in a single combustor liner. The pilot stage is normally located concentrically and outside, and is used for idle conditions, i.e, low fuel/air ratios and low temperatures, to achieve good ignition and low CO and HC emissions. The main stage section is located concentrically inside, and is used for high temperatures and relatively high fuel/air ratios, e.g, take-off conditions. This main stage was designed to provide a lean[15] flame with minimal time for NO_x formation. The DAC appeared in the 1950s, with the J34 engine, but this concept was ahead of its time, so there was a lack of interest on this combustor, until GE came and adopted it in their CFM56-5B engine, in the mid 1990s [23].

Another effort in reducing emissions resultant from the combustion process, was the invention of the Twin Annular Premixing Swirler (TAPS) combustor, in 1995, as a emissions reduction program between GE and the National Aeronautics and Space Administration (NASA) [24]. The TAPS was developed through the lessons learned with fuel staging of the DAC and from the experience gained with Dry Low Emissions (DLE) lean-premixing combustors in aero-derivative gas turbines[16]. The TAPS combustor concept is a lean burn system, in which each fuel injector contains a centre pilot and a concentric outer main, as shown in figure 1.4. The central pilot burns in a similar manner to traditional combustors. The fuel is 100% in the pilot, when the engine is starting and when operating at low power. At high power, the fuel is injected through the main, which is a large effective area to burn fuel lean. The aim is then to reduce pollutant emissions, resultant from the Landing and Take Off cycles (LTO), which are defined by ICAO.

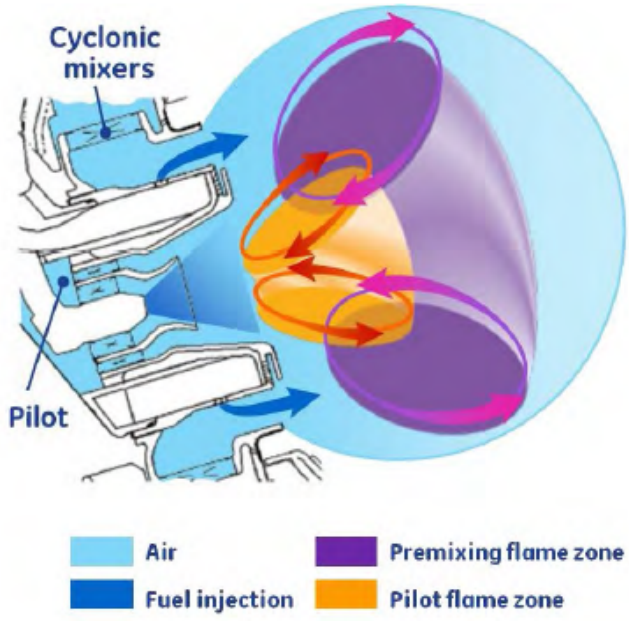

Figure 1.4: TAPS Fuel Injection Concept [24].

[15]Lean mixture refers to a low fuel to air ratio, i.e, there is excess air in the combustion process.

[16]The concept of DLE and lean-premixing combustors, regarding industrial gas turbines, is later explained in this historical review.

Industrial Gas Turbines and their quest to achieve Dry Low Emissions (DLE)

When Industrial Gas Turbines appeared from aero-derivative engines for power generation purposes, they did not have the same impact that aero engines had with the aviation industry. These industrial gas turbines were not competitive at the time due to the fact that they produced low power and low thermal efficiency. However these were improved, and by the end of the 20th century, gas turbines were capable of outputs of up to 300 MW and thermal efficiencies of up to 40%, which made them, along with steam turbines, the major source of power generation [15]. When gas turbines made an entry in markets such as pipelines, electricity generation and mechanical drives, they were immediately subjected to emission regulations, such as aero gas turbines were subjected when they were implemented in civil aircraft. These restrictions were mostly concerned with the reduction of NO_x, CO_2 and UHC. The main manufactures of large industrial gas turbines; Alstom, GE, Siemens and Mitsubishi, started then to develop low-NO_x combustion systems, which were the key for competitive gas turbines.

The easiest way of controlling unwanted emissions to the atmosphere, was to prevent their production in the first place through changes in the combustion design, which led to the use of DLE or Dry Low NO_x (DLN). DLE combustion systems address the production of NO_x at source with a design that does not rely on injected diluents, hence the term "dry"[17]. Promising technologies like Lean-Premixed Pre-vaporized (LPP) combustion, staged combustion, catalytic combustion and rich-burn lean quench combustion, all had the aim to reduce NO_x formation, by the reduction of the combustion peak temperature. The lean premixed system, however, was and still is the combustion system of choice with millions of operating hours recorded [25]. As explained before in this work, the term "lean" refers to the combustion of fuel with excess air, which lowers the temperature of the reaction, thus reducing NO_x formation. The main features that a lean pre-mix combustor design comprises are a Fuel/air injection device, stability device, pre-mixing zone and a flame stabilization zone. The differences in the exit temperature of a diffusion combustor, e.g. Single Annular Combustor (SAC), and a lean premixed combustor are demonstrated in the CFD calculation in figure 1.5. As we can verify, conventional diffusion flame combustors have a very high temperature primary zone due to the high turbulence; premixing and leaning out the mixture, as is the case of the DLE combustor, achieves the desired effect of a more uniform and lower peak combustor temperature, thus resulting in low thermal NO_x formation [25].

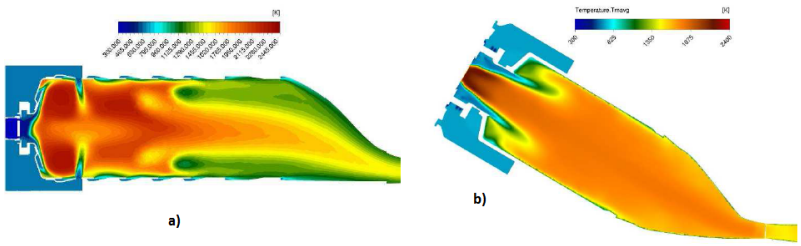

Figure 1.5: CFD calculation temperature distribution in a diffusion flame combustor (a) and in a DLE lean premixed combustor (b) [25].

The lean premixed combustor system has not yet been implemented in aero GTE, because it has

[17] Initially NO_x reduction resulted from the injection of water into the primary zone, Wet Lean Emissions (WLE), but WLE technology demanded cleaning large amounts of water, it was heavy and was difficult to install offshore.

some disadvantages that do not influence that much an Industrial GTE; generally speaking, DLE technology is not yet fully matured when compared to SAC, leading to reduced reliability, but the main disadvantages of running in lean conditions are the marginal blow-out limit and risk of high CO/UHC emissions at low combustion temperatures, due to the incomplete combustion. This possibility cannot even be considered in aero GTE, because if a blow-out does occur a possible disaster may take place. Also lean premixing combustors do not have the emission advantages at low power conditions, such as idle, at which aircraft spend a considerable time in this power setting, which means that at operating loads below 60%, there is a big increase in NO_x and CO emissions [26].

Important developments in order to achieve low emissions were also held by Alstom. With the introduction of the two similar GTE, the GT24 and the GT26 came the sequential combustor, adding the reheating principle to GTE, which offered superior operating flexibility, low emissions and high part-load efficiency. This combustion system is based on the environmental (EV) burner combustion concept, followed by the Sequential Environmental (SEV) burner in the second combustion stage, both held in an annular combustor. The concept is presented in figure 1.6. The compressed air is firstly heated in a first combustor, the EV combustor, with the addition of about 50% of the total fuel. Combustion gases then expand through the High- Pressure (HP) turbine, lowering the pressure by approximately a factor of 2. The remaining fuel is then added with some cooling air in the second combustion chamber, the SEV combustor, where the combustion gases are reheated in order to maximize the turbine inlet temperature and finally expand in the four-stage Low-Pressure Turbine (LPT) [27]. Lower emissions are achieved through this concept, because a reheat combustor makes a more efficient use of the oxygen by burning twice in the lean premix mode, and because there is a increased flexibility due to the flame stabilization by autoignition, which allows the GTE to operate in a wide range load, with low NO_x emissions.

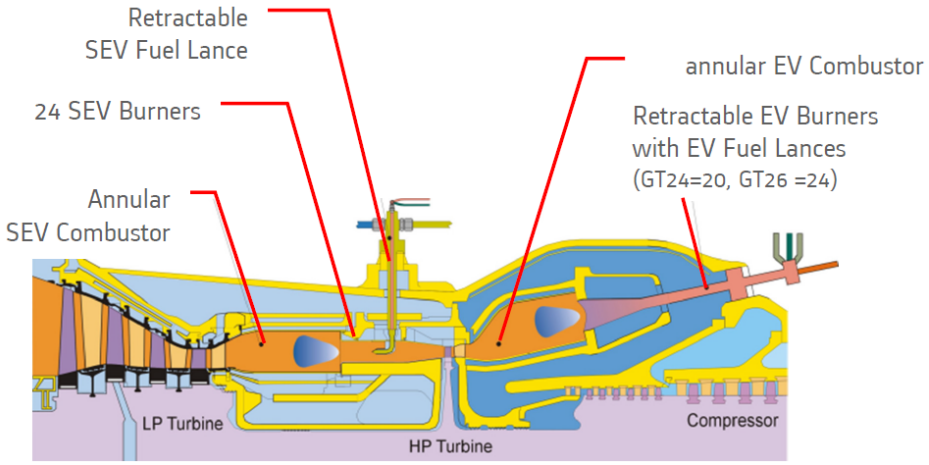

Figure 1.6: Alstom's GT24/GT26 sequential combustion system [28].

Although there was some modifications in the combustor systems throughout its development, the basic design features of aero-engines combustors have remained largely unchanged, meaning that combustor technology has developed gradually and continuously, rather than through a dramatic change, which is why most of the aero-engine combustors now in service tend to resemble each other in size, shape, and general appearance. The main components of the combustor are then a diffuser, a combustion chamber, the fuel injectors, the casings and in

the case of can combustors, Interconnectors. Within the liner itself, the distribution of air is arranged to ensure that the primary combustion zone operates in a much higher fuel/air ratio then the rest of the combustor zones. Extra air is admitted downstream the combustor, and it has two functions; the extra air admitted in the primary zone is to complete the combustion process; the air injected more downstream serves as wall cooling purposes and to dilute the combustion products to a temperature acceptable for the turbine. These components and their fundamentals will be explained with more detail in section 2.2.

1.5 Bibliographic Review

With the invention of the GTE came the need to develop models to simulate the entire engine and each of its components, in which the combustion section was among those that most interest was held. However, it took quite a long time to develop such models, due to limitations in the existing computational hardware, thus in the first years of GTE development, practical studies were dominant. As computers became more powerful, better analytical/numerical models were developed, especially Computational Fluid Dynamics (CFD) modelling, which is now widely applied as a combustion optimization tool. Combustion engineers are now able to model reacting multi-phase flows in a realistic geometry with good mesh resolution, thus increasing greatly CFD applications in industries, which enhances the rapid growth and sophistication of these.

In the following studies presented, focus was made on those that had the aim to analyse the emissions and the energy extracted, resultant from the combustion of biofuels in GTE's. Each of the following reviews present different and important aspects to consider in this thesis. Both experimental and computational studies will be presented, in order to verify if these achieve similar results, making it possible to conclude if biofuels are or not a viable option for the future of aviation fuel.

Regarding biofuels, a very detailed review of typical biofuels for aviation alternative fuel purposes was performed by Reksowadojo et al. [29]. Here he presented several studies performed with various types of biofuels, namely Fatty Acid Methyl Ester (FAME), Bio-derived Synthetic Paraffinic Kerosene (Bio-SPK) and Fischer-Tropsch Synthetic Paraffinic Kerosene (FT-SPK). He then concluded his review by analysing real flight test demonstrations using the previous biofuels. The result of this work is a very good understanding of what has been done in the research of biofuels for aviation alternative fuel purposes.

Experimental Studies/Methods

Lobo et al. [30] performed the first tests of PM emissions in a commercial jet engine, a CFM56-7B, when burning conventional Jet-A1 fuel, Biomass (FAME) and FT fuels. The exhaust samples were obtained from the exhaust of the engine, which was mounted in an open air test cell, and these were extracted using a PM probe and rake assembly coupled to a sample train. The PM size and distributions and its associated combustion CO_2 concentrations, were measured by a particulate spectrometer, the Cambustion DMS500. The ICAO LTO Cycle[18] was adopted for the engine power settings along with a 3% and 65% power setting, which are not included in

[18] ICAO LTO Cycle is defined by the following power settings: 7%, 30%, 85% and 100% and these correspond to idle/taxi, approach, climb-out and take-off, respectively.

ICAO LTO cycle. In order to accomplish a comparison between fuels at the same engine power settings, the measured fuel flows at each power condition were adjusted to account for the different heats of combustion of the considered fuels.

Results show that for the fuels studied, and for the considered power settings, the overall PM number based emissions for a 50% blend of FT fuel were reduced by 34 $\pm$ 7%, and the PM mass reduction was in the order of 39 $\pm$ 7%. For a 40% FAME the reduction of PM number and PM mass was 35% $\pm$ 6% and 52% $\pm$ 5%, respectively. However the FAME fuels PM reductions were mitigated, due to the fact that these present a higher oxygen content of methyl esters, which permits decarboxylation, leading to the formation of CO_2. Another mitigation factor is that these FAME fuels are more viscous then Jet-A1, which increases the fuel viscosity impacts, in both the spray pattern and the size of the fuel droplets in the combustor, leading to incomplete combustion, which in turn enhances CO formation. The authors than concluded that although the alternative fuels offer the potential for large PM emissions reductions, they do not meet current standards for aviation fuel, thus they cannot be considered as certified replacement fuels

An evaluation of the combustion characteristics of Second Generation Biofuels (SGB), in a diffusion burner was performed by Kumaran et al. [31]. The diffusion burner is a simplified replication of the combustion characteristics of a Gas Turbine Combustor (GTC). The SGB was obtained through the improvement of a First Generation Biofuel (FGB), obtained from waste cooking oil. The aim was then to evaluate the combustion characteristics of the improved biodiesel in terms of fuel burning rate, flame length and emissions. The results would then be compared to the FGB and Distillate Diesel (DD). The equipment used for this study consisted on a kerosene burner[19], continuous emission monitoring system, glass chamber, weighing balance, metal ruler and a temperature probe. Combustion efficacy[20] was calculated for heat loss calculation purposes, due to incomplete combustion based on CO concentration.

Results show that the improvement process was a success, improving SGB physical properties in terms of viscosity, surface tension and density; the SGB was also expected to have a higher thermal efficiency than FGB, during the GTE operation. In terms of flow rate, SGB and its blends have a higher flow rate than FGB and are comparable to DD with a blend of up to 50% of SGB. The emission of NO_x resultant from the combustion of SGB and FGB, decreased when compared to DD.

The final conclusions that can then be obtained from this preliminary investigation, is that SGB has better combustion characteristics, when compared to DD and FGB, in terms of burning rate, flame length and emissions. Thus, these conclusions will be helpful for the improvement of SGB, in future gas turbine applications.

In 2010, Klassen et al. [32] developed a Lean Premixed Pre-vaporizing (LPP) combustion technology in order to achieve clean combustion of liquid biofuels in gas turbines, for renewable power generation. This technology converts liquid biofuels, such as ethanol and biodiesel, into a synthetic natural gas. The result of this LPP in a DLE gas turbine, results in a low emission power plant with no net GHG resultant from the combustion of biofuels. Other benefits of this technology are the clean use of biofuels in combustors without having to use post-combustion

[19]The kerosene burner was used because it replicates and represents similar combustor dynamics to a GTC.

[20]The reason why the author used the term efficacy instead of efficiency is due to the fact that only heat loss due to incomplete combustion was considered.

pollution control equipment, and it can easily be implemented into existing GTE power plants. The testing of biofuels using this LPP combustion technology, was held in an atmospheric pressure combustor rig, using a Solar Turbines Centaur 50 natural gas nozzle. The biodiesel adopted was soy-oil based Soy-Methyl-Ester (SME), and the ethanol used was ASTM D-4806 transportation grade, which is used to blend with gasoline. For comparison, conventional fuels were used, which were named as fuel oil #1 and fuel oil #2. Results show that biodiesel and ethanol emissions are similar to those obtained from natural gas and fuel oil #1, but NO_x emissions obtained by the previous fuels, are lower than fuel oil #2[21]. Very low CO emissions were also obtained with the combustion of biofuels, using this LPP combustion technology, and unlike other combustion systems, it is achieved both low NO_x and CO emissions when burning liquid fuels.

The final conclusion that the authors made is that pollutant emissions levels achieved with LPP combustion technology are much lower, when compared with the combustion of these liquid fuels in GTE or reciprocating engines, representing the cleanest use of biofuels and achieving natural gas levels of criteria pollutants (NO_x, SO_x, CO and PM).

The study of emission characteristics when burning a FT[22] jet fuel in a research combustor and in a T63 turboshaft engine, was held by Corporan et al. [33]. These were fueled with conventional military jet fuel, JP-8, a natural-gas-derived FT synthetic jet fuel, referred in this study as synjet, and with blends of the two. The engine was operated at two power settings, idle and cruise, and the combustor at several equivalence ratios, in order to evaluate the emission production over a wide range of combustion temperatures. The T63 was initially operated with JP-8 and then transitioned to operation with the fuel blend and the neat FT fuel, with each test running about 30 minutes. The instruments used to quantify the Particle Number (PN) and PM were conventional aerosol instrumentation, and a Fourier Transform Infrared analyzer was used to quantify the gaseous species. In order to quantify the effects of the FT fuel on the formation and oxidation of particles in the primary combustor zone, of the research combustor, planar laser-induced fluorescence and laser-induced incandescence were used.

Test results indicated dramatic reductions in particle concentration and mean size, on both combustion platforms, using neat FT and synjet fuel blends, when compared to the operation with JP-8. The PN reduction was in the order of 90%, on both combustion platforms, with the FT neat fuel. A reduction of 80% in the smoke number of the engine was observed with neat synjet. However, minor impacts were observed for other gaseous emissions. It was then concluded that PN emissions decreased proportionally with the concentration of FT fuel in the blend and the higher hydrogen-to-carbon (H/C) content in the synjet fuel contributed to the reduction in soot.

A big program of flights and engine tests burning biofuels, were reported by Rahmes et al. [34]. The identification and the search of sustainable feedstocks, along with the use of a new fuel processing method, engine operability, performance and emissions tests were included in this program. Three Boeing aircraft models; 747-400, 737-800, 747-300 equipped with RB211-524G2-T, CFM56-7B and P&W JT9D engines, respectively, were used to perform the real flight tests. The process used to produce the biofuel was BIO-SPK. A 100% blend of this BIO-SPK fuel was then tested to compare its properties with conventional jet fuel; a blend of BIO-SPK and conventional jet fuel was made in order to satisfy standard requirements for conventional jet fuel[23].

[21] This was expected due to the fact that biodiesel and ethanol contain no significant fuel-bond nitrogen.

[22] The FT technology is important because it can be used to convert biomass into synthetic fuels. This technology will be explained with more detail in chapter 3.

[23] The ASTM D1655-08 is the standard specification for aviation fuels.

The sustainable feedstocks identified in this study were Jatropha, Algae and Camelina. These were identified as so, based on an evaluation on environmental, economic and social impacts. The authors then mentioned that using Bio-SPK blended fuels from these feedstocks, had the potential to reduce life cycle CO_2 emissions and that they could be compatible with current aircraft, systems and infrastructure. From the results obtained with the real flight demonstrations, it was concluded that the BIO-SPK fuel blends did not have any adverse affects on the aircraft systems.

With respect to experimental studies when using biofuel in a GTE, this review has been concluded. The following reviews address the same subject, using computational methods.

Computational Studies/Analyses

A review regarding the use of CFD in GTC analyses, was performed by Bhimgade and Bhele [35]. Here the authors focused on the GTC performance and evaluated the scope of CFD use, to increase this aspect. After presenting some works regarding CFD's role in combustor analyses, the author states that computational analyses are more advantageous over the experimental methods, due to the fact that CFD analyses includes computers capacity to analyse systems involving fuel flow, heat transfer and other associated phenomena, such as chemical reactions based on numerical approach. This does not mean however that the conclusions between both experimental and computational are different, stating that CFD results show a good agreement with experimental results. The computational techniques mentioned are *ANSYS Fluent*, KIVA, VECTICS and STAR-CD, along with codes using finite volume such as C++ and FORTRAN.

The author then emphasis the role of the computer in solving numerical correlations, mentioning the basic governing equations, which are mass conservation, momentum conservation, energy conservation and in the case of a reacting mixture[24], species conservation. It was then presented governing equations used in combustion modelling for unsteady, reacting flows assuming single step chemical reaction with negligible radiation. It is then concluded that CFD (CFX, *ANSYS Fluent*) has the greater scope to analyse the combustor using biofuels as an alternative fuel in a GTE, and that in the present, the focus is held on how turbulence leads to increased mixing, in order to be used to compensate for the inaccurate prediction of the chemical reaction rate.

Uryga-Bugajska et al. [36] performed a study in which kerosene, a biofuel and a blend was examined in a Modern Airspray Combustor (MAC) using CFD (*ANSYS Fluent*) modelling. The fuel combustion was calculated using a 3D commercial solver using a mixture fraction/Probability Density Fraction (PDF) approach. For modelling purposes, only 1/22 of the total combustion chamber was considered. The mesh created for the MAC consisted of 198.000 hexahedral and 3.600 prismatic wedge elements. The good quality of the mesh resulted from the extrusion of the surface grid, in the z direction. The boundary conditions were provided by QinetiQ[25], and includes profiles for the swirling air at the injection section and the mass flow for the remaining slots. The operating pressure value considered was of 700 kPa, and the total mass flow of air and fuel was 12.815 kg/s and 0.4746 kg/s, respectively. In this study, the Reynolds-Averaged Navier-Stokes (RANS) approach was chosen in order to solve the turbulent flow. It was used two

[24]Species of fuel which is comprised by many hydrogen and carbon atoms, which again produces different species after reacting with oxygen, e.g. NO_x.

[25]QinetiQ is a British multinational defence technology company, which focuses on aviation, security, defence, energy and environment.

turbulent models: the *Standard* $\kappa - \varepsilon$ was selected as a starting point, and later the Reynolds Stress Model (RSM) was used because of its improved capability of predicting swirling flows. Regarding the chemistry component of the process, this was solved by using the Laminar Flamelet Model (LFM) due do its previously demonstrated accuracy in predicting turbulent combustion, within a MAC [37]. This has then enabled predictions for the aviation biofuel to be made. Regarding thermal NO_x formation, this was determined by the extended Zeldovic reactions, and in order to predict NO_x formation correctly, the partial equilibrium option was assumed for the concentration of O and OH radicals.

The results obtained with kerosene were validated against the indicated experimental measurements provided by QinetiQ. Once validated the kerosene model, the predictions for the further two fuel mixture cases, in which no empirical data was available, where further on compared with the results obtained with kerosene. It has then been shown that using blended fuel produces similar performance to that of 100% kerosene, however for the given operating conditions, there was a significant reduction in performance, due to the reduction in combustion enthalpy, when 100% biofuel was used. Results also showed that NO_x formation when using 100% biofuel are much lower when compared with kerosene, these are in the order of 225 Part Per Million (PPM) and 800 PPM, respectively. Regarding the two turbulence models that were implemented, the *Standard* $\kappa - \varepsilon$ was found to be faster and demonstrated a higher level of stability than the RSM. However, the results in this study were obtained using the RSM, because the accuracy of the simulation using this model was significantly improved.

The first Large Eddy Simulation (LES) of soot evolution in a Rich-Quench-Lean (RQL) combustor, was performed by Mueller and Pitsch [38]. This study is of particular importance for this thesis, due to the fact that it describes with great detail the LES model for soot[26] evolution in turbulent reacting flows. Two fuel-to-air ratios (FAR) were simulated in order to access the ability of the model to perform predictions at the chosen operating points and to perform predictions when a parameter is varied. The detailed soot model used in this study was obtained from Mueller et al. [39]. The combustion model considered was based on the Flamelet/Progress Variable (FPV) model proposed by Pierce [40], in which the solutions of this model are parametrized by the mixture fraction Z[27] and a reaction progress variable C[28]. The LES governing equations were presented; these are spatially filtered in order to remove the smallest scales of the flow. Regarding the liquid spray model, a Lagrangian approach was used and its equations presented, in which the evolution of individual droplets were tracked in the flow. These models were then implemented in VIDA™ [29], and the flamelet solutions were computed with FlameMaster.

Results show that large quantities of soot are formed in the fuel-rich recirculation zone and that the overall FAR dictates both the dominant soot growth process and the location of maximum soot volume fraction. Using the LES model, the soot emissions were overpredicted by about 50%, which is a substantial improvement when compared to previous works using RANS, plus, the FAR predicted by LES compared very favourably with experimental measurements.

An interesting study was held by Wolters et al. [11], in which the impact of alternative fu-

[26] In propulsion and power applications, soot particles are undesired because these are usually accompanied by large amount of UHC, CO and other combustion inefficiencies.

[27] A conserved scalar, which is chemistry independent.

[28] This is typically the sum of the mass fractions of the major products of combustion.

[29] VIDA™ is a fully unstructured low Mach number LES solver for turbulent reacting flows in complex geometries.

els on engine performance, fuel consumption and CO_2 emissions was analysed on engine and flight mission levels. Two engine models were used; a two-spool turbofan for short-haul applications and a three spool turbofan for long-haul applications. Engine design parameters were chosen to be similar to the IAE-V2500 and the Trent 700 series. The evaluation was performed by using the German Aerospace centre, DLR, performance synthesis program GTlab and an aircraft performance tool, VarMission, by the same entity. Drop-in fuels from biomass feedstock were the focus of this investigation, so the alternative fuels considered was switchgrass, forest residue obtained by Fischer-Tropsch (FT) synthesis, jatropha, camelina and algae obtained by Hydroprocessed Esters and Fatty Acids (HEFA). GTlab was then used for an evaluation of these alternative fuels, with the thermodynamic data for gas properties being derived using NASA's 7-term polynomials. The fuel model was based on [41], which proposed a reduced five-step fuel kinetic mechanism for jet fuel simulation. Based on this simplified fuel composition, generic fuel models were created representing Jet A-1 (JetRef) as the baseline reference, neat Synthetic Paraffinic Kerosene (SPK), (SPK100) and a 50/50 blend of Jet-A1 and SPK (SPK50), as two alternative fuel configurations. The fuel models were calibrated to meet the respective average hydrogen (H) mass content of fuel, whereas any sulphur content within the fuel was neglected.

The authors concluded that the use of alternative fuels improved fuel consumption in both operating points. For the short haul mission, defined by the authors as 860 km, using JetRef, a fuel consumption of 3654 kg was calculated. With the introduction of SPK50 and SPK100, a fuel consumption of 3620 kg and 3588 kg, respectively, was obtained, proving that the more neat the SPK blend, the more fuel efficient the engine will be. This results from the improvement of engine performance in combination with the indirect effect from a reduced take-off weight. Regarding the Emission Indices (EI) of CO_2, the use of SPK50 and SPK100 presented a reduction of 1.9% and 3.7%, respectively, when compared to JetRef. For the long-haul mission, 6500 km, the reduction of fuel consumption when compared to JetRef, with SPK50 and SPK100 was respectively, 1.1% and 2.0%. The EI_{CO_2} of the corresponding fuels are a 2.0% reduction with SPK50 and a 3.9% reduction with SPK100. The simulations than suggested that improvements of fuel efficiency and CO_2 emissions by alternative fuels are in the order of a few percent, thus reducing life cycle emissions of these alternative fuels, are of considerable magnitude.

Based on the previous reviews, it can be concluded that in general, both experimental and computational studies proved that biofuels, more specifically SGB and Third Generation Biofuels (TGB) [42], represent a feasible solution in order to reduce fuel price and GHG emissions. These were successfully implemented in experimental flight tests, but cannot be yet implemented as an alternative fuel choice, because aviation alternative fuels have to satisfy very strict requirements, due to the high safety in commercial aviation industry.

The experimental results and the semi empirical correlations for calculating emissions such as CO, UHC and NO_x, when different operating parameters are used, also proved to be of great importance to the design and further development of the GTC. Computational analyses, especially CFD techniques *ANSYS Fluent* and CFX, provide the best means to analyze the combustor using biofuels as an alternative fuel in the gas turbine. Even with existing physical models, CFD can offer cost-effective solutions for many complex systems of interest to the power generation, aero-engines and process industries.

Chapter 2

Combustor Basic Considerations

In order to fully understand the role of a combustor in a GTE, it is important to first comprehend the fundamentals and systems behind a GTE, because the combustor's performance is hugely dependent of these. Thus, the first section of this chapter will be dedicated to explaining these aspects of a GTE, with more emphasis given to the combustor's engine in study, the CFM56-3.

2.1 Jet engine principles and mechanics

A GTE, commonly known as jet engine, is a heat engine that uses air as a work fluid, as means to provide thrust. This principle is based on Sir Isaac Newton's theory, that for every action, there is an equal and opposite reaction. In simple terms, we can look at a garden sprinkler that uses water to provide its rotating motion, or even a balloon, when we suddenly release the gas from the neck, the balloon is then propelled in the opposite direction of the jet.

All jet engines[1] work on the same principle. The air is firstly sucked in the front of the engine, by a fan. This air then passes through a compressor, which has the function to raise the pressure of the air to enhance the combustion. The compressed air is then injected into the combustor along with fuel, which is injected through fuel injectors, and then a spark plug lights the mixture. Here the mixture's temperature rises, and the burning gases expand and gain velocity through the nozzle, but in the way these pass through a set of blades, that are called the turbine, making them spin, which in turn produces power. The turbine is attached to the same shaft as the compressor, and the power output of the turbine drives the compressor. By the time the hot gas reaches the turbine, its pressure is still above that of the surroundings, and the final expansion takes place in the nozzle, in which the exhaust gas velocity increases. It is then this high-velocity jet that produces the thrust to propel the aircraft through the air.[2]

Further on this work, the author presents a deeper insight in each of this systems, and a very detailed view of the combustor.

2.1.1 The Working Cycle

The working cycle of a GTE is somewhat similar to the working cycle of an internal reciprocating engine (ICE), i.e., intake, compression, ignition and exhaust, but unlike ICE's, in which combustion takes place at constant volume and the processes are intermittent, in a GTE combustion takes place at constant pressure, and the processes are continuous. This said, the thermodynamic path over which the gas turbine operates is the Brayton Cycle, which is represented by the P-V cycle in figure 2.1.

The processes of the Brayton Cycle are the following:

[1] The author is referring to air-breathing engines, because non-air breathing engines, likes rockets, have their own oxygen supply, to make propulsion possible in outer space.

[2] In the process of producing high-velocity exhaust, the jet engine also produces electrical power, hydraulic power, pneumatic power for A/C and pressurization and hot air for anti-icing protection.

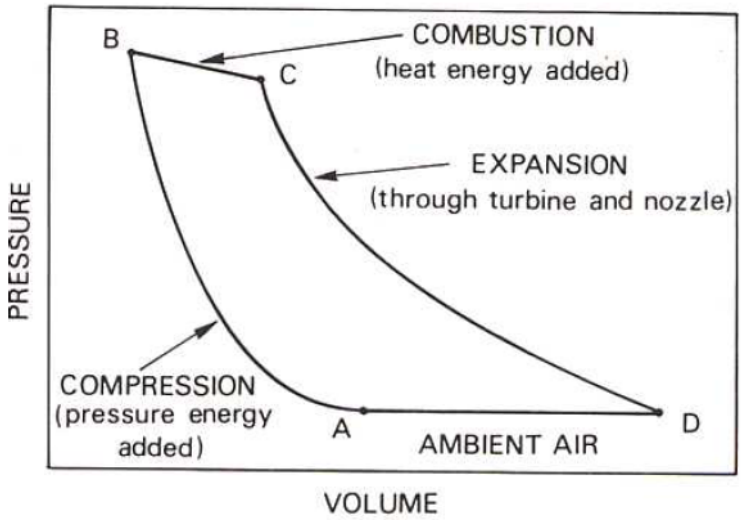

Figure 2.1: Pressure-Volume diagram of the Brayton Cycle [43].

- A-B – Point A represents air at atmospheric pressure, this air is then compressed along the line AB, which represents the compressor cycle. The compression of air between these two points is accompanied by an increase in the temperature of the air. Thus, the air exits from the compressor, and enters the combustor at both elevated pressure and elevated temperature. The pressure ratio $(r_p = p_2/p_1)$, which depends on the performance of the compressor, is a major factor in establishing the overall thermodynamic efficiency of the engine. The higher the pressure ratio, the higher the overall thermodynamic efficiency will be.
- B-C – Heat is added from B to C, by introducing fuel at constant pressure, thereby considerably increasing the volume of air. This fuel[3], which normally is natural and petroleum products, is the source of energy required to drive the cycle. The drop between these two points, represent the pressure drop in the combustion chambers, which in turn should be very low.
- C-D – From C to D, the gases that result from the combustion process expand through the turbine and jet pipe, to the atmosphere. During this part of the cycle, some of the energy in the expanding gases is turned into mechanical power by the turbine, and the remainder of these gases provides a propulsive jet.

It is important to note that because the GTE is a heat engine, the expansion of the gases will be greater with the rise of the combustion temperature. However, this must not achieve values greater than those that the turbine can withstand. Thus, air cooling techniques for the turbine blades, have been developed to permit higher combustion temperatures. These techniques are described in 2.1.3.

2.1.2 The Compressors

The compressor is the first component of the engine core. It is made by a set of fans attached to a shaft, and these fans are made up of blades. The compressor has the function to squeeze the air into progressively smaller areas, which in turn results in an increase in the air pressure. Today,

[3] In chapter 3, the author presents a deeper insight on alternative fuels for aviation purposes.

great part of the jet engine's utilize axial-flow[4] compressors. In these types of compressors, the air flows generally in one direction, along the shaft that connects the compressor and the turbine. The air moves through alternate rows of stationary and rotating sets of blades, that are called stators and rotors respectively. Each of these sets of rotors and stators are called a "stage". These blades are arranged in a manner that permits that the velocity of the entering air decreases, and its pressure increases, when the air reaches each of its stages. The CFM56-3 engine has 13 stages in its compressor, in which four are the High Pressure Compressor (HPC), and nine are the Low Pressure Compressor (LPC).

The earliest commercial jet engines had only one shaft, which are called single spool engines. In this configuration, the shaft connects one turbine section to one compressor. This however did not allow that each of the stage could be more accurately matched to the airflow through the engine, thus a second shaft was introduced allowing the engine to have two independent stages of compression, powered by two independent power turbines. The compressors and turbines could now be more accurately matched to the characteristics of the airflow, creating an improvement in efficiency. The addition of this second shaft created then the twin-spool engine, represented in figure 2.2. A note of interest is the incorporation of the triple-spool design, in RR's engines. These have the aim to achieve better fuel efficiency, by yet again, increasing the match of each compressor and turbine to the airflow.

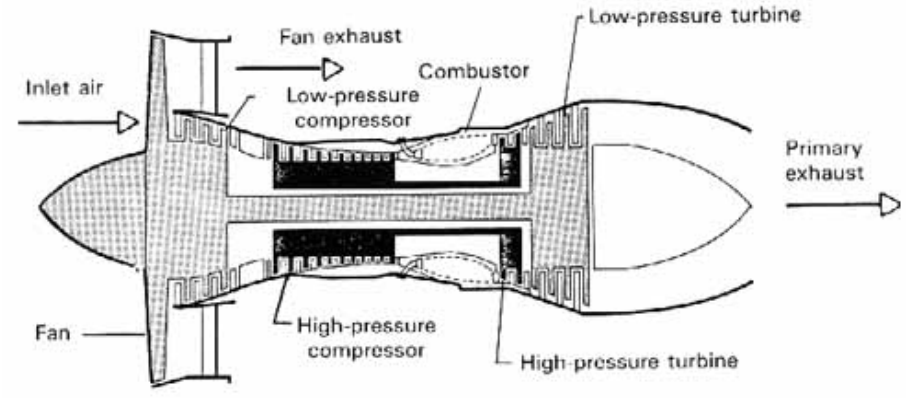

Figure 2.2: A cut view of a twin-spool turbofan engine [44].

This twin-spool compressors can be used in pure jet engines, however it is more suitable for the bypass type of engine, in which the LPC is designed to handle a larger airflow than the HPC. The bypass ratio is the ratio of the air which exits the engine without going through the engine core (secondary flow), compared to the amount of air which goes through the engine core (primary flow). The bypass is characteristic of the turbofan engine. Here, and depending on the bypass ratio, most of the thrust is developed by the fan, which is in fact part of the LPC (figure 2.2), powered by the Low Pressure Turbine (LPT). Turbofan engines produce lower noise than earlier jet engines and are more fuel efficient, this is because the core of these engines do not produce the amount of thrust as they produce in a pure jet engine. Thus, the work done by the core of the engine is mainly to drive the large fan in front of the engine. Current bypass ratios in commercial jet engines, are very high, and for these engines, the fan stage provides 75-85% of

[4]Centrifugal compressors were used in early jet engines. In this type of compressor, air entered at the center of an impeller and was compressed in a radial or outward direction. Lower efficiencies, a limited pressure rise and large diameters led to the disuse of the centrifugal compressor in aircraft applications.

the total thrust produced by the engine [45]. The CFM56 is a twin spool turbofan engine, with a high bypass ratio of 5:1 [46].

All of this compressor work, has the function to deliver air in the right pressure and temperature conditions, in order to enhance the combustion process in the combustor, and to provide a significant quantity of cooling air, to provide a film cooling in the walls of the combustor. The cooling process will be explained with more detail in section 2.2.7.

2.1.3 The Turbines

The function of the turbine is to provide the power to drive the compressor and accessories, and in the case of applications that do not require solely the propulsive jet, the turbine can provide shaft power for a propeller or rotor. Likewise compressor stages, the turbine also have stages, which are composed with one row of stationary nozzle guide vanes and one row of moving blades. These stages are divided into the HPT and LPT, and each of these have their own shaft. The HPT is the stage which is closest to the combustor, where the temperature of gases are greater, and so combustion engineers and HPT engineers have to work together, in order to solve the numerous challenges associated with this section of the engine.

When the hot gases resultant from the combustion process force there way through the discharge nozzles of the turbine, they are accelerated close to the speed of sound, due to the convergent shape of the nozzles. At the same time, the gas flow is given a spin in the direction of rotation of the turbine blades by the nozzle guide vanes. During the expansion of these gases through the vanes, energy is absorbed which causes the turbine to rotate at high speed, and so providing the power necessary to drive the turbine shaft and its corresponding compressor. This process however involves high stresses in the turbine blades, and in order to achieve efficient operation, the turbines may be exposed to temperatures between 850 and 1700 °C, and may reach a velocity of 762 m/s in certain parts of the turbine [43].

What defines this turbine inlet temperature, is the temperature resultant from the combustion process. In theory, in order to achieve the best performance, the burning temperature should be as high as that can be achieved from the complete combustion of the fuel and oxygen in the air. Despite the advances in nickel alloys for the turbine blades, that are both strong and lightweight, these cannot fully withstand this high complete combustion temperature, so blade cooling techniques have been developed, in order to provide a film of cool air that protects the blade wall from the hot gases. The HPC provides the air for this blade film cooling, in which the air passes through internal channels in each blade and ejects at the leading and trailing edges. Ceramic coating can also enhance the heat resisting properties, and reduce the amount of air cooling required, thus improving engine efficiency.

The CFM56 has five turbine stages, in which one is the HPT and the remaining four are the LPT.

2.1.4 The Nozzle

The nozzle is the exhaust duct of the engine, and has an important role in providing thrust for the aircraft. The energy of the airflow that passed the turbine stages, in addiction to the cooler air that bypassed the engine core, meet at the exit of the nozzle and produce a force that acts to propel the engine forward, which is called thrust. In order to make the engine quieter, a mixer is implemented before the nozzle, to combine the high temperature air coming from the engine core, with the lower temperature air that bypasses in the fan.

The Bernoulli Principle

Thrust is generated in the propelling nozzle by means of a convergent duct. As the exhaust gases pass to the atmosphere through this propelling nozzle, the velocity of the gases increase, thus creating thrust. The Bernoulli principle explains how the velocity of the flow is increased in a convergent nozzle; a convergent nozzle is a nozzle that starts big and then progressively its cross-sectional area gets smaller. As the fluid (air) enters the smaller cross-section, it has to increase its velocity due to the conservation of mass, i.e., to maintain a constant amount of fluid moving through the restricted portion of the nozzle, the fluid must move faster.

The design of the exhaust system is of great importance, because it exerts a considerable influence on the performance of the engine. This is because the areas that belong to the nozzle, affect the turbine entry temperature, the mass airflow and the velocity and pressure of the exhaust jet.

2.1.5 Jet Engine Performance

The engine thrust is proportional to the mass flow rate that goes through the engine, and the excess of the jet velocity over flight velocity. Thus, the specific thrust is an important engine design parameter for scaling engine size with thrust, at a given flight conditions, and is defined as the ratio of the engine thrust to its mass flow rate. Eq. 2.1 represents this relation:

$$F/\dot{m} = (V_5 - V_0) + (p_5 - p_0)A_5/m \tag{2.1}$$

Another important parameter is the Thrust Specific Fuel Consumption (TSFC), and it represents the ratio of the mass flow rate of fuel consumption to the engine thrust, as shown in Eq. 2.2:

$$TSFC = \dot{m}_f/F \tag{2.2}$$

The efficiency of the air-standard Brayton - Joule cycle, presented in figure 2.1, is given by Eq. 2.3:

$$\eta_{joule} = 1 \; - \; \frac{1}{r_p^{(\gamma-1)/\gamma}} \tag{2.3}$$

2.2 The Combustor

The goal of the combustor is to convert the chemical energy bound in the fuel into thermal energy. This thermal energy, is the energy used by the turbine to produce the power required to operate the various stages of compressors, or in the case of an industrial GTE, the turbine produces the power required to turn a generator, which in turn produces electricity.

It is important to understand the difference between the combustor and the Combustion Chamber (CC). The combustor includes all of the combustion systems, i.e. the combustor is the conjunction of the diffuser, the combustion chamber, the inner an outer casings, the spark plugs and the fuel injectors, whereas the CC[5] refers to the exact place in which combustion takes place.

[5] In some literatures, the authors adopt names as flametube, liner or even burner for the CC.

The combustor is a critical component in the GTE, because it must operate reliably at extreme temperatures, it has to provide a suitable temperature for the turbine inlet, and it must produce a minimum amount of pollutants over a long operating life. All of the challenges of these aspects, along with combustor fundamentals, will be explained with detail in this section.

2.2.1 Combustor Performance Requirements

An aircraft combustor must satisfy a larger range of requirements than industrial GTC. However, the basic requirements of all combustor are the following:

1. High Combustion efficiency - the fuel should be completely burnt so that all its chemical energy is liberated as heat.
2. Good combustion stability - the combustor should be able to burn over a wide range of FAR.
3. Reliable and smooth ignition - both on ground and high altitudes[6].
4. Low pressure loss - In figure 2.1, the drop between the point B and C illustrates the pressure loss occurring in a practical combustor. It can be seen that this pressure loss reduces the area within the P-V diagram, thus this reduces the work output of the engine.
5. Clean exhaust - At the exit of engine's exhaust, low emissions of smoke and gaseous pollutant species must be presented, i.e. UHC, CO and NO_x.
6. A good pattern factor - This represents the outlet temperature of the combustor. The hot gas stream entering the turbine should be at a uniform temperature at any point at the exit of the combustor. This is tailored to maximize the lives of the turbine blades and nozzle guide vanes.
7. Design for minimum cost and ease of manufacturing.
8. Maintainability and Durability.
9. Multi-fuel capability, i.e., Petroleum, synthetic and biomass-based fuel capability.

It is important to add, that for aircraft engines, size and weight are important requirements, whereas with industrial GTE's, a long operating life is the biggest consideration. However, the requirements for low fuel consumption and low pollutant emissions are priority for all types of engines.

2.2.2 Basic design features

In order to define the essential components needed to carry out the primary function of a combustion chamber, it is of interest to begin by examining the simplest possible combustor, and then discuss the modifications that have to be made in order to produce a combustor that meets the performance requirements presented in section 2.2.1.

In figure 2.3(a), it is presented the simplest possible combustor, in which fuel is sprayed into the centre of a parallel-sided duct. This arrangement, however, is not practical because the velocity of the airstream in which combustion takes place is equal to the compressor outlet

[6] In the case of aircraft engines, it must be able to reignite after a flameout occurs at high altitude.

velocity, which is in the order 150-200 m/s [47]. The major drawback to this system is that the fundamental pressure loss incurred to this system is too excessive, because the fuel would be burning at a very high velocity. Pressure loss then occurs whenever heat is added to a flowing gas, and is represented in Eq. 2.3. For $U = 150m/s$ and for typical values of T_3, T_4 and ρ, the ΔP_{fund} is in the order of 25% of the inlet pressure.

$$\Delta P_{fund} = 1/2\rho U^2[T_4/T_3 - 1] \tag{2.4}$$

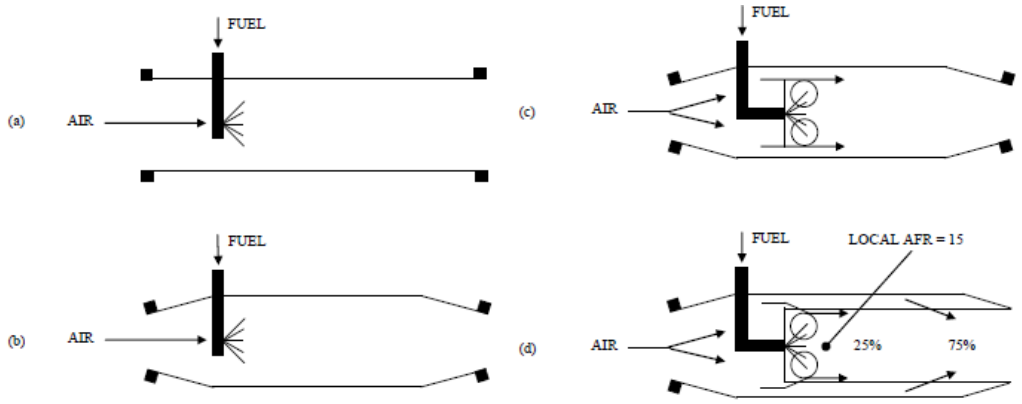

Figure 2.3: Stages in the evolution of the 'conventional' aircraft combustor [47]

In order to reduce this pressure loss to an acceptable level, figure 2.3(b) shows the use of diffuser to lower the air velocity to achieve a tolerable ΔP_{fund}, e.g., if the velocity is reduced to $1/5^{th}$ of its original value, the ΔP_{fund}, will fall to $1/5^2$ = $1/25^{th}$ of its original value, i.e. to about 1% which is an acceptable value.

Despite the implementation of a diffuser, the velocity in the burning region is still too high for stable combustion, thus a flow reversal must be created in order to provide a low-velocity region to anchor the flame. To create this flow reversal, a backplate has been added in figure 2.3(c). This arrangement is particularly important to prevent flame blowout and facilitate reignition under low pressure conditions, i.e., at high altitudes. However, this system has a unacceptable defect, because to produce the desired temperature rise in the combustor, the overall FAR must be around 60 [47], whereas air-hydrocarbon mixtures will only burn with FAR between 8 and 30.

To deal with the problem above, Figure 2.3(d) illustrates a CC attached to the backplate, with air-admission holes. These holes allow that only part of the air is admitted into the primary combustion zone near the fuel injector, to provide the optimum stoichiometric[7] ratio of 15. This arrangement allows that a recirculating flow can provide a continuous source of ignition for the incoming fuel-air mixture. The air not required for combustion is then admitted downstream of the combustion zone, to lower the temperature of the hot gases so that they are acceptable to the turbine.

Modern combustors implement this last configuration, however an intermediate zone is included between the primary and dilution zones. These zones will better be explained in section 2.2.4.

[7]The stoichiometric FAR is that for which just enough air is provided to burn all the fuel to CO_2 and H_2O.

2.2.3 Types of Combustors

There are three main types of combustors for GTE's. These are the tubular, tuboannular and annular. The selection of which type of combustor to use depends of the overall engine design and by the need to use the space as effective as possible.

Tubular

A tubular combustor, also known as a can combustor (figure 2.4), is the simplest form of the combustor and was first used in early jet engines, such as the Whittle W2B and the Jumo 004. The major difference, however, between modern can combustors and the Whittle can combustor, is that this last had a reverse flow arrangement, as shown in figure 1.1, in order to permit a short shaft engine. This arrangement however, created a considerable pressure loss, thus the straight through can combustors where then developed by Joseph Lucas Limited [43].

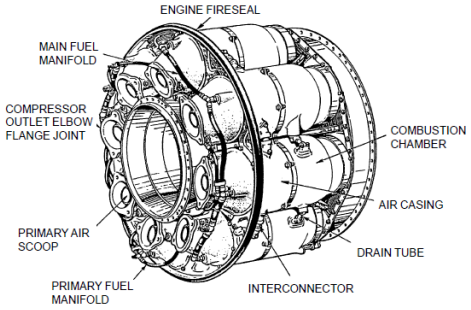

Figure 2.4: Tubular Combustor [47].

A GTE can have multiple combustors around the engine, with the air supplied by the compressor, directed through ducts into each can combustor. Each of these combustors comprise a cylindrical liner mounted concentrically inside an outer cylindrical casing, but are all interconnected. This is two allow that each of the combustors operate at the same pressure, and also allows combustion to propagate around the liners during engine starting.

Advantages:

1. It is easy to develop and when it comes to rig testing, if a engine has n chambers, the tests can be carried out by only using $1/n^{th}$ of the total engine airflow.
2. The fuel spray is well matched to the swirler air and to the secondary air jets. At all points the fuel spray spreads radially outwards while the secondary air jets penetrate radially inwards.

Disadvantages:

1. The can combustors, when compared with an annular combustor for the same mass flow, are much more heavier and lead to a larger engine diameter.
2. Between the compressor and combustor, and between the combustor and turbine, heavy and complex ducts are necessary.

Due to the above disadvantages, tubular combustors are no longer specified in new aero engines designs. However for industrial GTE's, they are still attractive.

Annular

The annular combustor consists of a single combustion chamber, which is annular in form, contained in a inner an outer casing. The chamber is opened at the front to the compressor and at the rear to the turbine nozzles. The combustor in study is of the annular type, and is illustrated in figure 2.5.

With the introduction of the annular combustor came the fuel spray nozzle. This type of fuel injection greatly improves the preparation of fuel for combustion by aerating[8] the over-rich pockets of fuel vapours that are close to the spray nozzle, thus big reductions in initial carbon formation are achieved. This type and other types of fuel injection will be better explained in section 2.2.6.

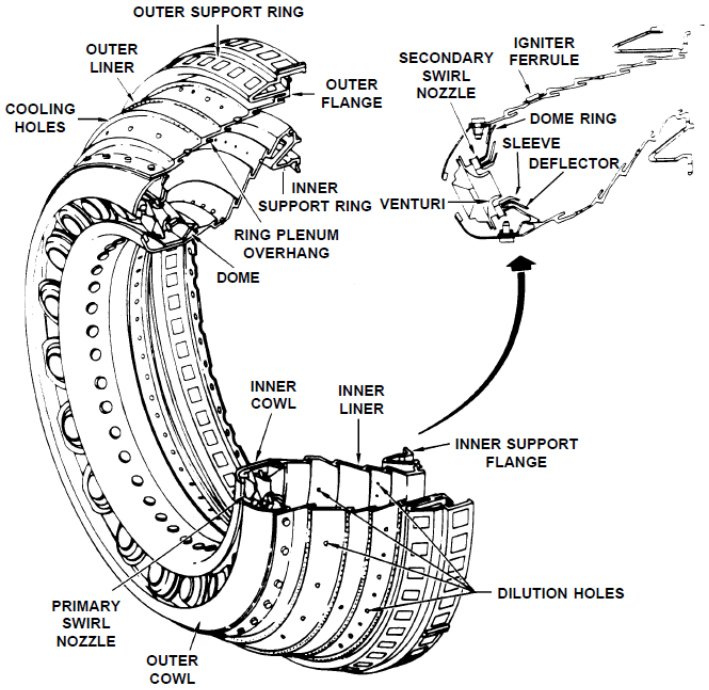

Figure 2.5: CFM56-3 annular combustor [48].

Advantages:

1. The amount of cooling air required to prevent the burning of the combustion chamber wall is less when compared to the other types of combustor. This reduction in cooling raises the combustion efficiency to practically eliminate unburnt fuel and oxidize CO to non-toxic CO_2, thus reducing air pollution.
2. Minimum overall length, weight and diameter.
3. Eliminates combustion propagation problems from chamber to chamber.
4. It has a low pressure loss due to its "clean" aerodynamic design.

Disadvantages:

1. It is much more difficult to obtain a stable uniform temperature profile temperature, when compared to the tubular combustor.

[8] Aeration is the process by which air is circulated through, mixed or dissolved in a substance.

2. The combustion chamber cannot be removed without having to disassemble the engine from the aircraft, which inhibits quick check-ups and maintenance.

3. In test rigs, this type of combustor necessitates full engine airflow, which can pose a problem in some facility test rigs.

Tubo-Annular

Due to the drawbacks of the tubular and annular combustors, the tubo-annular combustor was developed. These combustors are called so, or 'cannular', because they are basically a hybrid between the two basic types. They consist by a number of combustion chambers fitted in an annular casing. This arrangement combines the ease of overhaul and testing of the tubular type with the compactness of the annular type.

The tubo-annular also has a good match of fuel spray with airflow pattern and a low engine diameter, that can be obtained with the tubular and annular type, respectively. It is easy to develop and the rig testing is normally carried out using a segment containing a single combustion chamber. Tests including combustion efficiency, flame stability, ignition limits, combustion chamber temperature and exhaust smoke, can be carried out. However, on segment rigs of this kind, it is not possible to reproduce the outlet temperature profile obtained with an actual engine.

2.2.4 Combustion Process

The combustion of a given liquid fuel like kerosene, involves the mixing of a fine spray of droplets with air, the vaporisation of these droplets, the breaking down of heavy hydrocarbons into lighter fractions, the mixing of hydrocarbon molecules with oxygen molecules and the chemical reaction within themselves, completing the combustion process. In order to make possible that such combustion with a moving air stream, occurs in a small place, i.e. the combustion chamber, a high temperature, such as is provided by the combustion of an approximately stoichiometric mixture is necessary. Since the stoichiometric ratio is about 15:1[9], and the overall Air-fuel ratios (AFR) at which GTC operate at full power is between 33 and 40 [49], it is necessary to introduce the air through three stages, which are so called primary, secondary and dilution zones.

2.2.4.1 Primary Zone

The primary zone has as main objective to anchor the flame and provide sufficient time (residence time), temperature, and turbulence in order to enable the complete combustion of the incoming mixture of fuel-air. The air that exits from the compressor, is injected through 4 injection points, in which two are used to inject the air into the primary zone; these are the swirler and primary air wall jets. These have the function to control the structure as well as the mixing within the primary zone. This hole process is illustrated in figure 2.6.

The swirler

Swirler vanes, represented as an "X" in figure 2.6, are positioned at the front face of the combustor and typically surround the fuel injection points, and are the first entry point for the air that comes from the compressor. These swirl vanes induce a circumferential velocity component to the air, which in turn creates a pressure void at the centre line, and induces a backflow to fill the

[9] In section 2.4.3 this stoichiometric ratio is better explained, and represented by Eq. 2.27.

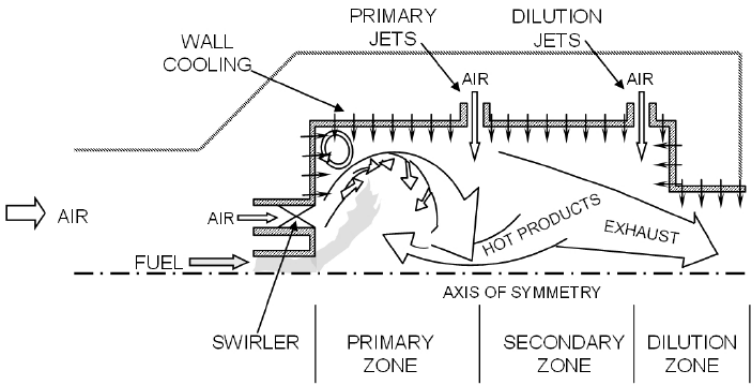

Figure 2.6: Combustor Features [50].

centerline pressure deficit. This creates a toroidal reversal flow that entrains and recirculates a portion of the hot combustion gases, to provide continuous ignition to the incoming air-fuel mixture. The downstream extent of this recirculation zone defines the primary zone. The efficiency of this recirculation zone, depends of the strength of the swirl, and is represented in Eq. 2.5. In order to induce a recirculation zone, the swirl number (S_N) must exceed 0.6 [14].

$$S_N = \frac{2G_m}{D_{sw}G_t} \tag{2.5}$$

Primary air jets

The mixing, stoichiometry and structure of the flows in GTC's, are affected by wall air jets. In the typical combustor, two sets of air wall jets are used in the primary and dilution zones (figure 2.6). The air jets for the primary zone have two functions: the first is to force the toroidal flow in staying within the limits of the primary zone, by providing a strong force against which the primary zone cannot easily penetrate; secondly, the primary jets bifurcate with a substantial percentage of the flow directed upstream, in order to mix with the toroidal flow that contains the fuel-air mixture, and the remainder air mixes downstream into the secondary zone.

The fluid mixing and the chemical kinetics occur in parallel throughout the primary zone, with a range of scales. The zone of recirculation, is within the macro scale, and within this zone, a range of turbulent eddy scales exists and persists during a finite life time (tens of milliseconds [50]), before breaking up and mixing with adjacent eddies, and forming a new eddy. Some of these eddies contain unreacted fuel and air, but will ignite; however others will not, in which these will have to wait to mix with other eddies, in order to acquire sufficient energetic species with the necessary mixture ratio, that is required for ignition.

2.2.4.2 Secondary Zone

The main functions of the secondary zone, also known as intermediate zone, is to allow imperfectly mixed fuel rich pockets to undergo complete combustion, i.e, oxidize the CO to CO_2, and reduce dissociation losses by allowing recombination of dissociated species before the dilution zone.

The principal elementary kinetic reaction that governs the oxidation is represented in 2.6:

$$CO + OH => CO_2 + H \tag{2.6}$$

As temperatures in the primary zone exceed 2000 K [43], dissociation reactions will start to occur, resulting in the appearance of significant concentrations of CO and H_2 in the gases of this zone. If these gases should pass directly to the dilution zone, and be cooled by large quantities of air, CO would be discharged from the combustor unburned.

To avoid such situation and improve the combustion efficiency, three strategies were adopted for the secondary zone [51]:

1. An overall lean mixture ratio (e.g.$\Phi \approx 0.8$) ,through the primary jet bifurcation was established;

2. The temperature was dropped to an intermediate level by the addiction of small amounts of air, encouraging the burnout of soot and allowing the combustion of CO and UHC to proceed to completion;

3. A residence time was provided to promote the oxidation.

The length of the secondary zone is ideally dictated partly by the minimum length needed to mix the intermediate air with gas flow and by the minimum residence time needed for complete combustion. The typical length is then 1/2 of the total length of the combustion chamber [51].

2.2.4.3 Dilution Zone

The dilution zone is located at the end of the combustor chamber, and is the zone in which the gases resultant from the combustion process exit, as shown in figure 2.6. The role of the dilution zone is to reduce the temperature of the combustion products so that a temperature to maintain the integrity of the turbine blades, is achieved. Just to clarify the importance of this zone, the gases may leave a modern combustor at a temperature around 1873 K, and the materials used in the turbine blades melt at a temperature of 1473 K [52].

This temperature reduction is accomplished by the second set of air jet, refered in section 2.2.4.1. These air jets are called in this zone as dilution air, and consists of approximately 1/4 of the total airflow that exits the compressor. However, to protect the integrity of the turbine, reducing the mean temperature is not enough. The radial and circumferential variation in local temperature of these hot gases can create hot spots in the turbine blades, which causes degradation or possible destruction of not only the blades but also other components of the HPT.

To avoid this from happening, combustion and turbine engineers have to work together so that the temperature profile at the exit plane meet design criteria. The temperature profile, commonly known as Temperature Traverse Quality (TTQ), is characterized by various indices, which include the "Pattern Factor", the "Profile Factor" and the "Turbine Profile Factor". The TTQ is one of the most important, and at the same, most difficult problems in the design and development of GTC chambers, because it is difficult to achieve satisfactory and consistent distributions of temperature from the hot gases that pass through the turbine; in fact the actual TTQ profile can deviate from the design profile, as shown in figure 2.7.

The Pattern Factor, represented by Eq. 2.7, reflects the extent to which the maximum temperature deviates from the average temperature rise across the combustor and is the parameter of most relevance to the design of nozzle guide vanes.

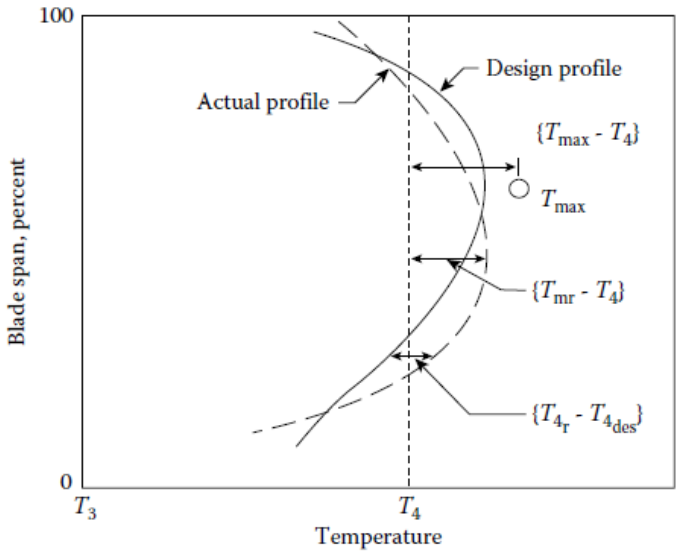

Figure 2.7: Exit plane temperature profiles [14]

$$Pattern\ Factor = \frac{T_{max} - T_4}{T_4 - T_3} \tag{2.7}$$

The temperatures with most significance for the turbine blades, are those that constitute the average radial profile. The profile factor characterizes the extent to which the maximum circumferential mean temperature, T_{mr}, deviates from the average temperature rise across the combustor, as shown in Eq. 2.8:

$$Profile\ Factor = \frac{T_{mr} - T_4}{T_4 - T_3} \tag{2.8}$$

The profile and pattern factor are best suited for situations were a perfectly uniform exit-temperature distribution would be considered ideal. However, this usually doesn't happen due to the fact that modern combustors employ extensive air cooling for the nozzle guide vanes and the turbine blades [14]; thus the desired average radial temperature distribution is far from flat, as we can see in figure 2.7, in which the actual profile peaks above the midheight of the blade.

The Turbine profile factor, presented in Eq. 2.9, then addresses the maximum temperature difference, by comparing the average given temperature in any given radius around the circumference (T_{3r}), and the design temperature for that same radius (T_{3des}).

$$Turbine\ Profile\ Factor = \frac{(T_{4.r} - T_{4.des})_{max}}{T_4 - T_3} \tag{2.9}$$

The dilution zone has then as main functions to dilute combustion gases with a large amount of air, provide an outlet stream of uniform temperature (low value of TTQ), and provide a suitable radial temperature distribution.

2.2.5 The ignition process

Most common fuel and oxidisers combine at a slow rate when subjected to ambient conditions, thus if an activation energy is not externally supplied, i.e. an ignition source, the acceleration of the reaction will not happen. Igniting the mixture will accelerate the reaction, and once ignited, the reaction self-propagates because the flame is an ignition source, as is any other hot object.

Regarding GTC's, the ignition process occurs in the following 3 phases [51]:

- Phase 1: Formation of a flame kernel

  This is the phase in which occurs the formation of a kernel of flame with of sufficient size and temperature, in order to permit propagation. The success or failure of this phase is governed by the energy and duration of the spark, which dictates the size and temperature of the kernel; local turbulence level, which affects the rate of heat loss from the kernel; FAR in the vicinity of the spark plug, which should be close to stoichiometric ratio; by the location of the spark plug, with importance in the extent to which the plug tip penetrates the wall of the combustion chamber.

- Phase 2: Propagation of the flame formed in Phase 1 to all parts of the primary zone

  The factors that influence success or failure in this phase are the primary zone turbulence level; the general air flow and distribution patterns; the overall FAR in the primary zone must be within flammability limits; the spark plug location is also important in this phase, because it determines whether the kernel is entrained in the toroidal flow of the primary zone, or if its swept away downstream.

- Phase 3: Light around (only applicable to tubular or tubo-annular combustors)

  This phase is only applicable for these types of combustor, because it refers to the ignition of the other combustion chambers through Interconnectors, in which the flow area of these is large to facilitate the flame passage, and whose length is short in order to minimize heat losses by external convection to annulus air.

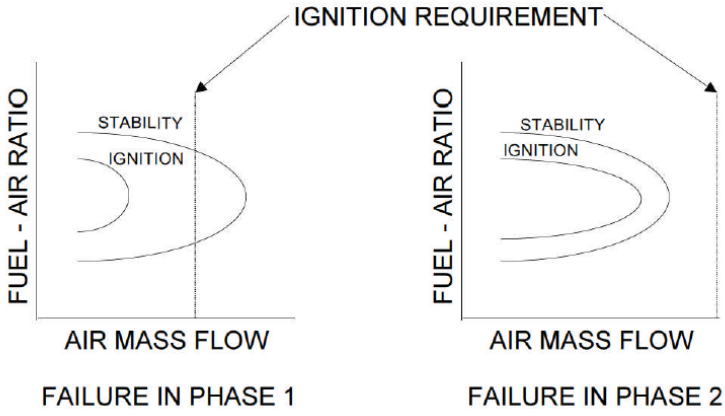

Figure 2.8: Curves illustrating failure in phase 1 and phase 2 [51].

Figure 2.8 represents cases of failure in phase 1 and phase 2. These curves show that if an ignition performance is unsatisfactory, by examining the position of the ignition loop in relation to the stability limits. The two limits are never the same because stability limits relate to

burning conditions, whereas ignition is associated with cold liner walls and high heat losses. However, the goal of ignition development is to ensure that these loops are separated only due to heat loss effects. So, if the ignition loop is well inside the stability loop, this indicates that the limitation on ignition performance is arising in phase 1, and if the ignition and stability loop are close to each other, the problems with ignition performance lie in phase 2.

From the analyses of lean lightup data acquired from a large number of combustion chambers, Lefebvre et al. [14] derived Eq. 2.10[10] for lean lightup FAR (q_{LLO}):

$$q_{LLO} = \left[\frac{B}{V_c}\right]\left[\frac{\dot{m}_A}{P_3^{1.5} exp(T_3/300)}\right]\left[\frac{D_r^2}{\lambda_r H_r}\right] \tag{2.10}$$

2.2.6 Fuel Injection

There are two distinct methods in which fuel can be supplied to the airstream, in order to form the fuel-air mixture; these are through vaporisers and fuel spray nozzles, in which the latter type compromises the two main types of pressure-jets and airspray injectors, and are the type of fuel injection adopted for the combustor in study. Due to this fact, this section will focus on the fuel spray nozzles, only giving a general view on the vaporizers.

2.2.6.1 Vaporisers

As said in section 1.4, a form of preparing a liquid fuel for combustion, is by heating it above the boiling point of its heaviest hydrocarbon ingredient, so that it is entirely converted to vapor before combustion. This is what a vaporizer fuel injector does, which is performed by injecting fuel and some air, into vaporizer tubes that are immersed in the flame. Thus, the fuel-air mixture is heated by the tube walls, and under the ideal conditions, emerges as a mixture of vaporized fuel and air.

Vaporisers however, have not been used on large civil aero engines because they present problems like low durability and high emissions. Other issues relate to the fact that vaporizers are fuel-cooled, which means that they are susceptible to overheating, which in turn is caused by blockage of the fuel feed tube. They are also unable to produce low smoke at the very high temperatures and pressures, seen in modern civil aircraft GTE's.

2.2.6.2 Fuel spray nozzles

Liquid fuels such as kerosene, have to be atomized and well mixed with air, before combustion. The process of atomization is one in which a liquid jet or sheet is disintegrated by the kinetic energy of the liquid itself or by exposure to high velocity air or gas. To achieve this, fuel spray nozzles are used, which can be distinguished by pressure, air-blast and air-assist atomizers.

Pressure atomizers

When a liquid is discharged through a small orifice into the surrounding air, under a high pressure, the pressure energy is converted into kinetic energy. If the velocity is low, the liquid

[10] D_r, H_r and λ_r are parameters relative to JP4 fuel, and are respectively the mean drop size, the lower calorific value and the effective evaporation; B is a constant whose value depends on the geometry and mixing characteristics of the combustion chamber as well as the amount of air admitted into the primary zone.

emerges as a thin distorted pencil, however if the pressures rises and exceeds ambient pressure by about 150 kPa [53], a high-velocity jet is formed, which rapidly disintegrates into a well-atomized spray, which in turn is enhanced by an increase in fuel-injection pressure. This type of atomizer is known as the plain orifice atomizer, and are disadvantageous for most practical applications due to the narrow spray angles that they exhibit. Thus, in order to achieve much wider spray cone angles, the pressure-swirl atomizer was developed.

The simplest form of this pressure-swirl atomizer is the simplex atomizer. The simplex spray nozzle is a pressure atomizer with a single fuel manifold. It consists of a chamber that induces a swirl into the fuel and a fixed area atomizing orifice. The rotating fuel flows through this orifice under both axial and radial forces, to emerge from the atomizer in the form of a hallow conical sheet. This nozzle performs a good atomization at higher fuel flows, but when the pressure drops, e.g. low engine speeds, the atomization is unsatisfactory. Thus, it was replaced in most installations with the dual-orifice nozzle, which offered better atomization at starting and idle conditions.

The dual orifice fuel nozzle, also known as duplex nozzle (figure 2.9), is the one that can be most found in modern-day engines. This fuel nozzle generally requires a dual manifold and a pressurizing valve or flow divider, in order to divide the primary and main fuel flow. These two manifold have two independent orifices, which are fitted concentrically, one inside the other. The smaller orifice handles with the lower flows, while the larger one deals with the larger flows, as the pressure increases. This arrangement allows the atomizer to offer an effective atomization over a wide flow range than the simplex spray nozzle, for the same fuel pressure [53].

In GTC's, it is desirable to have a consistent spray shape over the entire range of operating pressures and flow rates. A solid cone spray is ideal for many applications.

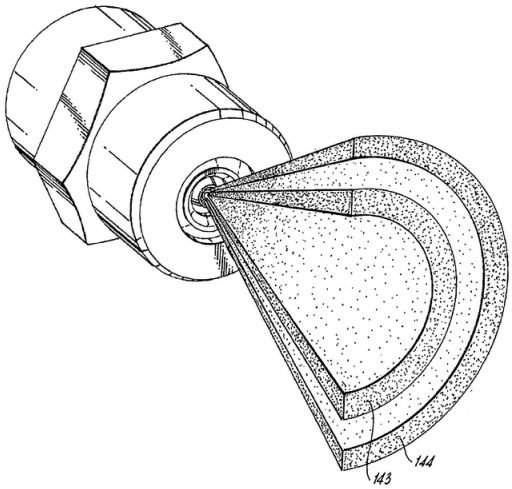

Figure 2.9: Dual orifice atomizer; 143 and 144 represents, respectively, the primary and secondary spray from their corresponding orifice [54].

Air-assist atomizers

Another solution that appeared to solve the problem in which a simplex nozzle cannot offer a good atomization at low fuel flow conditions, was the air-assist atomizer. The nozzle design adopted, was to size the fuel ports for the highest fuel flow rate, and then using a high-velocity

air flow, to enhance the atomization process at low fuel flows. The air assist atomizer comprises two configurations, the internal mixing and the external mixing. In the first type, the spray cone angle is a minimum for maximum air flow, and the spray widens, as the airflows reduced. The external-mixing type can be designed to provide a constant spray angle at all liquid flow rates, however, their utilization of air is less efficient, and consequently their power requirements are higher [53].

These air-assist atomizers are not used in aircraft applications, due to the fact that they need an external supply of high-pressure air, but in industrial GTE's, they are very attractive because this high-pressure air is only needed during engine lightup and acceleration conditions.

Air-blast atomizers

Air-blast atomizers functions exactly the same way in principle, as the air-assist atomizer, because both employ the kinetic energy of a flowing airstream to shatter the fuel jet into ligaments and then drops. The main difference between these two fuel atomizers lies in the quantity of air employed and their atomizing velocity. The Air-assist atomizers uses compressor discharge air to create a finely atomised fuel spray, and it is important to keep the rate flow down to a minimum. When there is no special restriction on air pressure, the atomizing air velocity can be made very high, thus these type of atomisers are characterised by their use of a relatively small quantity of air. However, the pressure differential across the combustion chamber, limits the air velocity that goes through an air spray nozzle, thus a large amount of air is required to achieve good atomization [55]. But unlike air-assist atomizers in which a large amount is wasted, with air-blast atomizers, this air transports the atomized drops into the combustion zone, and mixes with the additional air employed in the combustion process. Due to this and the fact that this atomiser produces a minimum of exhaust smoke, these have been installed in a wide range of applications, including aircraft GTE's.

2.2.7 Wall-cooling

As already stated previously in this work, the gases resultant from the combustion process usually peak above 1800 K, which is much higher than the melting point of both the combustion chamber and turbine blade materials. Thus, these surfaces must be adequately cooled, with a constant supply of cooling air. The most common way of cooling the combustion chamber walls, is by film-cooling. This basically consists of holes along the combustion chamber wall, in order to provide a thin film of air to protect the inner wall. However, the inner wall is coolest near each slot and increases in temperature in a downstream direction, to the next set of cooling holes, which means that a lot of cooling air is wasted.

Although film-cooling does not influence directly the quantity of emissions, it does have an indirect effect, due to the fact that the air required for film-cooling, is also required for emissions control.Thus, the aim of any wall-cooling device should be to effectively protect the CC wall, with a minimum of cooling air in order to maximize the air available for emissions control. There are numerous film-cooling techniques, however, this section will focus on the the film-cooling techniques applied to the combustor in study, which are stacked rings, machined rings and ceramic-coating tiles.

The primary film-cooling technique applied in the CFM56-3 combustor, is the stacked ring device

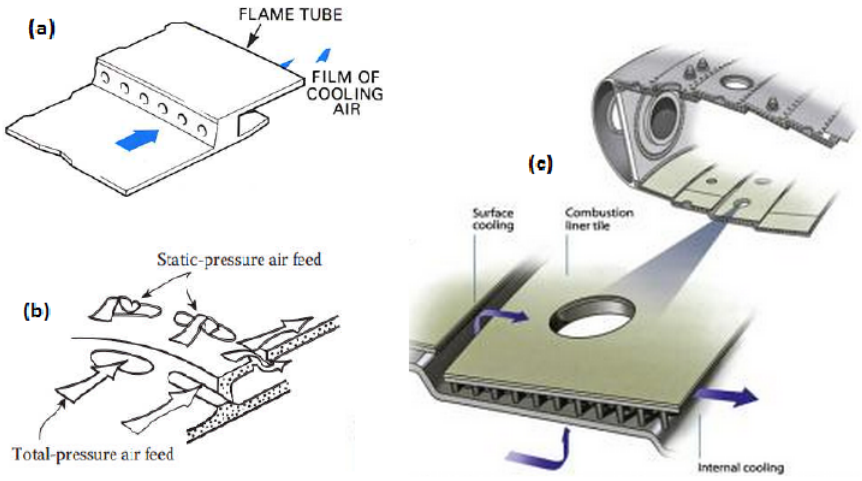

Figure 2.10: Combustion chamber wall-cooling devices; (a) stacked ring, (b) machined ring, (c) ceramic-coating tiles [43] [14] [52].

(figure 2.10(a)). It uses the total pressure feed[11] through holes that are drilled or punched in the wall of the combustion chamber. This results in a less rigid form of the combustion chamber construction, but their dimensional accuracy is higher than other film-cooling devices, which reduces the variations in cooling airflow rate. The flow area of these holes are calculated to meter the required amount of cooling air, and the gap between the lip[12] and the CC wall, is dimensioned to provide the required cooling-air velocity; this means that the cooling air velocity, can be fixed at the optimum value for maximum cooling effectiveness, regardless the actual pressure along the combustion chamber. The combustor in study presents 5 slots of stacked rings in each side of the CC wall, with an average of 600 holes in each slot.

One slot of machined rings (figure 2.10(b)) is also implemented in this combustor. These machined rings can be fed by static pressure, total pressure or both, however in these, only static pressure is fed, through rectangular holes. In relation to stacked rings, machined rings offer a more accurate control of cooling-air quantity and improve the mechanical strength of the combustion chamber.

Another important wall-cooling feature which is implemented in the CFM56 combustor is ceramic-coating tiles, illustrated in figure 2.10(c). The individual tiles are attached to a cold "skin", in which cooling air passes through holes in the combustion chamber wall and impinges on the tile. This air then moves through a series of pedestals, that are designed to improve the convective heat transfer coefficient, before exiting the front and rear of the tile, to form a insulating film that protects the CC wall. These tiles are designed to be removed for maintenance purposes.

[11] The difference between the total and static pressure feed can be noticed in figure 2.10(b).

[12] The lip or skirt, is the surface that allows that the individual cooling air jets, that pass through the holes, to coalesce and form a continuous film.

2.3 Combustion Chamber performance

2.3.1 Pressure loss

The pressure loss in a CC is of great importance, due to the fact that this last must be able to allow fuel to burn efficiently over a wide range of operating conditions, without occurring a large pressure loss. This can be achieved by providing adequate turbulence and mixing, with a pressure loss varying from 3 to 8% of the air pressure at the entry of the CC being incurred [43].

Saravanamuttoo et al. [15] states that when the pressure loss is expressed non-dimensionally in terms of the dynamic head, it will not vary much over the range of the Reynolds number, under which combustion systems operate. Thus, the overall Pressure Loss Factor (PLF) can be expressed by Eq. 2.11[13]:

$$PLF = \frac{\Delta p_0}{m^2/(2\rho_1 A_{max}^2)} = K_1 + K_2\left(\frac{T_{02}}{T_{01}} - 1\right) \tag{2.11}$$

There are various forms in which pressure loss can be verified in a CC, e.g., pressure loss due to heat addition, due to the diffuser configuration or either by the casing diameter. However, with Eq. 2.11 we can estimate the pressure loss when the CC is operating over a wide range of conditions of mass flow, pressure ratio and fuel input. Table 2.1 represents the PLF in the various types of CC's, representing only the cold loss, i.e., the losses that arise from turbulence and friction that can be measured with accuracy from cold-flow tests. The hot loss represents burning conditions, and for chambers of moderate temperature rise, ΔP_{hot} usually lies between 0.5 and 1% of the inlet pressure [14].

Table 2.1: PLF in CC's [14]

Type of chamber	PLF
Annular	20
Tubo-annular	28
Tubular	37

2.3.2 Combustion intensity

The combustion intensity is a very important parameter because it evaluates the maximum possible conversion rate of reactants for a given volume of the CC, i.e., to obtain a high power output, a small and compact CC must release heat at high rates. Thus, the combustion intensity is particularly important for aero GTE's, due to the need of their maximum size reduction. The combustion intensity $(f(\xi))$ is expressed in Eq. 2.12:

$$f(\xi) = \frac{\dot{Q}}{Vp^n} \quad [kW/m^3\ atm] \tag{2.12}$$

in which $\dot{Q}$ is the heat release rate and p is the pressure, and may employ p^{1-8} with the units $kW/m^3 atm^{1-8}$. In aircraft systems, the combustion intensity is in the region of $2 - 5 \times 10^4 kW/m^3\ atm$ [15].

[13] K_1 and K_2 are determined from a CC on a test rig from a cold run and a hot run, respectively.

2.3.3 Combustion efficiency

The combustion efficiency is one of the most important parameters in the CC performance, because if high values of combustion efficiency are not achieved, a waste of fuel and a rise in pollutant emissions, such as CO and $UHC's$, are taking place. Modern aircraft GTE's must be able to achieve almost 100% of combustion efficiency at take-off conditions, and at any point of the GTE operating cycle, the combustion efficiency must always be higher than 90% [49].

There are two different ways of calculating the combustion efficiency, these are based on heat release and temperature rise. However, this last method is via chemical analyses, and is not easy due to the fact that it is difficult to obtain samples from the high velocity stream, and because of the AFR[14] employed in GTC's, which means that the unburnt constituents to be measured, are a very small proportion of the whole sample. Thus, for this work, combustion efficiency (η_{comb}) of the combustor will be obtained from the theoretical heat release to the actual heat release, as shown in Eq. 2.13:

$$\eta_{comb} = \frac{Actual\ heat\ release}{Maximum\ heat\ release} \tag{2.13}$$

The actual heat release is also difficult to measure, however the exhaust gas composition can be measured, which gives information on the products resultant from incomplete combustion. As said before, these products are mainly CO and $UHC's$, and the quantity of these gives an indication of the actual heat release. The maximum heat release is related to the net calorific value[15].

The actual heat release is equal to the theoretical heat release, minus the loss resultant from products of incomplete combustion. Considering that we have CO in the exhaust, the extra sensible enthalpy released if it were to react to completion is shown in Eq. 2.14:

$$Q = CV_{CO} \times [CO]_{mass} \times \dot{m} = 10.1029 \times [CO] \times (AFR + 1) \times \dot{m}_f \tag{2.14}$$

The maximum heat release is given by Eq. 2.15:

$$Maximum\ heat\ release = CV_{fuel} \times \dot{m}_f \tag{2.15}$$

Thus, applying Eq. 2.14 and Eq. 2.15 in Eq. 2.13, the combustion efficiency can be calculated as 1 minus the ratio:

$$\begin{aligned} \eta_{comb} &= 1 - \frac{10.1029 \times [CO] \times (AFR + 1) \times \dot{m}_f}{CV_{fuel} \times \dot{m}_f} \\ &= 1 - 10.1029 [CO]_{mass} \left[\frac{AFR + 1}{CV_{fuel}} \right] \end{aligned} \tag{2.16}$$

Using this same procedure, it is possible to calculate the value for any other product of incomplete combustion. The above value of AFR may also be calculated based of $[O_2]$ and $[CO_2]$, making this a very convenient method of determining the combustion efficiency, based just on the exhaust gas analyses.

[14] This parameter is the inverse of the FAR (see section 2.4.2).

[15] The calorific value is related to the heat of combustion, which will be explained in section 2.4.5.

2.3.4 Stability Limits

In a CC, there is both a rich and a weak limit to the AFR, in which beyond the flame is extinguished. This may occur when there is a high airflow and only a small fuel flow, i.e. a very weak mixture strength (e.g. during a glide or dive with the engine idling). Thus, the range of AFR between the rich and weak limits, is reduced with the increase of air velocity, and if this last is increased beyond a certain value, it is impossible to initiate combustion with the fuel-air mixture. Figure 2.11 shows a typical stability loop, where the limiting AFR is plotted against air mass flow $[kg/s]$.

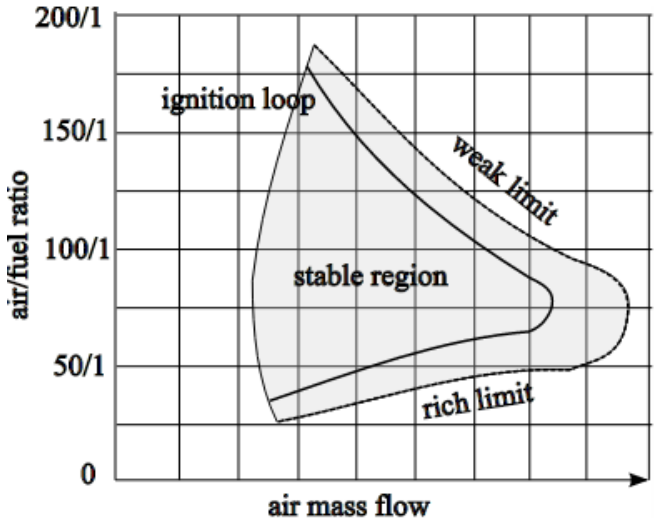

Figure 2.11: stability loop [43].

It is important to add that the stability loop is a function of the pressure in the CC, and a decrease in the pressure reduces the rate at which the chemical reactions proceed, which in turn narrows the stability limit. For aircraft GTE's this is irrelevant because it is important to check that the stability limits are sufficiently wide, with a CC pressure equal to the compressor delivery pressure which exists at the highest operating altitude [15].

2.4 Combustion Fundamentals

"*Combustion is generally recognized as a chemical reaction accompanied by the release of heat and light*" [56]. The overall objective of combustion in the present work, is the controlled generation of maximum combustion heat, with a minimum of harmful emission products. In this section, the author presents an insight off all the fundamental basic aspects regarding combustion.

2.4.1 Combustion flame types

A combustion reaction can be categorized by its flame type, i.e, combustion can be either a premixed flame or a non-premixed (diffusion) flame. The main distinction between these two types of flame gives respect to the mixture of the reactants. In the case of a premixed flame, the reactants are mixed prior to the reaction, at a molecular level. Regarding diffusion flames,

the reactants are initially separated, and the reaction only occurs at the interface between the fuel and the oxidizer [57]. The diffusion flame type categorizes the combustion system in study.

2.4.2 Definitions

Gravimetric and volumetric ratios

The quantities of the species in a mixture can either be defined by their weight (gravimetric), or by their volume (molar). These are commonly represented by χ_i and Ψ_i respectively. Needless to say that the sum of mass or mole fraction for all species in a mixture, has to be unity, as shown in Eq. 2.17:

$$\sum_N \chi_i \;=\; \sum_N \Psi_i \;=\; 1 \tag{2.17}$$

In order to convert from mole fraction to mass fraction, it is necessary to know the molecular weight, M (kg/kmol), for each of the individual species. Only after, the mass of all species are calculated by multiplying the volume fraction by the molecular weight. The final step is then to divide the mass of the individual element/molecule by the total mass[16]. Eq. 2.18 represents this conversion, while Eq. 2.19 represents the mass to molar conversion:

$$\chi_i \;=\; \frac{\Psi_i M_i}{\sum\limits_N \Psi_i M_i} \tag{2.18}$$

$$\Psi_i \;=\; \frac{\chi_i / M_i}{\sum\limits_N \chi_i / M_i} \tag{2.19}$$

Dry and wet ratios

The terms wet or dry serve to define a mixture ratio. For the present combustion study, the combustion products are indicated in a dry basis, i.e., after condensing and removing all water. So in order to calculate a dry mixture ratio, the sum of the mixture ratio of all of the molecules except water, are calculated.

Density of a mixture

Any given mixture, which can be gas, liquid or solid, is defined as the weight per unit volume. In the the case of a gas mixture, the density can be approximated using the ideal gas law, represented by Eq. 2.20:

$$PV \;= nR_u T \tag{2.20}$$

As the current study presents a gaseous mixture, in the form of combustion products, it is necessary to calculate the average molecular weight in order to perform the calculation. This average molecular weight, is represented by Eq. 2.21:

$$\overline{M} \;=\; \sum_{i-1}^{n} M_i \Psi_i \tag{2.21}$$

[16] It is important to note that it is virtually always volumetric compositions that are used in chemical equations, however usually the gravimetric composition is given since this is the easiest to measure.

Mixture ratios

The mixture ratio is one of the most important parameters in a combustor system, because it affects the combustor's performance, life span, efficiency and pollution characteristics.

The mixture ratio represents the ratio in which the fuel and air are present in a system. In premixed combustion systems, there is only one mixture ratio throughout the entire combustion process. However, in the present non-premixed combustion (diffusion flame) study case, there is an infinite range of ratios, that spreads from pure air to pure fuel. The mixture ratio can be defined through the FAR, the equivalence ratio, through excess air and by the mixture fraction.

The FAR is commonly used in the gas turbine industry, and is the inverse of the AFR, which is more used for internal combustion engines [49]. The FAR refers to the ratio of fuel to the air at any given moment, and is expressed through Eq. 2.22:

$$FAR = \frac{m_f}{m_a} \tag{2.22}$$

In order to determine if a mixture is rich or lean, i.e., excess fuel or air respectively, an equivalence ratio (Φ) is used, and is represented by Eq. 2.23. The stoichiometry describes the actual FAR compared to the chemically correct or stoichiometric ratio. The primary zone is typically rich ($\Phi >$1.0), in order to promote reaction stability (e.g. avoid flameout).

$$\Phi = \frac{FAR_{actual}}{FAR_{stoi}} = \frac{m_f/m_a}{(m_f/m_a)_s} \tag{2.23}$$

The mixture fraction (ξ) is a very useful variable in combustion modelling, in particular for diffusion flames. This is because of the fact that all parameters have a value of infinity when in the presence of pure fuel or pure air (FAR and AFR respectively). This is no good for computer modellers, since computers face many difficulties when they attempt to calculate infinities [58]. The mixture fraction is then defined as the ratio by mass of mixture which originated from the fuel, as opposed to the oxidizer stream, and is represented by Eq. 2.24:

$$\xi = \frac{m_f}{m_f + m_a} = \frac{m_f/m_f}{m_f/m_f + m_a/m_f} = \frac{1}{1 + AFR} \tag{2.24}$$

As we can verify with Eq. 2.24, in the air stream (when the $AFR \to \infty$) $\xi = 0$, and in the fuel stream (when $AFR = 0$), $\xi = 1$.

2.4.3 Combustion Stoichiometry

When it comes to the complete oxidation of a simple hydrocarbon fuel, there is always the formation of CO_2 from all of the carbon, and H_2O, from all of the hydrogen. This relation for a given hydrocarbon fuel, with the general composition C_nH_m, is shown in Eq. 2.25:

$$C_nH_m + \left(n + \frac{m}{4}\right)O_2 \longrightarrow nCO_2 + \frac{m}{2}H_2O \tag{2.25}$$

Placing kerosene ($C_{12}H_{24}$) as the hydrocarbon in Eq. 2.25, and replacing the values n and m with 12 and 24 respectively, we obtain Eq. 2.26, which represents the oxidation reaction of kerosene:

$$C_{12}H_{24} \ + \ 18O_2 \ \longrightarrow \ 12CO_2 \ + \ 12H_2O \tag{2.26}$$

Looking up at the atomic weights of the atoms C, O, H which are 12.01, 16 and 1.008 respectively, and multiplying them with the number of moles of each of them in Eq. 2.26, it can be calculated that kerosene has a molecular weight of 168.312 $kg/kmol$ and that oxygen molecule has a molecular weight of 576 $kg/kmol$. Dividing the oxygen-fuel mass ratio we obtain a value of 3.425, which means that for every 1kg of fuel, we need 3.425 kg of kerosene. Since it is known that approximately 23.2% of the mass of air is oxygen, we can obtain the stoichiometric AFR of kerosene with Eq. 2.27:

$$\frac{3.425}{23.2} \times 100 \ \approx \ 14.76 \tag{2.27}$$

However, even with the idealized case of complete combustion represented by Eq. 2.25, there are more species present in the combustion products, then simply the H_2O and CO_2. This is because in most cases, fuels are burned in air and not in pure oxygen, which means that the nitrogen present in the air may participate in the combustion process, which in turn produces the unwanted NO_x. Other aspect to take into account while analysing Eq. 2.25, is that combustion is not always complete, and the effluent gases contain unburned and partially burned products in addiction to CO_2 and H_2O.

The air is composed by its majority of N_2 (76.8%), O_2 (23.2%), and small amounts of CO_2, argon and other trace species. This means that for every mole of oxygen required for combustion, 3.78 mol of N_2 must be also introduced. N_2 does not alter significantly the O_2 balance, however it does have a major impact on the thermodynamics, chemical kinetics, and formation of pollutant in combustion systems [59]. This said, the complete stoichiometric relation for complete oxidation of a hydrocarbon fuel (C_nH_m) is given by Eq. 2.28.

$$C_nH_m \ + \ \left(n \ + \ \frac{m}{4}\right)(O_2 \ + \ 3.78N_2) \ \longrightarrow \ nCO_2 \ + \ \frac{m}{2}H_2O \ + \ 3.78\left(n \ + \frac{m}{4}\right)N_2 \tag{2.28}$$

Analysing Eq. 2.28, it can be verified that for every mole of fuel burned, $4.78(n \ + \ m/4)$ mol of air is required and $4.78(n \ + \ m/4) + m/4$ mol of combustion products are generated. The gas compositions are usually reported in terms of mole fraction, due to the fact this last does not vary with temperature nor pressure, as does the molar concentration. Thus, the product mole fraction (y) of CO_2, H_2O and N_2, is represented by Eq. 2.29, Eq. 2.30, Eq. 2.31, respectively:

$$y_{CO_2} \ = \ \frac{n}{4.78(n \ + \ m/4) \ + \ m/4} \tag{2.29}$$

$$y_{H_2O} \ = \ \frac{m/2}{4.78(n \ + \ m/4) \ + \ m/4} \tag{2.30}$$

$$y_{N_2} \ = \ \frac{3.78(n \ + \ m/4)}{4.78(n \ + \ m/4) \ + \ m/4} \tag{2.31}$$

2.4.4 Absolute enthalpy, enthalpy of formation and enthalpy of combustion

The Absolute enthalpy (h_i), also known as standardized enthalpy, is very a very important variable in chemical reacting systems. For any given specie, it is possible to define an absolute enthalpy, which is the sum of the enthalpy of formation (h_f) and the sensible enthalpy change (Δh_s). The first takes into account the energy associated with the chemical bonds, while Δh_s is associated only with the temperature. Eq. 2.32 represents the absolute enthalpy at a temperature T:

$$\bar{h}_i(T) \;=\; \bar{h}^{\circ}_{\mathrm{f,i}}(T_{ref}) \;+\; \Delta\bar{h}_{s,i}(T_{ref}) \tag{2.32}$$

where $\bar{h}_{s,i} \;\equiv\; \bar{h}_i(T) \;-\; \bar{h}^{\circ}_{\mathrm{f,i}}(T_{ref})$

The subscript ref presented in Eq. 2.32 refers to the standard reference state. Thus, the standard state temperature and pressure are $T_{ref} = 25°C\ (298.15\ K)$ and $P_{ref} = P° = 1\ atm\ (101.325\ Pa)$, respectively, which are consistent with Chemkin and NASA thermodynamic databases [57]. The enthalpy of formation are conventionally adopted as zero for the elements that are in their natural state, and for enthalpies of formation other than the reference state, these are tabulated in many literatures.

Once expressed the enthalpy for mixtures of reactants and mixtures of products, it is possible to define the enthalpy of combustion, when it comes to combustion reactions. For any given complete combustion process, for the products to exit at the same temperature as the entering reactants, heat necessarily has to removed from the combustor. Applying the first law of thermodynamics (Eq. 2.33), the amount of heat removed can be related to the absolute enthalpies of the reactants and the products, as shown in Eq. 2.34:

$$q_{cv} - w_{cv} \;=\; h_0 \;-\; h_i \;+\; \frac{1}{2}(v_0^2 - v_i^2) + g(z_0 - z_i) \tag{2.33}$$

$$q_{cv} \;=\; h_0 \;-\; h_i \;= h_{prod} - h_{reac} \tag{2.34}$$

thus, the definition of enthalpy of combustion (or enthalpy of reaction (Δh_R) per mass of mixture), is given by Eq. 2.35, or in terms of extensive properties, which is given by Eq. 2.36:

$$\Delta H_R \;\equiv\; q_{cv} \;=\; h_{prod} - h_{reac} \tag{2.35}$$

$$\Delta H_R \;=\; H_{prod} - H_{reac} \tag{2.36}$$

2.4.5 Heat of combustion

The heat of combustion (Δh_c), commonly known as the heating value, is the energy released as heat when a compound undergoes complete combustion with oxygen, and is symmetric to the enthalpy of reaction. There are two heating values; the Higher Heating Value (HHV) and the lower Heating Value (LHV). The HHV is the heat of combustion calculated, with assumption that all of the water in the products has condensed to the liquid state. Is within this state that most of the energy is released. The calculation of the LHV, assumes that none of the water is condensed. The standard state of the heating values for a variety of hydrocarbons are present

in several literatures.

The HHV and the LHV can be related by Eq. 2.37:

$$HHV = LHV + h_v \times (n_{H_2O,out}/n_{fuel,in}) \tag{2.37}$$

2.4.6 Adiabatic flame temperature

For a given combustion process, the adiabatic flame temperature (T_{ad}) is the maximum temperature that the products can achieve, for given reactants. Lower temperatures can occur due to heat transfer, incomplete combustion and dissociation. The maximum (T_{ad}) for a given mixture occurs at stoichiometric proportions [57].

In combustion studies, two adiabatic flame temperatures can be used; one for the combustion at constant-pressure and the other one for constant-volume. However, only the first is relevant for this work, as GTC's operate at constant-pressure. If combustion occurs at constant-pressure, the absolute enthalpy of the reactants at T_{ref} is equal to the absolute enthalpy at the final state ($T = T_{ad}, P = 1\ atm$). The first law statement, represented by Eq. 2.38, is what defines this constant-pressure adiabatic flame temperature, and was obtained by applying Eq. 2.33:

$$h_{reac}(T_i, P) = h_{prod}(T_{ad}, P) \tag{2.38}$$

Another parameter of interest is the heat capacity (C), which is defined as the ratio of heat added (or removed from an object), to the resulting temperature, as shown in Eq. 2.39:

$$C \equiv \frac{Q}{\Delta T} \tag{2.39}$$

More heat is required from the system to achieve the same temperature change for an ideal gas at constant pressure, than it is required at constant volume. This is because at constant volume, all heat added is used to raise the temperature. In the other hand, at constant pressure some of the heat performs work. The specific heat capacity at constant pressure (c_p) is represented by Eq. 2.40:

$$c_p = \left(\frac{\partial h}{\partial T}\right)_p \tag{2.40}$$

The enthalpy rise requirement of a GTC is set by the cycle pressure ratio, by the properties of the working fluid and fuel, and by the material limitations [60]. These factors are balanced in Eq. 2.41:

$$\frac{\dot{m}_f}{\dot{m}_a} = \frac{c_p}{Q_f}(T_3 - T_2) \tag{2.41}$$

2.5 Emissions

As could be realized during this work, the pollutants emitted by GTE's that are of most concern are CO, UHC, NO_x and PM (or smoke). At low power conditions, the inlet combustor pressure and temperature are relatively low, which implies that the reaction rates for kerosene-type fuels are low. These fuels must be adequately atomized, evaporated and combusted, with a sufficient

residence time at high enough temperatures to achieve the best combustion efficiency, i.e., maximum conversions of the fuel into CO_2. When this is not the case and the flow field permits fuel vapor to exit the combustor without any reaction (or partially reacted), to species of lower molecular weights, UHC will be formed and be present along with the exhaust gases. If a portion of this flow field intersects with a zone in which temperature has been decreased, e.g. due to film-cooling, these incomplete or quenched reactions, lead to the production of CO.

With the increase of engine power, the high air pressures and temperatures lead to fast reactions, meaning that CO and UHC are virtually zero. However, at these high temperatures the formation of NO_x and PM become prevalent. This as we can see presents a problem, because as efforts are held to, e.g., reduce CO and UHC, this leads to an inevitable increase in NO_x and PM emissions, as can be seen in figure 2.12. This is a problem that persists due to the configuration of modern combustors, thus in order to solve these problems other combustor configurations have to be developed, and staged combustion is a very interesting alternative[17].

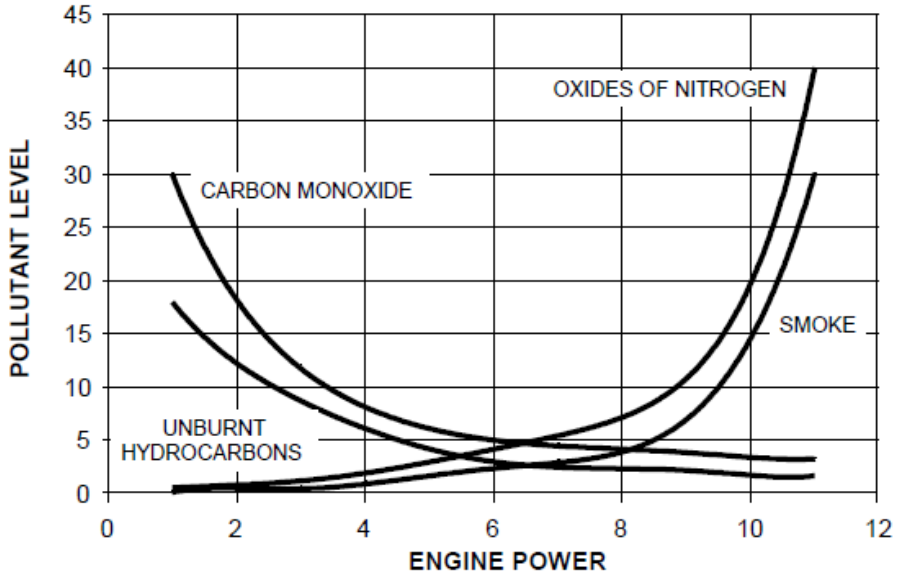

Figure 2.12: GTE emissions [47].

The hazardous effects of these pollutants and their limitation strategies have been mentioned throughout this work, thus in App. A.2, table A.2 has been created summarizing these effects and limitation strategies.

2.5.1 Hydrocarbon oxidation and CO formation

CO is an intermediate specie in the oxidation of hydrocarbon fuels to CO_2 and H_2O. Within fuel-rich regions of the flame, the CO levels are high because there is not enough oxygen for complete combustion. Thus, CO can only be oxidized when a sufficient amount of air is mixed with the hot gases. The extent to which CO is actually oxidized depends greatly on the kinetics of oxidation reactions and the manner of cooling [59]. The following four equations describe the oxidation of CO [62]:

[17] Staged combustion is a NO_x control method, in which these are controlled by creating a rich-lean staging of combustion, e.g, by adjusting some CC to run rich and some lean. The NO_x reduction that can be obtained from staged combustion is between 10 and 40 percent [61].

$$CO + O_2 \leftrightarrows CO_2 + O \tag{2.42}$$

$$O + H_2O \leftrightarrows OH + OH \tag{2.43}$$

$$CO + OH \leftrightarrows CO_2 + H \tag{2.44}$$

$$H + O_2 \leftrightarrows OH + O \tag{2.45}$$

Eq. 2.42 serves as the initiation of the chain sequence but does not contribute significantly to CO_2 formation, due to the fact that it is a slow reaction. Eq. 2.44 is also a initiation chain sequence but is the principal reaction in the overall scheme; it produces H atoms that react with O_2 to form OH and O (Eq. 2.45). These radicals react with CO and H_2O, through Eq. 2.44 and Eq. 2.43 respectively.

2.5.2 Zeldovich reaction and NO_x formation

In GTC's, there are two mechanisms that are responsible for the formation of NO_x; these are thermal NO_x and prompt NO_x. NO_x is also produced through the fuel-bond, but this is usually of less importance for normal fuels [63], i.e, with high British Thermo Unit (BTU) fuels[18]. When there is no fuel-bond nitrogen, thermal NO_x mechanism is predominant in combustion systems with flame temperatures greater than 1800 K [64]. Thermal NO_x is then associated with the formation of NO_x through high temperature oxidation of diatomic nitrogen (N_2) and O_2, found in the air for combustion. These then dissociate into their atomic states and participate in a series of reactions that produce thermal NO_x. The greater the residence time of nitrogen at that temperature, higher will be the NO_x formation [47].

The three principal reactions that produce thermal NO_x, are represented in Eq. 2.46, Eq. 2.47 and Eq. 2.48, which are known as the extended Zeldovich mechanism. Zeldovich was the first to notice the importance of Eq. 2.46 and Eq. 2.47 for thermal NO_x formation [65]. Eq. 2.48 was added later by [66], which describes the reaction of the nitrogen atom in 2.46 with an OH radical to form NO. Eq. 2.48 makes a significant contribution to the formation of NO_x, however Eq. 2.46 is the rate-limiting step for the formation of thermal NO_x, because of its high activation energy [64].

$$N_2 + O \leftrightarrows NO + N \tag{2.46}$$

$$N + O_2 \leftrightarrows NO + O \tag{2.47}$$

$$N + OH \leftrightarrows NO + H \tag{2.48}$$

The rate at which NO_x can be produced by the Zeldovich reaction, can be estimated through the equilibrium concentration of O_2 in the post-flame zone, using Eq. 2.49:

[18] The BTU content of fuels, along with its context in biofuels is explained in chapter 3.

$$\frac{d[NO]}{dt} = 6 \times 10^{16}\ T_{eq}^{-0.5} exp\left(\frac{-69.090}{T_{eq}}\right)[O_2]_{eq}^{0.5}\ [N_2]_{eq} \quad \left[\frac{moles}{cm^3 sec}\right] \tag{2.49}$$

Pollutant emissions are generally expressed as Emission Index (EI), defined as grams per pollutant per kilogram of fuel (g/kg fuel), for a certain power setting. Regarding EI_{NO_x} for annular combustors, these are expressed by Eq.2.50 [67]:

$$EI \approx 32 \times S_{NO_x} \tag{2.50}$$

Where S_{NO_x} defines the NO_x Severity Parameter, which is expressed in Eq. 2.51:

$$S_{NO_x} = \left(\frac{P_3}{2965kPa}\right)^{0.4} \times e^{(\frac{T_3 - 826K}{194K} + \frac{6.29 - 100 * war}{53.2})} \tag{2.51}$$

Prompt NO_x occurs in the earliest stage of combustion and is associated to the reaction of molecular N_2 with radicals such as C, CH and CH_2, which are fragments derived from fuel. This reaction results in the formation of nitrogen species such as Cyanonaphthalene (NCN), which in turn undergo a fast oxidation with OH and O radical species to form NO [68], through Eq. 2.52 and Eq. 2.53 respectively:

$$NCN + OH \leftrightarrows NO + HCN \tag{2.52}$$

$$NCN + O \leftrightarrows NO + CN \tag{2.53}$$

It is important to note that there is very little prompt NO_x formation in the post flame zone[19], but this mechanism can be a great source of NO_x formation when at low combustion temperatures of oxygenated fuels, such as biodiesel [69].

2.5.3 Soot formation

CFD modelling of soot formation and oxidation within the combustion system in study (turbulent, diffusion flames) is difficult because of the complexities of the physical and chemical processes involved, and because of the typical dimensions of the computational grids used for complex geometries [64]. Thus, soot modelling remains one of the greatest challenges to computational modelling of combustion products, and as it isn't a priority for this work, it will not be considered.

2.5.4 ICAO's LTO cycle

Due to the increasing air pollution surrounding the airports, driven by the growth of air travel, ICAO created a reference LTO cycle to limit or reduce the impact of aircraft engine emissions on local air quality. Thus, the emission inventories of aircraft in the vicinity of the airports are calculated using this cycle.

The ICAO LTO cycle is divided in 4 phases, as illustrated in App. A.1. These phases are then the following:

- Take-off: Average thrust setting from take-off release, to the point of main throttle back;

[19] This is because the concentration of hydrocarbon radicals is quite small away from the flame front.

- Climb: Thrust setting from the point of throttle back to the ICAO LTO cycle maximum altitude of 3000 ft (914.4m);
- Approach: Average thrust setting from the ICAO LTO cycle maximum altitude, over the touch down point at the end of the roll-out on the runway;
- Taxi/Ground idle: This phase extends to the beginning of the take-off phase and the end of the approach phase, i.e., it is the average thrust setting from engine start to the point of take-off brake release for taxi-out, and from the end of the rollout after landing and parking, and main engine shut down for taxi-in.

Table 2.2: LTO cycle measurements for the CFM56-3 [46]

Mode	**Power setting**	**Time**	**Fuel flow**	**EI** (g/kg)			**SN**
	$(\%F_{00})$	$(mins.)$	(kg/s)	UHC	CO	NO_x	
Take-off	100	0.7	0.946	0.04	0.9	17.7	4
Climb out	85	2.2	0.792	0.05	0.95	15.5	2.5
Approach	30	4.0	0.290	0.08	3.8	8.3	2.5
Idle	7	26.0	0.114	2.28	34.4	3.9	2.2

Table 2.2 shows the typical power settings, as well as the time spent in each phase for ICAO's LTO cycle[20]. The engine fuel flow (SFC) and the emissions indices are also provided by ICAO. The engine used for emission measurement was the CFM56-3, and these emissions can simply be calculated by Eq. 2.54 and then compared with table A.1 (in App. A.1), which shows ICAO's emissions standards for the type of aircraft.

$$Emission\ [g/kN] = EI\ [g/kg\ fuel] \times SFC\ [kg\ fuel/hr\ kN] \times Time\ in\ mode\ [hr] \tag{2.54}$$

Furthermore, if the data regarding the fuel flow in table 2.2 was not available, this could be calculated by knowing the power output of the engine at take-off conditions [40 kW], and the LHV of the fuel, which in this case is kerosene [43.1 MJ/kg], by Eq. 2.55:

$$\dot{m}_{fuel} = \frac{P\ [kW]}{LHV_{fuel}\ [MJ/kg]} = \frac{40}{43.1} \approx 0.93\ [kg_{fuel}/s] \tag{2.55}$$

It can be seen through Eq. 2.55 that the $\dot{m}_{fuel}$ obtained through Eq. 2.55 is approximately the same as provided by ICAO in table 2.2, and as so, this equation can be used to estimate the $\dot{m}_{fuel}$ of the biofuels studied in this work.

Still regarding table 2.2, the SN is the ICAO's standard for smoke measurement, i.e. the smoke concentration, and has the aim to eliminate any visible smoke from the engine exhaust [14]. The SN can be expressed by Eq. 2.56:

$$SN = 83.6(F_{00}^{-0.274}) \tag{2.56}$$

[20]The data presented in table 2.2 was obtained from ICAO's emission data sheet, for the CFM56-3.

Chapter 3

Biofuels for Aviation

Since the first powered flight from the Wright brothers in 1903, the dependency on oil products has been predominant due to their favourable weight to volume characteristics, and low cost. However, with the rise of the oil price, along with the dependency on foreign oil, which is generally appointed as the primary cause for some big conflicts that took place in the last 30 years; combined with the growing concern of aircraft impact on climate change, has led the aeronautic industry (and not only), to seek and develop alternatives for petroleum-derived fuel.

Nowadays, there are a wide variety of alternative fuels, but all of them present some challenges to implement when compared to conventional jet fuel. However, among all of these alternatives, biofuels and in longer term hydrogen, have the potential to replace conventional jet fuel, as the first could be easily implemented in the present and future aircraft, thus being a drop-in fuel which would require little or no modification to current aircraft design [70].

The aim of the present chapter is to access among others, the life cycle characteristics of aviation fuels from feedstocks, and to explain why were the biofuels *jatropha*, *algae* and *sunflower* chosen for this work; to study the fuel properties that must be considered to make the fuel a viable candidate for the future of aviation industry; all of the challenges associated to these feedstocks as a future aviation fuel, are also explained in detail, so that the reader can acquire a clear image of all the potential that biofuels have to offer.

3.1 Conventional Jet fuel

A GTE has the capability of burning almost anything that can burn, and as so the decision of what to burn comes with some side factors such as availability, cost, emissions, cross section temperature and handling (among others). Kerosene was chosen over other fuels such as gasoline because it presents the best combination of these properties. Today's commercial aviation industry uses mainly Jet-A and Jet-A1. The main difference between these two fuels, is that Jet-A1 has a lower freezing point than Jet-A[1], which makes the first more suitable for polar routes during winter. This however comes at a price, as refineries can produce a few percent more Jet-A than Jet-A1, because a broader distillation cut can be held [10].

Thus, the oil dependency is comprehensible for several reasons; oil products are liquid at atmospheric temperature and pressure, and as so allows easy handling; as they do not contain oxygen atoms, their thermal stability is high, which prevents corrosion; the fact that they have the highest energy content per unit mass, might make them the paramount of all liquid fuels [71]. Conventional jet fuel also offers many other physical and chemical advantages over alternative fuels such as biofuels, and a deeper insight of these properties can be investigated in Chevron's Aviation Fuels Technical Review [10].

[1] Jet-A: -40^oC; Jet A-1:-47^oC

3.2 Biofuels

Biofuels can be defined as combustible liquids, that are manufactured from renewable sources such as plant crops. Crops with high oil content such as sunflowers, should be the starting point for any biofuel implementation, as these can produce high energy outputs. This oil can be obtained by first cleaning, cracking and conditioning the beans. These oils are triglyceride's of fatty acids, and the process of producing biofuel, involves a process named transesterification which applied to these triglyceride's with methanol, produce the so called Fatty Methyl Esters (FAMEs). These FAMEs are responsible for the close similarity to conventional jet fuel, as they have similar physical and chemical properties [10]. The FAMEs composition of the biofuels selected for this study, are presented in table D.2.

These properties however, can vary depending on the feedstock, which in turn can present a big drawback for the implementation of these biofuels, as aviation fuel has strict requirements which accord to ASTM D1655. FAMEs also present a lower energy content than that of kerosene, and also are subjected to an increase bacterial growth due to the fact that small amounts of oxygen are present within the FAMEs. This bacterial growth can limit the storage time of biofuels to 6 months. Moreover, the freezing points of biofuels are generally around 0 ^{o}C, opposed to the -40 ^{o}C of jet fuel, which is a critical limitation as aircraft fuels are exposed to very low temperature at cruise altitude. All of these problems however, can be overcome by a deeper investigation (which also means a higher investment), on all the aspects regarding biofuel production and refinement [70].

Biofuels can be described through three generations; **Generation One** of biofuels refers to the fuels that are made from food feedstock, e.g. soy bean, which in turn compete with the food supply chain; unlike generation one, **Generation Two** biofuels can be obtained from non-food feedstocks such as *jatropha* and *Algae*; **Generation Three** of biofuels gives respect to the use of biotechnologies to make fuel from biomass which is specially modified for biofuel purposes. This last should offer the required productivity, but because the technology is not yet mature, the production of second generation biofuel should be the focus for the next decades, as these biofuels use a sustainable resource to produce fuel which can replace conventional jet fuel, while not competing with food, land and water resources [72]. Moreover, several studies have concluded that by replacing fossil fuels with biofuels most of the harmful emissions resultant from the combustion of these would be reduced, and regarding CO_2 this reduction could be in the order of 80% [73].

Even so, and assuming that future biofuels could fulfil aviation's tight fuel requirements, these biofuels have to comply to several social, economic and environmental factors. These requirements were released by The International Roundtable for Sustainable Biofuels, which released 12 criteria to which biofuels had to comply for them to be considered sustainable; these criteria are organized in a preamble called "version zero" [74]. According to the author, the three most importing principles that can be seen in this list and that must be complied, is the non-competition with food nor land, and the mitigation of climate change by significantly reducing GHG emissions as compared to fossil fuels.

Furthermore, the fuel properties of any alternative fuel has to be accessed and subjected to rigorous tests by regulatory agencies before even considering these as future aviation fuels.

Properties like the high flash point that biofuels present, are very good for handling but as combustors are not prepared for these high ignition temperatures, higher pressures would have to be supplied [70]. Other fuel properties such as aromatics, sulphur content, density and viscosity are also extremely important, but will not be described as these are not relevant for the goals of this study. Thus, for a complete review in all of these important properties, and their affect in biofuels, it is advised to consult the works of Dagget et al. [70] and Stanford et al. [75].

3.2.1 *Jatropha curcas*

Jatropha is a plant that produces seeds which contain the so called FAMEs in the form of oil, which can be used to produce biofuel. The fact that this plant is not a food source (it is toxic for humans and animals), and also due to the fact that *jatropha* can be cultivated in non-arable areas[2], which leaves the arable land available for food crops, makes *jatropha curcas* a very appreciated feedstock for biofuel production. Moreover, the solid waste resultant from the processing of *jatropha curcas*, can be used to burn on fires and in stoves, which means that nothing goes to waste with the production of this biofuel [72].

A life cycle assessment of the production of biofuel using *jatropha curcas* as feedstock, conducted by the Yale school of Forestry, estimated that cultivating this feedstock in agro-pastoral land, would reduce GHG emissions in up to 85%, and if natural woodland were converted for the cultivation of this plant, the GHG emissions would suffer an increase of 60% [76]. This feedstock also proved cultivable with only water that came from rain, a fact that excludes the water competition disadvantage. It can then be concluded that the cultivation of feedstocks for biofuel production, should be conducted in areas in which deforestation would not take place, minimizing any side affects that may come with biofuel production. Other food crops may not supply 5% of their dry weight in oil, but *jatropha* feedstock can supply up to 40% of its dry weight in oil [76].

The oil from *jatropha curcas* can be converted to biofuel using transesterification, however the type of this process is subjected to the content of FAMEs present in the oil. In turn, the amount of FAMEs can vary depending on the oil, and as so it is crucial to optimize the biofuel production, so that the *jatropha curcas* yield can be maximized. While analysing several literatures, it was verified that there is little research on this optimization. In the end, this optimization was obtained from the work of Goyal et al. [77], in which was reported the optimization of the conversion of high fatty acid, *jatropha curcas* oil to biofuel, with the use of response surface methodology.

Jatropha biofuel was among the chosen biofuels, due to the fact that there are several studies and entities, like the government of India, which assign top priority to the production of biofuel from *jatropha curcas* plants. In fact these plants are already being cultivated in India, occupying an area of about 4000 km^2, and to which the oil is expected to be available for biofuel production in the near future [77].

[2]The non-arable areas extends to wastelands and areas where no other plant would survive.

3.2.2 Sunflower

In the past years, the production of biofuel from sunflower feedstock has been quickly gaining popularity. This is due to the fact that sunflowers can grow well in a variety of conditions, and can be grown easily with good economic incomes at both small and large field scales. The high oil content of sunflower seeds are also very high (generally over 40% [78]), a fact that makes these feedstocks appreciated for biofuel production. The by-products (meal) that come from the production of *sunflower* biofuel has also great potential to feed livestock such as cows.

Although *sunflower* feedstock can grow in a variety of soil conditions, they perform best in well-drained soils, because in drier regions they often need supplemental irrigation for best yields [78]. The fact that these feedstocks are susceptible to a variety of pests presents another drawback. However by implementing crop rotation, modified cultural practises and chemical control, a more resistant feedstock can be cultivated.

As biofuel from *sunflower* would inevitably compete with *sunflower* food oil products, and as this last should not be considered a sustainable biofuel, it may be asked why the author opted for this biofuel feedstock. The main reason is due to landscape reasons. One could imagine that throughout the world there could be thousands of square kilometres of land which *sunflower* could be cultivated, and as these landscapes could be magnificent by their own, by associating these landscapes to a green sustainable energy source, a feeling of a bright future in terms of energy and global warming care, would be guaranteed.

3.2.3 Algae

Probably the most promising feedstock for producing large quantities of sustainable aviation biofuel, comes from *algae* [72]. Their capability of being harvested in inhospitable areas like deserts, polluted and salt water makes *algae* the best option for a sustainable biofuel. *Algae* can then be harvested in these environments and with the use of sunlight and CO_2, the biomass can be created. The fact that this feedstock thrives from CO_2 is of great importance, as most of the CO_2 associated with the production of *algae* biomass, could be captured when sunlight is available. Generally speaking the water demand is very low when compared to other crops, especially when photobioreactors[3] are being used. These photobioreactors can be more expensive and more difficult to use, but they may provide a higher level of control and productivity [79]. Once the technology of *algae* biofuel is available for aviation scale, the amount of land required for the feedstock cultivation is very low when compared to other crops[4] (see figure 3.1), and the fact that these can grow quickly puts *algae* biofuel at the top of the most promising biofuels, to fulfil aviation's fuel demands.

So given all of the benefits that *algae* biofuel could provide to the aviation industry, why is it not yet implemented? This question can be simply answered with the investment matter. The main drawbacks of the current state of *micro-algae* biotechnology drift to the fact that there is a high investment associated with the production of *algae* and the processing of the biomass into biofuel. Once this investment barrier is overcome, the world has all what is need to produce a

[3] Photobioreactors are artificial environments in which the specific conditions for *algae* biomass production could be carefully controlled.

[4] *Algae* biofuel also has the highest concentration of FAMEs (up to 80% [79]), which justifies why the required production for aviation consumption, needs so little land.

fuel that could fully supply its energy demands, while at the same time being environmentally clean and renewable.

3.2.4 Land usage

Even though biofuels might prove to be a suitable substitute for Jet-A, their feedstocks must grow at a rate and occupy a certain land area to which aviation demands can be fulfilled. Regarding this particular subject, a study held by Boeing concluded that the land required to produce the required amount of biofuel for aviation, is in the order of 2.7×10^{-6} [72]. As can be seen from figure 3.1, Australia by its own could easily produce the required amounts of biofuel, from *jatropha* feedstock. Moreover, as there is other places in the world were *jatropha* could be grown, one can conclude that there is enough land to cultivate *jatropha* on the necessary scale. Still by analysing figure 3.1, it can be verified that *algae* biofuel only needs 0.0025% of the land for the production of biofuel on the necessary scale, from *jatropha* feedstock, which represents the area of Ireland.

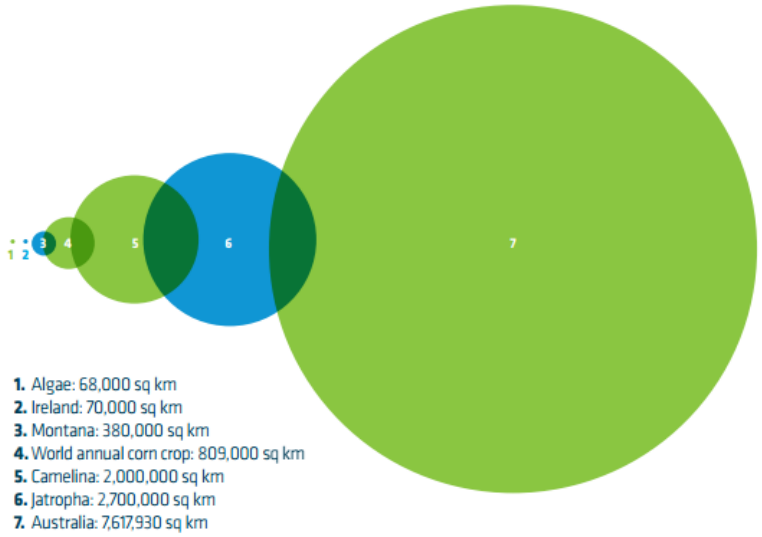

Figure 3.1: Land area equivalents required to produce enough fuel to completely supply the aviation industry [72].

In sum, biofuels have both advantages and disadvantages, and these have to be weighted in order to determine if these are suitable for a future aviation fuel. These pros and cons are then the following:

Advantages:

- Comparing to fossil fuels, biofuels can be much less expensive, as the availability of these are rising, while fossil oil supplies are decreasing.

- Probably the greatest advantage of biofuels, is the fact that these can be produced from a wide range of crops, and unlike the production of fossil fuel sources, biofuels are much more easily renewable as crops can be grown in a much more faster pace, and at the same cultivation locations.

- The reduction of the dependency on foreign energy sources, also comes as a great advantage, as any country would be able to produce their own biofuel, which in turn will produce a large amount of work posts which will not only favour employment (mostly in the agriculture industry), but could also stimulate the economic development of rural areas.
- And finally the focus of this work, which is the emissions from the combustion of these biofuels. The biofuels studied, proved to produce less emissions, when comparing to Jet-A, making these biofuels an environmental friendly alternative for aviation fuel.

Disadvantages:

- Due to the lower calorific value of biofuels, it is necessary more fuel to produce the same amount of energy, while burning Jet-A[5].
- The lower emissions mentioned previously, resultant from the combustion of biofuels, can be mitigated by analysing the carbon footprint of the biofuels, i.e. the process that involves the production of biofuels, which include the fabrication plants and the machinery necessary to cultivate the crops, can make insignificant the emission deficit.
- An initial huge investment is necessary to build the fabrication plants, to provide all of the machinery needed for the cultivation of the crop and to refine the biofuels to higher energy outputs. This is probably the main reason why biofuels are not yet considered a serious alternative for aviation fuel.
- Another disadvantage that many claim the most responsible for the non-development of biofuels, is the competition with food, if the source of the crop is e.g, corn. However, this disadvantage is not even considered in this work, as non-food crops are being used.
- According to the author, the main disadvantage derives from the fact that the crops intended for the production of biofuels will consume large quantities of water. This can be a serious problem, not only because the water price would increase, but the possibility of cultivating the crops in rural areas, were the water source is already scarce, would have to be carefully considered. However, *jatropha curcas* can be cultivated with rain water, and *algae* biofuel can be produced from sea water, which discards the water competition disadvantage.

Despite there is still not enough investment on the research on the viability of biofuels to sustain the demands of aviation fuel, there have been quite a few flights which had the aim to test biofuels performance; an example of a biofuel powered flight was held by Continental Airlines. Here a Boeing 737-800 was powered by burning a 50-50 blend of Jet-A and a *algae-jatropha* derived biofuel, and as verified in other biofuel flights, no problems were reported [29]. In 2012, the NRC performed the first flight on a civil aircraft, using a 100% unblended biofuel obtained from the plant *Brassica Carinata*. Overall, this flight test was a success. Tests results show that this biofuel reduced emissions and provided a better fuel efficiency than petroleum aviation fuel [12]. There are several other biofuel powered successful flights, and to see a complete review on these flights, it is advised to check the work of Reksowadojo et al. [29].

[5]The results of the energy output of the biofuels studied, are presented in section 5.2.

Chapter 4

Numerical Modeling and Planning

In the last decade an increase in computing power has been achieved, which in turn improved modelling capabilities. Now it is possible to work towards realizing the goal of a CFD-based analytical design approach. The readiness of CFD to be used for design is assessed by its prediction capability of certain critical performance characteristics like emissions, exit temperature profiles, wall temperatures, lean blowout (LBO) and fuel-air ratio.

Regarding gas turbine combustion calculations, the following four steps must be taken into account, in order to ensure that CFD is a reliable tool [80]:

1. A study regarding the available turbulence models against standard benchmark cases. This is important because it is possible to predict the capability of the solver and to choose the adequate turbulence model for CFD modelling.

2. An accurate prediction of the cold flow field that goes through and around the combustor, which includes the air flow that goes through multiple inlet ports of the CC, pressure, velocity and turbulence distribution.

3. A state-of-the-art modelling of the fuel atomization process, which in turn results in an accurate estimation of the spray quality.

4. An appropriate choice on the chemistry model, along with a turbulence/chemistry interaction model, and a well established process for exercising them. These aspects are very important to predict the critical characteristics of the chemical reacting flow within the combustor.

Except the fuel atomization model, all of the points mentioned above are considered for this work. Although the fuel atomization is one of the most important aspects to be considered in these type of studies, as it directly affects combustion efficiency and emissions, it is not considered due to the complexity of the present study. Moreover, the first and second phases of the fuel atomization have to be correctly studied, which by itself can be the subject of master's and PhD studies [81].

4.1 Turbulent flow analysis

There is a lot to talk about when it comes to turbulent flow combustion modelling, because this is a very broad subject area. Thus, it will not be possible to review all of the important aspects regarding this subject in the present work. The focus in this section will then be to introduce the CFD-based modelling techniques used in this work, to introduce the governing equations that will be solved in the CFD code (*ANSYS Fluent*), and to present the closure schemes that are used to calculate and understand turbulent transport and mean burning rates in turbulent flames.

4.1.1 CFD-based modelling techniques

Techniques have been developed throughout the years in order to obtain useful information and to allow predictions of turbulent flows. These techniques can be divided into two basic levels; the First-order Eddy Viscosity/diffusivity (EVM) models and the second order Reynolds Stress Models (RSM); within these models several variants exist, however the predictions obtained from this study will rely on the RSM. The RSM was chosen among other models such as the standard k-ε model, because it was verified that better results were obtained from the RSM, despite being more CPU expensive and more difficult to converge then EVM. It was also chosen because it is proven that RSM is more advantageous over other models, in complex 3D swirling flows such as the combustor in study, and consequently it is an efficient way to improve the simulation accuracy [81].

4.1.2 Governing Equations

One of the best methods of analysing turbulent flows is to write out the partial differential equations that embody the basic conservation principles[1], i.e, mass, momentum, energy and species; perform a Reynolds decomposition and then average the equations over time [57]. The result of this decomposition is then the so called Reynold Averaged Navier-Stokes (RANS) equations, and are the following [83]:

- Continuity:

$$\frac{\partial \bar{p}}{\partial t} + \frac{\partial}{\partial x_i}(\bar{p}\widetilde{u}_i) = 0 \tag{4.1}$$

- Momentum:

$$\frac{\partial}{\partial t}(\bar{p}\widetilde{u}_i) + \frac{\partial}{\partial x_j}(\bar{p}\widetilde{u}_i\widetilde{u}_j) - \frac{\partial}{\partial x_j}(\overline{pu_i''u_j''}) - \frac{\partial}{\partial x_j}\left[\mu\left(\frac{\partial \widetilde{u}_i}{\partial x_j} + \frac{\partial \widetilde{u}_j}{\partial x_i} - \frac{2}{3}\partial_{ij}\frac{\partial \widetilde{u}_i}{\partial x_i}\right)\right] = -\frac{\partial \bar{p}}{\partial x_i} \tag{4.2}$$

- Scalar transport:

$$\frac{\partial}{\partial t}(\bar{p}\widetilde{\Upsilon}_\alpha) + \frac{\partial}{\partial x_i}(\bar{p}\widetilde{u}_i\widetilde{\Upsilon}_\alpha) + \frac{\partial}{\partial x_i}(\overline{pu_i''\Upsilon_\alpha''}) - \frac{\partial}{\partial x_i}\left(\Gamma_\alpha\frac{\partial \widetilde{\Upsilon}_a}{\partial x_i}\right) = \widetilde{\omega}_\alpha \tag{4.3}$$

In a laminar flow, the fluid stress is proportional to the rate of strain with the viscosity being a constant of proportionality. In a turbulent flow however, the turbulent stress is related to the mean rate of strain through turbulent viscosity (μ_T). This is the so called Boussinesq's hypothesis, and is represented in Eq. 4.4:

$$-\overline{\rho u_i'' u_j''} = \mu_T\left(\frac{\partial \widetilde{u}_i}{\partial x_j} + \frac{\partial \widetilde{u}_j}{\partial x_i}\right) - \frac{2}{3}\bar{\rho}k\partial_{ij} - \frac{2}{3}\mu_T\frac{\partial \widetilde{u}_k}{\partial x_k}\partial_{ij} \tag{4.4}$$

The turbulent viscosity is calculated from the kinetic energy of turbulence (k) and from the dissipation rate (ε); these are related through Eq. 4.5:

$$\mu_T = C_\mu\bar{\rho}\frac{k^2}{\varepsilon} \tag{4.5}$$

[1] A complete review on these basic conservation principles of reacting flows, can be reviewed in [82].

The transport equations for k and ε are used, and the scalar flux is set proportional to the mean scalar gradient, as shown in Eq. 4.6:

$$-\overline{\rho u_i'' \phi''} = \left(\frac{\mu}{\sigma} + \frac{\mu_T}{\sigma_T}\right)\frac{\partial \widetilde{\phi}}{\partial x_i} \tag{4.6}$$

4.1.3 Regimes of turbulent combustion

In order to derive models for turbulent combustion, a physical approach is required. This approach is based on the comparison of the various time scales present in turbulent combustion. The Damkohler number is very important because it compares the turbulent (τ_t) with the chemical (τ_c) time scales, through Eq. 4.7:

$$Da = \frac{\tau_t}{\tau_c} \tag{4.7}$$

When the Damkohler number is very large ($Da \gg 1$)[2], the flame front is thin and its inner structure is not affected by turbulence, which at most can wrinkle the flame surface [84]. This occurs when the Kolmogorov scales, which are the smallest turbulence scales, have a τ_t greater than τ_c, which means that the turbulent motions are too slow to affect the flame structure. The Karlovitz number (Ka) describes the transition, and is inversely proportional to Da.

4.2 Model Construction

As occurs with many other studies, it is very difficult to obtain the blueprint of a given combustor, due to the confidentially that the GTE manufacturing companies tend to maintain. This case was no exception; TAP kindly provided us a CFM56-3 combustor, and in order to obtain an accurate model of the combustor's geometry, a 3D scan had to be performed followed by a CAD design. A detailed insight of each of these procedures of the model construction is explained in this section.

4.2.1 The scanning process

The 3D scanning device used was the Artec Spider™, from Artec group, which was provided by UBI. This device has an outstanding accuracy for small objects, and offers unlimited possibilities in reverse engineering, i.e., scanning an existing model and importing it into a CAD software enables modifications in the model, in order to achieve desired improvements. However, this scanner is not indicated for bigger objects, such as the combustor in study, due to the fact that it has a narrow field of view[3]. After attempting several approaches to this problem, the scanning methodology adopted, was to scan latitudinal sections of the combustor at a time, and then join these sections in the Artec Studio 9.2 post-processing software. But even this methodology presented some problems; initially the scanner was loosing track, this occurs when the scanner achieves a certain point in which it can no longer continue the scan because it is unable to

[2]The typical Da for GTC's is 150, 6.5 and 1.3 for take-off, idle and altitude relight conditions, respectively [83].

[3]The indicated 3D scan device for this object size is the Artec Eva™, which was not available at the time.

identify different textures in the model, to serve as reference for the rest of the scan; this was solved by adding adhesive tape crepe along the latitudinal sections, and marking large "X_s" along it, as can be seen in figure B.1. Another problem that appeared when post-processing the scans was that the beginning and the end of these latitudinal scans were not coinciding; this was solved by enabling a discrete option in the software, named "loop closure", which is described in section 2.2.12 of Artec Studio 9.2 user's guide.

The scanner is inoperative without the software and will not start before it detects this. The Artec Studio 9.2, is a very sophisticated but user friendly, post-processing software and was the software used for the scanning process. It uses the unprocessed scans from the scanner device, and transforms them into an accurate 3D model, of the scanned object. The steps of this process are the following:

1. *Align*: After performing the scanning process, and identifying which of these scans can or not be used (due to their quality), it is necessary to align them. The software provides a nice align option, which enables the user to identify two identical points in two scans, and these usually are enough to permit a correct alignment of these scans. If the alignment does not perform correctly, the user can identify more similar points in these two scans in order to aid the alignment.

2. *Global Registration*: Even after a successfully alignment, there might be some frames that are not aligned, and are not noticeable with the naked eye. Thus, global registration is an algorithm that performs the alignment of any given frame that is not aligned, and also eliminates any noise within the scans. This step is required to perform the model fusion.

3. *Model Fusion*: After a successful global registration, all the processed data can be fused into a single polygonal 3D model. There are three types of model fusion; fast fusion, smooth fusion and sharp fusion, in which this last was the used one due to the fact that the detailing of the result is usually higher than in the first two cases [85]. After this step, the 3D model can then be exported in several formats, e.g., STL, OBJ, PLY.

4. *Model editing*: Even after the fusion is successfully performed, there are still irregularities in the surface and noise that require editing, which makes the file more CPU expensive. The software provides quite a few editing options, e.g, surface smoothing, small objects filter, hole filling and mesh simplification.

After the completion of these post-processing steps, other functionalities are available as is the case of measures, i.e, the software can accurately measure the distance between selected points. This tool was very useful for obtaining measures for the CAD design, and is illustrated in figure B.3. The Artec Studio 9.2 software, requires a potent computer, and the bigger the model to scan, more will be the system resources required from the computer. In this case, the highest required RAM was 28 GB and was accomplished with a computer that was kindly provided by Dr. Francisco Brojo, which was also used for the *ANSYS Fluent* simulations, presented in this work.

Overall the scanning process was a success. Only the exit section of the combustor could not be scanned due to the fact that the turbine support structure that was attached to the combustor was not removable, which prevented the view of the scanner to that part of the combustor. Without accounting for the learning time and the scanning process, the post-processing of the

3D model took roughly 1 week. The scanning of the combustor was held at UBI while the scanning of the fuel injectors and the dome, were held at TAP facilities. Some images of the scanned 3D model combustor, can be seen in App. B.2.

4.2.2 CAD design

After obtaining a 3D model of the combustor through the scanning process, this cannot be used directly for meshing and simulation purposes in *ANSYS Fluent* due to two reasons; first this 3D model only presents a shell of the combustor, i.e, the 3D model does not have any thickness, and secondly this model even after the post-processing step, still lacks some detail which is required for the model simulation (see figure B.2). Thus, it is necessary to perform a CAD design, with the aid of the STL format exported from Artec Studio 9.2.

The CAD software chosen was *CATIA V5 R19*. This choice was mainly because the author was more familiar with this software and also because it offers a wide variety of tools to enable all sorts of drafts. Initially CATIA was having a big problem importing the STL file, because as this was relatively big for an STL format ($\approx$ 200MB), the software was always crashing after tempting to import it. Even after a few editing and mesh simplifications of the STL file in *Artec Studio 9.2*, *CATIA* was still unable to import the file. An alternative STL importing method to *CATIA* had to be investigated.

Fortunately, this alternative method was discovered while exhaustively attempting other importing methods offered by *CATIA*. The solution was then to open the *Shape workbench*, select the *Digitized Shape Editor* toolbar and open the *Cloud Import* function. Here, several import formats are available, which include the desired STL format. Importing this file with this methodology results in an import time of less then a minute, for this case. The reason the importing process is so smooth, is due to the fact that the imported file is just a "shell", while in traditional importing methods, all of the polygons of the STL file are displayed in *CATIA*, which in turn enables measurements and other functionalities with the STL file.

Initially the intention of the CAD process was precisely this. But with the discovery of this importing alternative, came an outstanding functionality for the manipulation of this STL file, which elevated the preciseness of the final CAD model. This functionality is named as *Activate* and is located within the *Quick Surface Reconstruction* toolbar. This basically enabled the selection of a given part of the STL file, and deleted the rest of the STL model, making it possible to precisely draw the very complex curves that are present in the cross section of the combustor, and represent details like the cooling lips. This step can be visualized in image B.5, presented in App. B.3.

The CAD focused firstly on the design of the combustor walls. All of the details present in the combustor were represented, including the bolts that attach the combustor wall to the dome, and the cooling lips. Next came the representation of the dome section. This was a tricky phase, as the dome has a precise inclination, which in turn affects the inclination of the fuel injector. The degree of inclination could not be figured out through the scans that were obtained from this section, because only a quarter of this section was scanned. However, this inclination was accurately represented in the final CAD model, due to a document that TAP provided which indicated the degree of inclination that the dome had to have, after maintenance. The swirlers

also presented a problem in the beginning, because the airflow that comes from the primary and secondary air swirler to the CC, could not be distinguished from the scans nor from the pictures taken. TAP again provided a document which illustrated the path in which the flow that comes from these swirlers follow, which enabled an approximate[4] CAD representation, as can be seen in figure B.7.

Finally, the CAD phase was a success and the hole combustor was represented (combustor walls, dome, fuel injectors, primary and secondary swirlers). However, only a quarter section of this combustor will be used for simulation purposes in order to decrease the simulation time and effectively represent the four fuel injectors that supply a richer mixture, i.e, there will be one fuel injector within the five fuel injectors, present in each quarter section of the model combustor, that supplies a richer mixture. Also, for simulation purposes only the tip of the fuel injector is represented in the final CAD model (see figure B.4). Figure 4.1 represents this quarter section[5], shading with its base alloy material, Nickel.

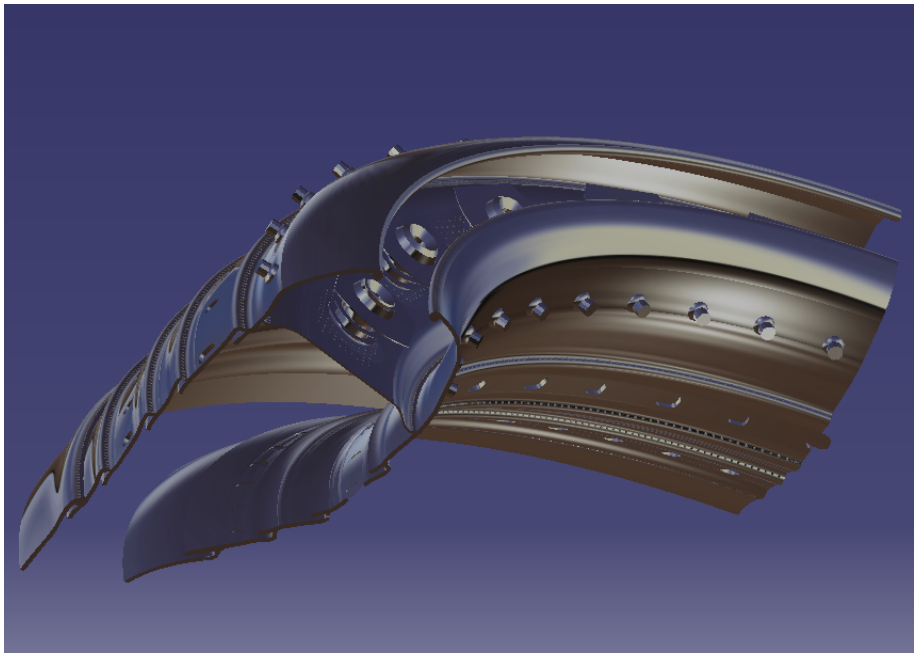

Figure 4.1: Quarter section of the combustor CAD model, shading with a Nickel alloy.

4.2.3 Generation of the Numerical Mesh

The most important aspect in a CFD simulation, is the generation of the model mesh. The aim of this mesh is to provide a distribution of points where the solution will be calculated, and the finer the grid better will be the resolution of all the flow features. However, it is important to note that the finer the grid, or in order words, increasing the number of elements will inevitably lead to an increase in computational cost (CPU) and time, thus it is important to study all of the important aspects of the mesh, such as the grid spacing ratio and the cells aspect ratio, in order to achieve the best comprise between mesh size, computational cost and solution accuracy.

[4]The exact geometry of these swirlers was not achieved because there were certain measures that still lacked from the available documents.

[5]A multi-view of this quarter section is represented in figure B.6.

The mesh generation was performed using *HELYX-OS*, which is based on *SnappyHexMesh*. This selection was based on the work of Carlos [86], which concluded that *HELYX-OS* had many advantages over other mesh generating software's like *ICEM* and *Pointwise*. Advantages include a quicker mesh generation time and a user friendly software which enables the user to better refine any given part of the mesh. *HELYX-OS* is an *OpenFoam* program, and as such is not available for Windows in the free version. Thus, Linux is the operating system in which *HELYX-OS* can be freely handled, and as such another computer, with 8GB of RAM, provided by Dr. Francisco Brójo was used for this phase.

Before setting the parameters for generating the mesh, each of the boundaries/surfaces from the model, has to be converted into the STL format in CATIA V5. This is done by performing a tessellation in each of the surfaces and then extracting them into the STL format. After this step is done, and all of the surfaces are converted into STL, these are still not ready to be imported to *HELYX-OS*, because these STL files were created in Windows, and Linux requires its own STL format. Thus, Blender[6] was used in the Linux system to import the STL files to Windows format, and convert them into a Linux STL format; this step has to be performed separately for each STL file.

After all of the STL files being converted, we now have everything to begin the mesh generation setup. Firstly the base mesh spacing has to be defined, and the smaller this value, better will be the mesh definition [87]. The value of 0.009 was chosen because it was noticed that decreasing this value, no improvements were observed in the mesh. Next the STL files are imported, and the box indicating that the model was created in mm, has to be checked. Within each of these STL's, the refinement level and layer addition has to be defined. The refinement level defines how much refinement is performed with respect to the base mesh, and the higher the refinement level, finer will be the mesh around the selected surface. Here the intent was to refine the areas where the solution is expected to change rapidly, like the fuel injection region. Other regions, like the walls were kept at a relatively low refinement level[7], so that the mesh would not have an excess of cells, without it being necessary. When it comes to layer addition, it is very important to study how and where to introduce layers in order to achieve the desired $y+$ value. *HELYX-OS* offers four parameters regarding layer addiction; Number of layers (n_l), final layer thickness (δ_f), layer minimum thickness and layer stretching (δ_s). As the name suggests, n_l is the number of layers which are intended to add to push away the mesh from the surface, in order to get a better quality mesh in that region. δ_f is the ratio between the last layer thickness[8] and the Surface Cell Size (SCS) of the model surface. The ratio between the minimum layer thickness desired for the model's surface and the SCS was left in blank in order to induce a constant layer growth and avoid a conflict of parameters, which in turn avoids errors within the mesh generation. The last layer parameter is δ_f, and is defined as the expansion rate of the layers starting from the surface.

The last step in the mesh setup is to define a point where a mesh cell will exist. To do so, the material point has to be selected and positioned within the volume of the combustor. This will

[6] Blender is a professional open source software, used to create, among others, animated films and 3D printed models.

[7] The level of refinement at these regions were reduced to a level at which the mesh quality in this region would not be affected.

[8] The last layer thickness is the layer in contact with the surface of the model.

then define a mesh within the closed boundaries of the model combustor. The setup is then concluded, and the mesh generation can now commence. *HELYX-OS* will start iterating, and will only create a mesh when all of its parameters are achieved, and normally no errors within the mesh will arise.

Although *HELYX-OS* is more user friendly then other mesh generating software, a lot of problems and errors were still encountered in the initial phase due to the complexity of the model. Initially, *HELYX-OS* was creating a box that contained the model when generating the mesh. It was only after discovering some holes in the geometry that were not covered, that this problem was resolved. Another error that was occurring was due to layer creation at the walls. Because the walls have some complex curvatures, the software was intersecting the layers at this region, which created errors. It was figured out, after several variations within the layer parameters, that the maximum n_l had to be set to a value of 3, and that δ_f must had a maximum value of 0.08. Other problems did appear, but fortunately these were overcome after exhaustively attempting various setups. The final setup, as well as the mesh characteristics are shown in table 4.1.

Table 4.1: Mesh generation inputs and results using *HELYX-OS*

Boundary type	**Refinement level**	**Layers**			**Base mesh spacing**
		n_l	δ_f	δ_s	
Air mass flow inlets	4	3	0.08	1.25	
Fuel mass flow inlets	7	6	0.04	1.25	0.009
Swirlers	6	6	0.04	1.25	
Walls/pressure outlet	4	3	0.08	1.25	
Number of cells : 2.120.300 | Number of faces: 7.029.105 | Number of points: 2.979.832					
Mesh generation time (s): 3664					

It is also important to mention that after verifying that the upper part of the dome (defined initially as "top"), in which the air first enters the combustor, was not necessary to represent because the mass flow inlets will be defined individually for the swirlers and the holes of the dome. This removal of the upper part didn't have to be performed in CATIA V5, because it was verified in *HELYX-OS*, that by adding a surface at the swirl cone inlet[9], it would lead *HELYX-OS* to ignore the upper part, and only perform the mesh of the inner part of the dome, which is in fact the volume of the combustor. This procedure reduced the size of the mesh in about 300.000 cells, which resulted in a significant reduction in CPU cost. The mesh before and after the upper part of the dome being removed, can be seen in App. C, in image C.1 and image C.2, respectively. Also in the same appendix, we can see a sectioned view of the layers in image C.3, which was obtained using *Paraview*. The final mesh presented in table 4.1 was using almost all of the 8GB RAM, available in the PC; trying to refine even more the mesh, led to the interruption of the program, due to lack of RAM. Aspects regarding the mesh quality in *ANSYS Fluent*, are explained in section 4.3.

[9]This surface is represented by the number 6, in image C.2, App. C.

4.3 Problem Setup

Once the mesh is ready[10], the problem setup can now begin. *ANSYS Fluent* 15.0 is the software used to perform this simulation, due to its proven results discussed in section 1.5.

When initiating *ANSYS Fluent*, a window named Fluent Launcher is displayed. Here it is necessary to ensure that 3D dimension is checked, and it is also necessary to choose whether the calculation will be performed in single or double precision. If double precision is enabled, the solution will be slower but the results will be more accurate. After verifying that the results obtained with double precision did not justify the greater amount of simulation time[11], single precision was the chosen calculation scheme. Still in the same window, it is possible to run the simulation with single or parallel processors, in which the latter reduces significantly the computational time. Thus, parallel was chosen and the number of processes was set to 8, which is the maximum processors available in the computer.

Once *ANSYS Fluent* is launched, the quality of the mesh must be checked as this greatly affects the solution's convergence and results [88]. It is then firstly necessary to check if there is any negative cell values, which was not the case. Following this, reporting the mesh quality will display in the command window some important aspects regarding mesh quality; these are the aspect ratio, orthogonal quality and mesh skewness. Here some issues did appear regarding the last two parameters, but these did not impose a concern as Carlos [86] also stated similar mesh issues in *ANSYS Fluent*, and was able to obtain good results with his work. This said, the maximum values[12] obtained regarding the aspect ratio, orthogonal quality and mesh skewness were 40, 3.22248×10^{-2} and 0.96251, respectively.

4.3.1 Models

ANSYS Fluent is a very versatile code, and as so there are a variety of models that can be chosen, depending on the necessity of the simulation. For this setup, five models are used:

1. Energy model - The energy model must be activated as this regards the energy related to the temperature change within the combustion process or heat transfer.
2. Radiation model - The Discrete Ordinates (DO) radiation model was the chosen one, as it produces a more accurate solution than the P1 radiation model, but its drawback is a higher CPU cost [89].
3. Viscous Model -Through this model, inviscid, laminar and turbulent flows can be studied. As discussed in section 4.1.1, the chosen model was the RSM with all its constants maintained at the default values.
4. Species model - This model allows *ANSYS Fluent* to model the mixing, transport and combustion of chemical species. Due to the importance of this model for this work, the inputs will be explained in detail.

[10] Before trying to import the mesh into *ANSYS Fluent*, it is necessary to transform the mesh format with the code *foamMeshToFluent*, which writes out the *OpenFoam* mesh in *ANSYS Fluent* mesh format.

[11] Running the simulation with double precision, resulted in roughly 4 to 5 times more time then running the simulation in single precision.

[12] Orthogonal Quality ranges from 0 to 1, where values close to 0 correspond to low quality and the mesh skewness ranges from 0 to 1, where values close to 1 correspond to low quality. The values that limit the aspect ratio depend on several factors, and if this value is unacceptable, *ANSYS Fluent* will display a warning [88], which was not the case.

First-off, non-premixed combustion is selected as this describes the combustor system in study. Regarding the PDF table creation, inlet diffusion is selected as this includes the diffusion flux of species at the flow inlet. In the *chemistry tab*, chemical equilibrium is selected and as for the energy treatment, non-adiabatic is enabled.

The operating pressure values vary with the GTE's power setting, and are displayed in table D.3[13]; as for the Fuel Stream Rich Flammability limit (FSRFL), a value larger than 10% of the stoichiometric mixture fraction can be used [89]. The stoichiometric value of Jet-A is relatively simple to calculate (see Eq.2.27), but as the biofuels used in this study are composed by several hydrocarbons/species, it becomes more difficult to calculate the stoichiometric ratio. Thus NASA's Chemical Equilibrium with Application (CEA) was used for this purpose. CEA allows the user to introduce each of the species, as well as their concentration in the fuel, and then calculates several user defined output thermodynamic properties, which include the stoichiometric ratio[14]. The stoichiometric ratios obtained with CEA, are presented in App. D, table D.1. The last thing to check in the *chemistry tab*, is to ensure that the *thermo.db* file, in which the thermodynamic properties of the fuel species will be introduced, is correctly chosen.

The specification of the fuel species name and concentration is done in the *boundary tab*. It is important to check if the species that are intended to introduce are presented by their thermodynamic properties, in the *thermo.db* file[15]. For the present study, besides Jet-A, all of the species which compose the biofuels had to be introduced. This was done by accessing Burcat's [90] thermodynamic data base, which presents a great range of the species thermodynamic properties, in the 7 term polynomial form, initially published by NASA [91]. It is important to note that the introduction of this thermodynamic data in the *thermo.db* file, has to agree with CHEMKIN format [92], otherwise *ANSYS Fluent* will not add the new specie to the fuel. Each of the species added, as well as their concentration in the biofuels are presented in App. D, table D.2.

Still in the *boundary tab*, the oxidizer species and concentration, as well as the temperatures of the oxidizer and the fuel have to be introduced. The oxidizer (air), was considered composed only by nitrogen and oxygen with concentrations of 0.78992 and 0.21008, respectively. As for the fuel temperature, this gives respect to the flash point of each fuel, which is presented in table D.1. The oxidizer temperature varies through the GTE's power setting, and its values are explained in section 4.3.2.2, and presented in table D.3.

After the previous steps being performed, the last step in the species model is the calculation of the PDF table in the *table tab*. Here all of the table default parameters were maintained, and the *Automatic Grid Refinement* was enabled. Finally the PDF table can be calculated, and as a result the quantity of species created can be checked in *Materials*.

5. NO_x prediction - The final model to setup is the NO_x model. This has to be enabled, oth-

[13] These values are explained in section 4.3.2.2, and presented in table D.3.

[14] The data obtained from CEA was validated by comparing the stoichiometric ratio of Jet-A in CEA by the value obtained in Eq.2.27. The result was the same stoichiometric value.

[15] This can be done by checking directly in the *thermo.db* file or by clicking *List Available Species*, which will display the species that are present in the command window.

erwise *ANSYS Fluent* will not display any information regarding NO_x formation when the solution is calculated. Here, as described in section 2.5.2, Thermal and Prompt NO_x has to be selected, and the species that are present in the fuel must also be chosen. *Partial-equilibrium* must be chosen in the *Thermal tab* as this predicts the *O* radical concentration required for thermal NO_x prediction [89]. The fuel carbon number (table D.2) as well as its equivalence ratio must be introduced, and *temperature* is important to be selected in the PDF mode as this will enable the turbulence-chemistry interaction[16] [89].

4.3.2 Boundary Conditions

Probably the most important phase of this entire work is the calculation and set-up of the boundary conditions, as this greatly affects convergence and results. To have an idea on how important the correct input values must be calculated, it was verified in the simulations that by deceasing in 30% the total air cooling mass flow, an increase in 300 K at the combustor's exit was achieved. Thus, all of the input values for the boundary conditions are explained in this section.

As explained in section 4.2, manufacturers maintain most of their GTE's technical information confidential. It was extremely difficult just to achieve the total $\dot{m}_a$ that is ducted through the fan stage, and practically no information is provided regarding this aspect. Thus, initially this value was estimated through Bernardo's work [93], in which the flow around a fan blade of the CFM56-3, was analysed. From this value (8.36 kg/s), we could then multiply by the number of fan blades (38), and then obtain a total $\dot{m}_a$ of 317.68 kg/s. As it is known that the bypass ratio of the CFM56-3 is 5:1, it is possible to conclude that the air that reaches the combustor is about 52.95 kg/s. Although this value is a good estimative, it does not account for the bleed air[17] that is extracted from the primary flow, nor for the air that is extracted for HPT cooling, which does not enter the combustor. Consequently a solution to these problems had to be investigated, and were indeed encountered in Pedro's work [94].

Pedro investigated the thermodynamic model of the CFM56-3, using *GasTurb*[18]. It was obtained through this work important aspects regarding each stage of the GTE, namely the $\dot{m}_a$, temperature and pressure, at full power. The relevant information for the present study is presented in table D.4, App. D. From Pedro's work, the $\dot{m}_a$ that is present at the fan stage was initially compared with Bernardo's work, in order to verify if there was a big discrepancy, which was not the case as Pedro reported a value of 314.82 kg/s (0.9% difference). The $\dot{m}_a$ present in the primary flow estimated from Bernardo's work was also very similar, as Pedro reported a value of 51.52 kg/s at the HPC exit (2.7% difference).

The most important information obtained from the work of Pedro, is the $\dot{m}_a$ that effectively reaches the combustor which will prove to be the foundation for the present study. Here a value of 41.51 kg/s was reported, and comparing to the $\dot{m}_a$ that exits the HPC it can be concluded that $\approx$ 20% of the primary air flow is extracted for bleed air and turbine cooling. From this value, the input values for the boundary conditions can now be calculated.

[16] If the turbulence interaction is not enabled, NO_x formation will be computed while neglecting the important influence of turbulent fluctuation on the time-averaged reaction rates.

[17] Bleed air refers to the compressed air that is extracted from the compressor stage of a GTE, used for (among others) starting the remaining engines, cabin pressurization and wing anti-icing.

[18] *GasTurb* is a powerful cycle program used for simulating the most common types of GTE's.

4.3.2.1 Determination of the boundary conditions input values

The boundary conditions where determined by dividing by four[19], the total $\dot{m}_a$ and $\dot{m}_f$, and from the overall AFR. The typical values for GTE's operating AFR are stated by Bryn Jones [49], and are between 33-40 at 100% power, and $\approx$ 100 at 7% power. At full power the overall AFR calculated in this work was 43.6, which represents a difference of 7% from the upper limit stated by Bryn. In order to achieve an AFR between the stated values, the total $\dot{m}_a$ would have to be reduced; thus it was opted to use the calculated AFR as this used all of the air obtained from Pedro's work (10.36 kg/s).

The first step was then to ensure that at the PZ, the AFR was at stoichiometric conditions. The $\dot{m}_a$ that enters the PZ is done through the primary and secondary swirlers[20], and as so its $\dot{m}_a$ can then be determined. Knowing the overall AFR and fuel flow, it is possible to determine the total $\dot{m}_a$, and then calculate the total cooling $\dot{m}_a$, by subtracting the PZ $\dot{m}_a$ from the total $\dot{m}_a$. It was then necessary to distribute this cooling $\dot{m}_a$, through the boundary conditions. The determination of which percentage to apply in each boundary was only possible through an extensive trial and error approach through the simulations, in which the aim was to achieve the exit temperature reported by Pedro. Once this exit temperature was achieved, the percentage of cooling air that is applied to each boundary was then known. It is important to note that this trial and error approach was performed burning Jet-A as fuel, at full power. The boundary conditions for the remaining power settings were then similarly determined from this reference. All of the relevant data for the boundary condition while burning Jet-A are presented in table 4.2, and in turn, table D.6 presents these values when burning the biofuels. In these tables, the total $\dot{m}_f$ is divided with the 5 fuels injectors, and 10% more fuel was considered in the richer fuel injector than the remaining four [49]; the biofuel $\dot{m}_f$ was determined with Eq. 2.55.

4.3.2.2 Determination of the operating pressure and oxidizer temperature

The determination of the operating pressure and oxidizer temperature was calculated by a linear regression. Regarding the operating pressure it is known through Pedro's work [94] that the compressor delivers a pressure of 2343.346 kPa at full power, and at 7% power the pressure at the HPC exit can be considered atmospheric (101.325 kPa) as the power is very low. With these values the operating pressure can then be calculated at the intermediate power settings, through linear regression. The oxidizer's temperature was similarly calculated, in which the temperature corresponding to full power was also obtained from Pedro's work and the temperature produced at a 7% power setting was considered to be the fuels flash point. These values are presented in table D.3, App. D.

Three types of boundary conditions were applied; *mass flow inlet's*, *pressure-outlet*, *symmetry* and *walls*; these boundaries are distinguished in table C.1. The previous data, as well as the data presented in tables 4.2 and D.6, are intended to be introduced in the *mass flow inlet's*. Here there are still some parameters that have to be set-up; the direction of the flow is set to *normal to boundary* for all of the boundaries, except the swirlers, in which $\sin(60^o)$ and $\cos(60^o)$ was introduced in the "z" and "y" direction, respectively; this then simulates the entry of the air through the swirlers, with a 60º angle. The turbulent intensity and turbulent viscosity ratio can

[19] As only $1/4$ of the combustor is studied, the total $\dot{m}$ values have to be divided by four.

[20] Air also enters into the PZ through *Dome holes 1*, however it does not enter stoichiometric calculation as it is for wall cooling purposes.

Table 4.2: Air mass flow (kg/s) inputs for each boundary, at its respective power setting, while burning Jet-A

Fuel	**Jet-A**				**Cooling air flow**
Power (%)	100	85	30	7	%
Dome holes 1	0.0127	0.0129	0.0094	0.0045	0.1851
Dil 1.1	1.5000	1.5344	1.1189	0.5337	21,9534
Dil 2	3.0000	3.0688	2.2378	1.0674	43,9068
Dil 2.1	1.7000	1.7390	1.2681	0.6046	24,8805
Mix	0.3000	0.3069	0.2238	0.1067	4.3907
Mix 2	0.3000	0.3069	0.2238	0.1067	4.3907
Mix 3.1	0.0050	0.0051	0.0037	0.0018	0.0732
Mix 3.2	0.0050	0.0051	0.0037	0.0018	0.0732
Mix 4	0.0100	0.0102	0.0075	0.0036	0.1464
Swirler 1	1.7383	1.4553	0.5329	0.2095	- - -
Swirler 2	1.7383	1.4553	0.5329	0.2095	- - -
Total cooling $\dot{m}_a$	6.8327	6.9894	5.0968	2.4311	$\approx$ 100
Total $\dot{m}_a$	10.3092	9.9000	6.1625	2.8500	
Fuel flow $(\dot{m}_f)$	0.2365	0.1980	0.0725	0.0285	
Overall AFR	43.6	50	85	100	
PZ AFR	14.7				

be introduced, however it was opted to leave these parameters at their default values (5 and 10% respectively), as increasing these did not result in any improvement within the solution. In the *thermal tab*, the stream temperature[21] has to be introduced and in the *species tab*, the *Mean Mixture Fraction* has to be set to unity, when injecting fuel (fuel injectors). The *wall* boundaries were remained at default settings and the *exit gauge pressure*, regarding the *pressure-outlet*, was set to zero as this considers the system pressure at the exit to be the operating pressure[22].

4.3.3 Solution Methods, Solution Controls and Monitors

It is within this and the following section, that the main tasks which are involved in any CFD simulation have to be specified. These tasks include among others, spatial discretization schemes, solution controls, solution initialization, monitors and starting the simulation.

4.3.3.1 Solution methods

For this work, two approaches were opted regarding the solution methods; firstly the simulation ran on the default solution schemes until becoming stable, afterwords the schemes were changed to *Second Order Upwind*. This was done due to the fact that when running firstly the simulation with the default settings, the solution converges more smoothly; however, the results normally are not the best, and thus the scheme has to be changed to a higher order, in

[21] These temperatures have to be introduced accordingly these being air inlets (table D.3) or fuel inlets (flash point presented in table D.1).

[22] This means that there is no pressure loss within the combustor, which is what engineers aim for.

which this case *Second Order Upwind* was opted. This procedure will then lead to a converged solution, with more accurate results [95].

The original setting was then *SIMPLE* for the Pressure-Velocity Coupling scheme; Green-Gauss Cell Based for the Gradient spatial discretization; *Standard* for Pressure and *First Order Upwind* for the rest of the parameters. Regarding the modified settings, *Coupled* was chosen for the Pressure-Velocity Coupling; *Least Squares Cell Based* for gradient spatial discretization; *PRESTO!* for Pressure and *Second Order Upwind* for the rest of the parameters.

4.3.3.2 Solution controls

The default values for the solution controls are considered too aggressive for the type of combustion system in study [89], and as so, most of these values had to be reduced. Initially a lot of errors and divergence problems were appearing during the simulations. An example of a divergence problem that was appearing and what was done to solve it, is the following; *divergence detected in AMG solver: enthalpy*, was one of the most persisting errors, which was occurring before 50 iterations. It was only after decreasing the URF *density* to a very low number (0.3) that this particular error was solved. As said a large amount of errors appeared, and it was only by exhaustively trying various settings for the solution controls, that these were overcome.

The URF also proved very important when trying to reach convergence criteria, and again a lot of effort was held in order to achieve appropriate values for these factors. Table D.5, presented in App. D, shows the original settings against the new settings adopted for the solution controls.

4.3.3.3 Monitors

The purpose of the *monitors* is to set a value for a certain parameter and then check if each equation is converging to the defined value. The *monitors* by their-self should not be regarded as the unique factor to obtain good results, however it is important that these user defined values are achieved. The default values[23] were all changed to a convergence criteria of E^{-6}, to ensure that the convergence process is smooth. The *absolute convergence criterion* was applied, to ensure that at that point, the equation is converged [89].

4.3.4 Solution initialization and Calculation set-up

Good and appropriate initial values are necessary to be given in order to ensure that the solution converges as quickly as possible. In most of the cases, the option *hybrid initialization* provided by *ANSYS Fluent* generally is more than enough, however for the present case it was proved that these initial values were not adequate as the solution was not converging. Thus, *standard initialization* was used from *swirler 1*, and proved to be a good choice as the solution was converging smoothly and relatively quickly.

Regarding the calculation set-up, it is of good practice to first *check case*[24] before the calculation process starts, as this ensures that there are no errors within the case, and the model is ready to be simulated [95]. Next, the solution can then be commenced, and for this study the calculation was setup to 2000 iterations.

[23] With the exception of pollutant NO_x, energy and DO intensity in which E^{-6} is the converging limit.
[24] When a *check case* is held, the mesh, models, boundaries, materials and solver are being checked.

Chapter 5

Results

Over nearly a year in the development of this work, countless simulations were performed, in which the majority were held just to achieve the reference values provided by ICAO, while burning Jet-A. Most of these were not successful, as trying to achieve one reference value, resulted in a increase/decrease of other parameters, intended to be reported. Thus a trial and error approach was held, which proved the only way in trying to achieve good results for this study. Nevertheless, the results still present a margin of error, when compared to the reference values; however, taking into account the many variables present in this study, that may influence the final results, the results presented in the present chapter can be considered acceptable, and by comparison good conclusions can be made.

The results presented are the consequence of a mesh-independent solution. A mesh independent solution is considered achieved when the solution does not change when the mesh is refined. In this case, the mesh was refined by increasing the refinement level in *HELYX-OS*, and the solution was considered mesh-independent when the final results did not vary at all. The parameters which compose the final independent mesh, are presented in section 4.2.3.

The present chapter presents the results for the parameters that were intended to simulate, for the combustion of biofuels in the CFM56-3 combustor, throughout ICAO's LTO cycle. A total of 16 simulations[1] compose the final results, and are presented in a way to understand the relationship between the fuels, at different power settings. Initially, only the emissions and the energy extracted from the biofuels, were intended to be reported and discussed, however after verifying the importance of other parameters, these were also introduced in this chapter.

Thus, this chapter will start with an evaluation of convergence, regarding the quality of the numerical solution; an evaluation of the y^+ to make sure that this parameter is between the recommended range; a comparison of the energy extracted while burning biofuels and Jet-A, at full power; a validation of the numerical results by comparing the results obtained with Jet-A with those provided by ICAO; a evaluation of the combustor's exit temperature, and the influence of cooling air. The emissions, which are the primary goals for this study, are finally presented separately for each fuel, throughout the mentioned power cycle. To conclude this chapter, the conclusions obtained from the results are discussed, and future studies are proposed.

Two machines were used to calculate the results presented in this chapter: the first is an eight core processor with 28 GB of RAM, and the second, a quad core with 8 GB of RAM. Each solution took an average time of 20 hours for the first and almost 3 days for the second machine. All of the results and contours displayed in this chapter are done so through *Tecplot 360*, as *ANSYS Fluent* was having a problem when attempting to display the contours. This was maybe due to the fact that the mesh was too refined for the problem setting, and *ANSYS Fluent* was not

[1] As four fuels are being simulated, at four power settings (ICAO's LTO cycle), a total of 16 simulations are necessary.

being able to handle the huge amount of data. On the other hand, *Tecplot* proved to be a very powerful post-processing software, which took the graphs and contours presented in this chapter, to another level.

5.1 Convergence

The importance of convergence shall not be underestimated, as a converged solution might not mean a correct/accurate one, but does mean that the results agree with all of the parameters assigned in the problem setup. A solution can be considered converged when the monitors that were defined in section 4.3.3.3 are achieved, when the mass imbalances through the system is very small or when the maximum number of iterations is reached.

5.1.1 First order vs Second order method

For the present study, convergence criteria was set for a decrease in residuals to E^{-6}. For the *First order upwind* scheme, these residual values were in fact achieved, and convergence proved to be strong and smooth, as can be seen in figure 5.1. As discussed in section 4.3.3.1, the *second order upwind* scheme provided more accurate results than the first scheme, and as so it was the solution scheme opted for the final results. This scheme was not able to achieve the defined convergence criteria, but became stable at just 600 iterations (after the *First order upwind* scheme) and converged at 2250 iterations, as can be seen in figure D.1, presented in App. D. It is important to note that these 600 iterations were only achieved by an extensive trial and error approach, as initially the solution was highly unstable.

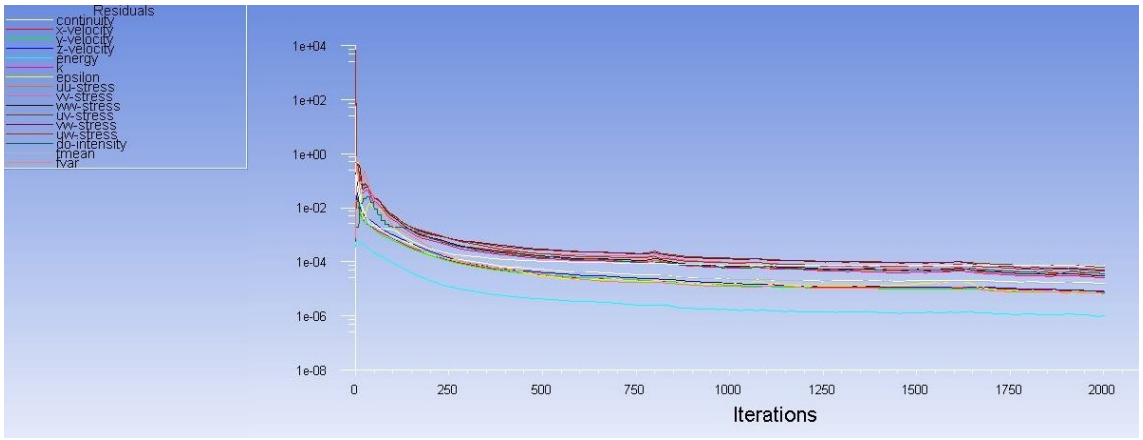

Figure 5.1: Converged solution.

A solution can be converged but still be wrong, if e.g. the residual tolerance are set to a high value. A way of checking if the residuals tolerance defined are correct, and the solution is completely converged, is through the mass imbalance. ANSYS [89] states that the net mass imbalance should be less than 0.5% of the total flux through the system, i.e. in a converged solution, the flow that enters the system should be equal to that going out. If a significant mass imbalance should be verified, the residuals should be reduced to at least an order of magnitude. For the present study, the mass imbalance was in the order of $E^{-5}\%$ (≈ 0), which is a strong proof that the solution is completely converged and therefore correct, for the problem setup.

5.1.2 y^+ analyses

The analyses of y^+ is not relevant for this study, as the heat transfer through the walls is not being considered. Yet, it is recommended that the values of y^+ shall be between 30 and 300 [81]. As can be seen in figure 5.2, most of the zones of the combustor are within this range. There are however some zones, like the cooling air lips, that acquire a high y^+ value. This means that the mesh in this zone has to be better refined, but again, this will lead to a heavier mesh and thus a higher CPU cost, without need as mesh-independence has already been achieved for the desired results[2].

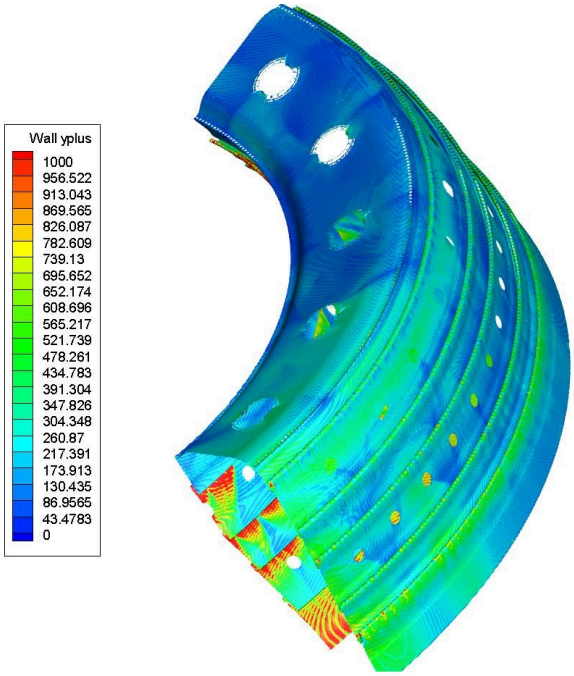

Figure 5.2: y^+ regarding the walls of the combustor.

5.2 Energy extracted

The energy extracted from the biofuels was calculated using Eq. 2.55, and the LHV of the biofuels, presented in table D.1. The energy extracted comes in the form of power output [kW], while burning a constant $\dot{m}_f$, which corresponds to the $\dot{m}_f$ of Jet-A, at full power. The results are presented in figure 5.3, and it can be instantly noticed that all of the biofuel have a lower power output, when compared to Jet-A. This is expected as biofuels have a lower combustion enthalpy, which means that more biofuel is needed to produce the same amount of energy, from that obtained from kerosene. Further analyses of the combustion chemistry of biofuels, has been discussed in several literatures [70][79].

Nevertheless, only a slight decrease is verified with *jatropha* and *Sunflower* biofuel ($\approx$ 7.5%), however a very significant power output decrease can be noticed with *algae* biofuel ($\approx$ 30.4%). This fact drifts of course by the quality of the fuel, which as explained in section 3.2, hugely depends on the production conditions of the biofuel. Every time a new study is made to improve

[2]Even if it was decided to refine these zones, section 4.2.3 already explains that this is not possible, due to the complexity of the model and due to the lack of RAM, available in the Linux PC.

a given biofuel, this goal is generally achieved, and in fact, regarding *jatropha* biofuel there are several older studies which report a LHV in the order of 34.4 MJ/kg, and for this study, the LHV of *jatropha* biofuel was 39.5 MJ/kg, and was obtained from the work of Goyal et al. [77].

The conclusion that can be then made from an energy point of view, is that *jatropha* and *sunflower* biofuel are viable, as the first only presents a 6,5% higher fuel consumption. In the other hand, *algae* is not viable at the moment, however as explained in section 3.2.3, it has a huge potential but until further improvement studies, it can not be considered as a replacement candidate for Jet-A.

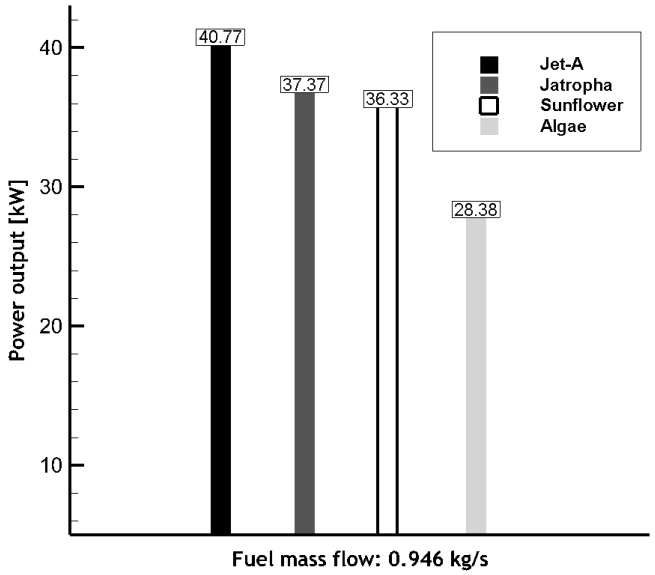

Figure 5.3: Energy extracted from the combustion of Jet-A vs the biofuels, at a constant $\dot{m}_f$.

5.3 Results validation

All of the results presented in this chapter where validated by firstly comparing the emissions calculated with the simulations while burning Jet-A, at full power, with ICAO's emissions measurements, presented in table 2.2. Only after obtaining reasonable results, could the other simulations take place, and therefore be considered acceptable.

The results of this comparison can be seen in figure 5.4. The main issue intended to analyse in this work, is the study of NO_x emissions, and as can be seen in figure 5.4, it was the emission that presented the smallest error, which is in average 16%. It is interesting to note that at 85% power, the error was at its lowest values, accounting to only 5%. On the other hand, CO and UHC emissions presented bigger differences from ICAO's values, especially at low power settings. This was expected as high values of CO and UHC result from combustion inefficiency at low power, due to the lack of high temperature to promote complete combustion[3]. The bigger difference however, from ICAO's values, was due to the fact that in this study, the fuel atomization was not considered, and so the mixing that promotes enhancements in combustion efficiency is not taking place, and so these differences within CO and UHC were expected.

[3]This fact is better explained in section 2.5.1.

The behaviour regarding the amount of NO_x emissions produced throughout ICAO's LTO cycle, was also the expected, as decreasing the power proved to produce lower emissions. Regarding UHC values, the expected behaviour of emissions reduction with the power increase, was also verified and at high power settings, the values obtained were very close to the reference values; however CO emissions resulted in an erratic behaviour, as increasing the power should not lead to an increase in emissions. This behaviour disagreement is explained in section 5.5.2. In sum good agreements were obtained with these comparison results, when it is taken into account that there are many variables present in this study, which can influence the final results.

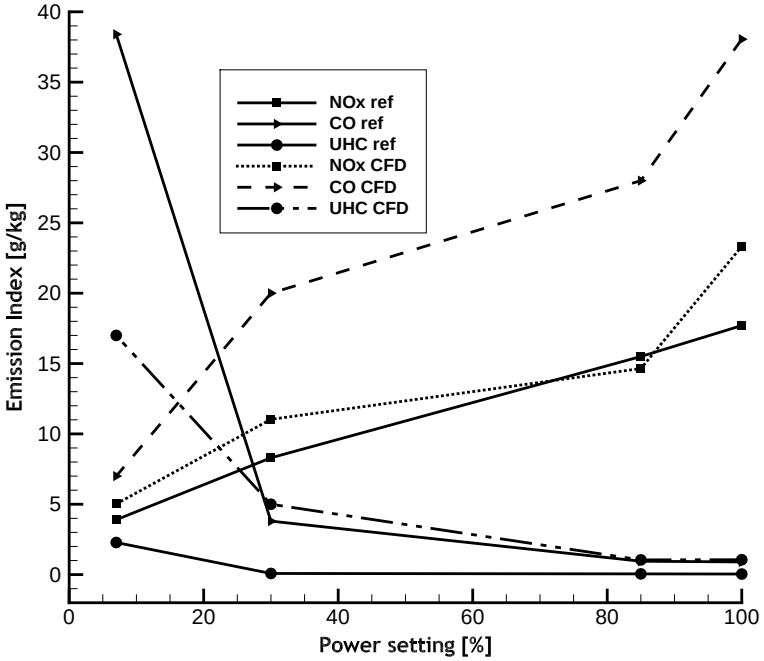

Figure 5.4: Results validation: ICAO's measures vs CFD calculations while burning Jet-A.

5.4 Combustor exit temperature

The combustor's exit temperature is another factor with which the results could be compared and validated. As explained in section 4.3.2.1, good reference values was obtained from Pedro's work [94], in which the relevant are presented in table D.4. For this section, the relevant data gives respect to the exit temperature of the combustor, and here Pedro reported a value of $\approx$ 1650 K, at full power. For the present study, the achievement of the exit temperature was of great importance, because the boundary conditions regarding cooling air, could be determined, from a trial and error approach. The final results were very good, as it was reported, through the simulations, a value of 1582 K, which represents an error of only 4.2% from the value reported by Pedro.

However, the exact value of 1650 K could be achieved if desired, by reducing the overall AFR. Nevertheless, it was opted to stick with the boundary conditions determined in section 4.3.2.1, as these were considering the total $\dot{m}_a$ of the CFM56-3 combustor, at full power. This said, figure 5.5 represents the combustor's exit temperature throughout ICAO's LTO cycle, while burning Jet-A and the biofuels. As can be seen, all of the biofuels simulated present a lower combustor exit

temperature when compared to Jet-A at the same conditions. This is a very good indication that biofuels can produce the same amount of energy as Jet-A, despite consuming more fuel, while at the same time being less aggressive to the combustor, i.e., the combustor and the HPT blades can take advantage of these lower temperatures, as with a decrease of temperature, comes a significant increase in their lifetime, due to the fact that they are subjected to lower thermal stress[4]. It can also be concluded that the three biofuels present identical exit temperatures throughout ICAO's LTO cycle, and that only *algae* biofuel presents a higher temperature at 100% power (1516 K).

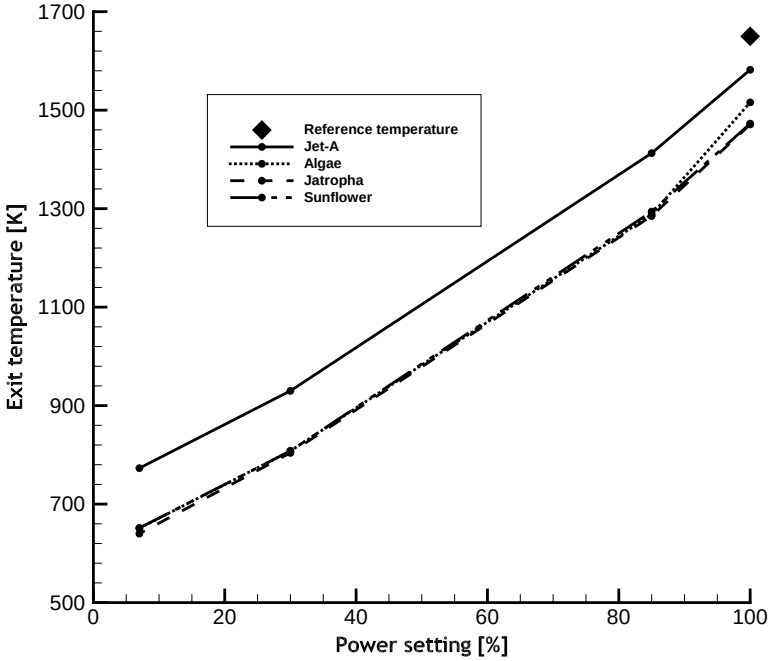

Figure 5.5: Combustor exit temperature throughout ICAO's LTO cycle, while burning Jet-A and the biofuels.

The contours of the combustor exit temperature, while burning *jatropha* biofuel are shown in figure 5.6. It can be noticed that the combustor exit temperature does not present a uniform temperature profile pattern[5], and instead hot spots are shown. These are extremely undesired in GTC's, as hot spots can, and will lead to a higher degradation of the turbine nozzle guide vanes, as well as the turbine blades (see section 2.2.4.3). These hot spots appearance can be explained by the absence of a cone angle, within the injection of the fuel. Initially, the cone angle was intended to be introduced, however it was verified that this cone angle has to be introduced within the atomization model, which was not considered for this study. The cone angle absence can also be noticed in the middle slice (figure 5.6), which represents the temperature resultant from the fuel/air combustion. Here the combustion of the mixture produces a quite narrow profile, in which the distance from the outer wall is significant, which means that not all of the area intended for combustion, is being used. The profile should be more concentrated in the

[4]However as the turbine blades are designed to operate with specific profile temperatures, at a given power setting, the effect of these lower exit temperatures verified with the combustion of biofuels, on the turbine blades performance, have to be better investigated.

[5]The results presented in figure 5.5, are the result of a mass-weighted average performed in *ANSYS Fluent*.

PZ, occupying a larger area in that zone, and should not extend as it does, to the combustor exit. However, this behaviour was observed only at full power, as at lower power settings, no hot spots were presented, meaning that higher quantities of cooling air are required for a cone angle absence.

These problems can then be solved by introducing a cone angle, to which in fact a working example has been performed to prove these statements. The result of this working example is presented in figure D.2, App. D, and it can be clearly noticed that with the introduction of a cone angle of 60^o, the flame front did concentrate within the PZ, occupying all of the cross area of the combustor, and that only the hot gases remained within the dilution zone.

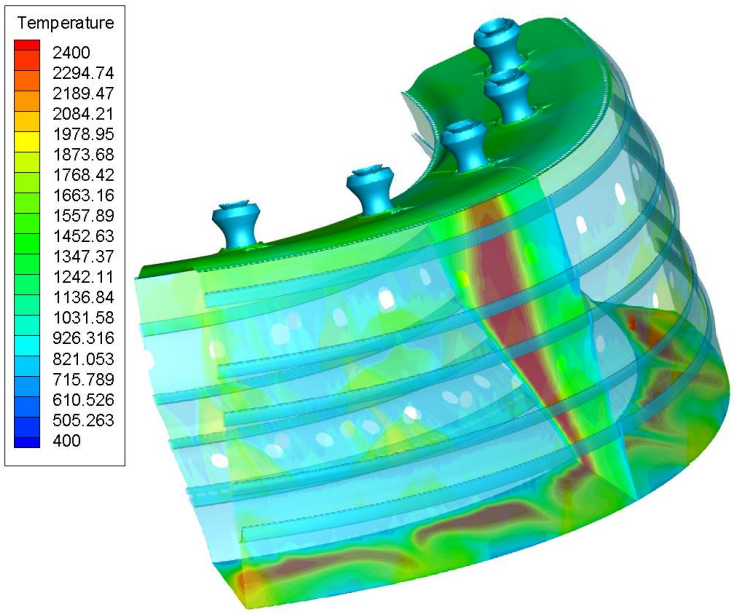

Figure 5.6: Contours of the combustor exit temperature (K), while burning *jatropha* biofuel, at full power.

5.4.1 Air flow distribution

The air flow distribution is a basic problem in combustor design and development, and while performing the trial and error approach, it was noticed that little fluctuations of the amount of cooling air employed, resulted in great variations regarding the combustor exit temperature, wall temperature and emissions. This last proved to be of great importance, as a reduction of cooling air resulted in a significant increase of NO_x emissions, due to the fact that there is less air available for cooling, which inevitability results in a increase of temperature, which in turn promotes NO_x formation.

The biggest effect that comes with the reduction of cooling air verified, was the combustor exit temperature. This proved to be the most dependent of the amount of cooling air employed, as it was verified through the simulations, that by decreasing in 30% the amount of cooling air, resulted in a increase of over 300 K of the hot gases present at the combustor exit. The wall temperature did not suffer this much with this reduction of cooling air, as the maximum temperature increase reported within the walls, was in the order of 100 to 150 K.

To conclude this section, figures 5.7(a), 5.7(b), 5.8(a), and 5.8(b), represent the contours of

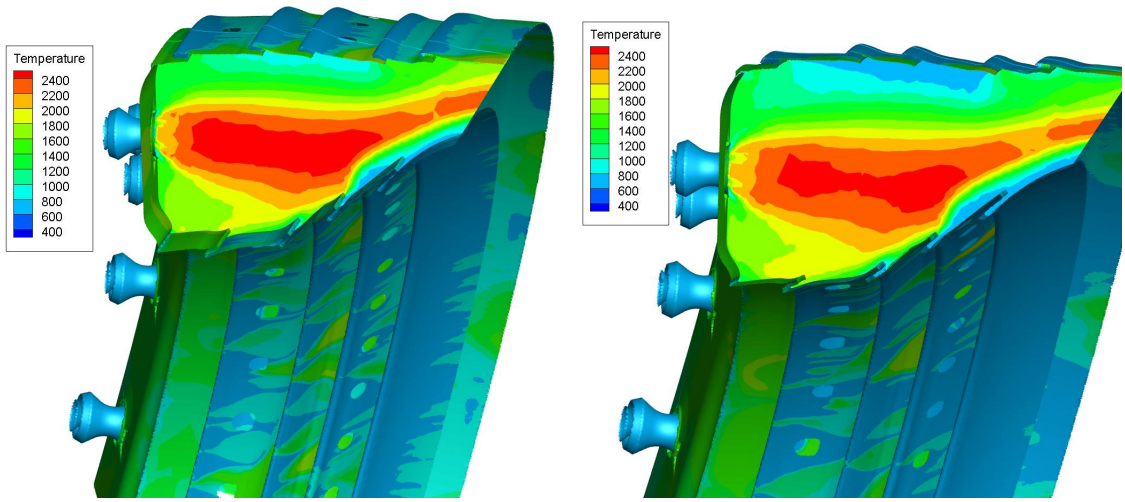

(a) (b)

Figure 5.7: Contours of the cross section temperature (K), while burning: (a) *jatropha* biofuel, at a 100% power setting and (b) *algae* biofuel, at a 85% power setting.

the combustion of the biofuels, throughout ICAO's LTO cycle. At a 100 and 85% power setting, there are two different goals; the first is the maximum energy output, as this gives respect to take-off conditions, and the second gives respect to a high energy extraction while having to increase the cooling airflow, as the engine spends three times more time in this power setting, when compared to a 100% power setting. Figures 5.7(a) and 5.7(b), shows the contours of these statements, while burning *jatropha* and *algae*, respectively. By analysing carefully these figures, it can be noticed that the maximum temperature is visualized in figure 5.7(a), in which the peak temperature value is 2400 K, while a larger amount of cooling air is presented in figure 5.7(b). It is curious to mention, that the boundary conditions calculated in section 4.3.2.1, were without knowing, according to this statement, which proves that the $\dot{m}_f$ at a 85% power setting, was determined by the manufacturer in such a way that larger quantities of cooling air are employed in this power setting, when compared to take-off conditions[6].

Regarding the lower power settings, 30 and 7%, shown in figures 5.8(a) and 5.8(b) respectively, it can be seen that the flame front is located almost in its entire, within the PZ, fact that mitigates the hotspots mentioned previously, which means that the hot gases are effectively being cooled, resulting in a uniform exit profile temperature. When it comes to the combustion of the biofuels, no major differences were noticed in the contours, when comparing to the contours of Jet-A.

In general the peak gas temperature is located in the PZ, and due to the dilution of the combustion products, the temperature is lower in the dilution zone and exit of the combustor. It can also be seen from figures 5.7(a), 5.7(b), 5.8(a), and 5.8(b), that as the power setting increases, so does the high temperature zone, due to the fact that more fuel is being burned (lower AFR).

[6]See table 4.2, for a clearer insight of these statements.

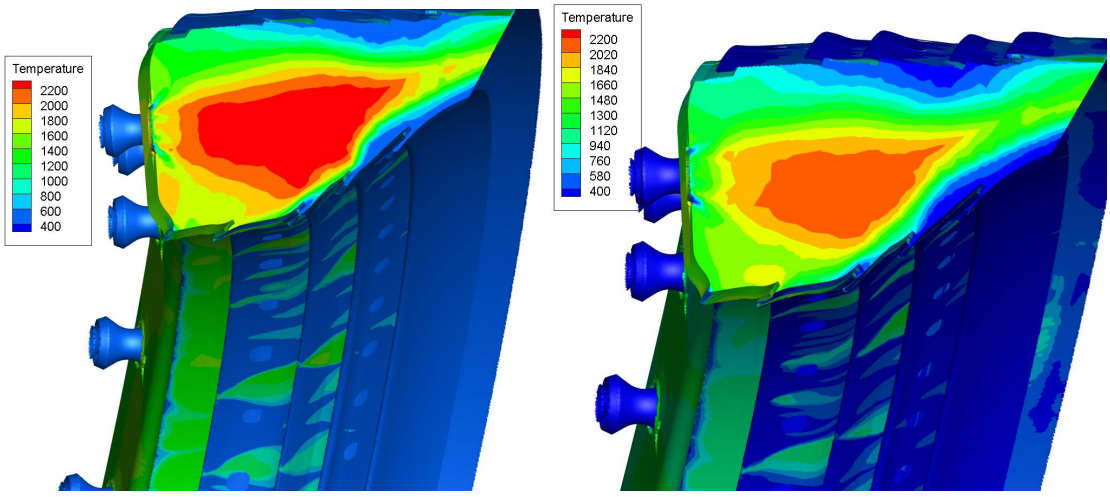

(a) (b)

Figure 5.8: Contours of the cross section temperature (K), while burning: (a) *sunflower* biofuel, at a 30% power setting and (b) *jatropha* biofuel, at a 7% power setting.

5.5 Emissions analyses

All of the results presented in this section, were obtained by reporting the emission *Flow rate* in *ANSYS Fluent*, then multiplying by 1000 and dividing by the total $\dot{m}_f$ at the inlet. The results are presented in the form $g\ [Emissions]/kg\ [fuel]$, which makes it possible to compare with ICAO's reference data. This procedure is represented by Eq. 5.1:

$$\frac{Emission\ flow\ rate\ [kg/s]\ \times 1000}{Inlet\ \dot{m}_f\ [kg/s]} = \frac{g}{kg_{fuel}} \tag{5.1}$$

5.5.1 Oxides of nitrogen

The investigation of the impact on NO_x emissions and formation while burning biofuels, was of prime importance for this study. Fortunately these were the results that presented the best agreement with ICAO's reference data, and as such the NO_x EI obtained from the combustion of biofuels, can be considered correct. Moreover, the expected behaviour of NO_x emissions decrease, with the decrease of power setting, was also achieved for all of the fuels, as can be seen in figure 5.9(b). As explained in section 2.5.2, the thermal NO_x formation is governed by the Zeldovich mechanism, and according to this theory NO_x is formed from atmospheric nitrogen at sufficiently high temperatures. These high peak temperatures are located within the PZ, but the oxidation occurs mainly in the post flame zone area, in which the concentration of the radicals O and OH are sufficient for the process to occur. This statement can be proved by analysing figure 5.9(a) and 5.10; here it can be seen that the major concentrations of NO_x are located after the flame front, and near the combustor's exit.

In section 2.5.2 it was also stated that thermal NO_x is the leading mechanism for NO_X formation at the high temperatures of the PZ, and that prompt NO_x is only formed in fuel rich regions. In this study it was verified that the concentration of prompt NO_x was higher in the region of the richer fuel injector, and only accounted for $\approx$ 7% of the total NO_x formed in the combustor; it also did not vary that much with the type of fuel. Thus, the EI NO_x results presented in figure

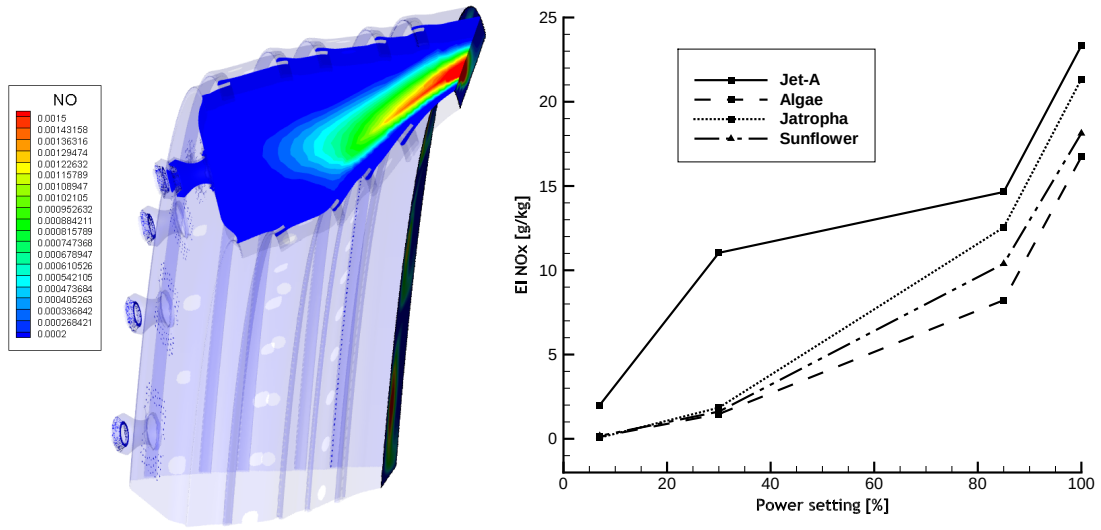

(a) (b)

Figure 5.9: (a) Cross section contours of NO_x concentration [kg/kg], while burning *algae* biofuel at 85% power, and (b) EI results of NO_x, resultant from the combustion of Jet-A and the biofuels, throughout ICAO's LTO cycle.

5.9(b) account for the total NO_x (thermal + prompt NO_x) that reached the combustor's exit.

The EI NO_x results from the combustion of the fuels throughout ICAO's LTO cycle, are presented in figure 5.9(b), and for all the biofuels, the predicted values show the correct trend of NO_x concentration increase, towards the combustor's exit (as can be seen in figure 5.10). Thus, by analysing figure 5.9(b) it can be noticed that all of the biofuels presented a lower EI of NO_x when compared to Jet-A. The biofuel that presented the smaller NO_x EI throughout the entire ICAO LTO cycle, was *algae* biofuel, and in which the biggest difference was verified at 30% power, where *algae* NO_x emissions were 87% smaller than those of Jet-A at the same power setting. In the other hand *jatropha* biofuel performed the worst among the biofuels, which at the power settings 100 and 85%, the values were very close to those of Jet-A.

It can be then concluded from the NO_x emissions analyses, that biofuels have the potential to dramatically decrease these emissions throughout all of the power settings. It is however interesting to note that as NO_x formation is strongly temperature dependent, the lower level of NO_x values may be primarily due to the lower temperature which take place on the combustor's exit, when biofuels are burned (as reported in section 5.4).

5.5.2 Carbon monoxide and unburned hydrocarbons

UHC and CO emissions are associated to combustion inefficiency (or incomplete combustion from the fuel), and this last is greatly related to fuel atomization, as the small fuel particles can be more easily mixed with the air, which in turn enhances combustion efficiency. CO are generally formed due to the lack of oxygen to complete the reaction to CO_2, and from the dissociation of this last if the mixture present in the combustion zone is stoichiometric, such as the conditions presented in the PZ (figure 5.11) [14]. UHC means that a waste of fuel is taking place as not all of the fuel that is injected is being burned, reaching the combustor exit in the form of drops or vapor, and as such UHC must be avoided at all cost.

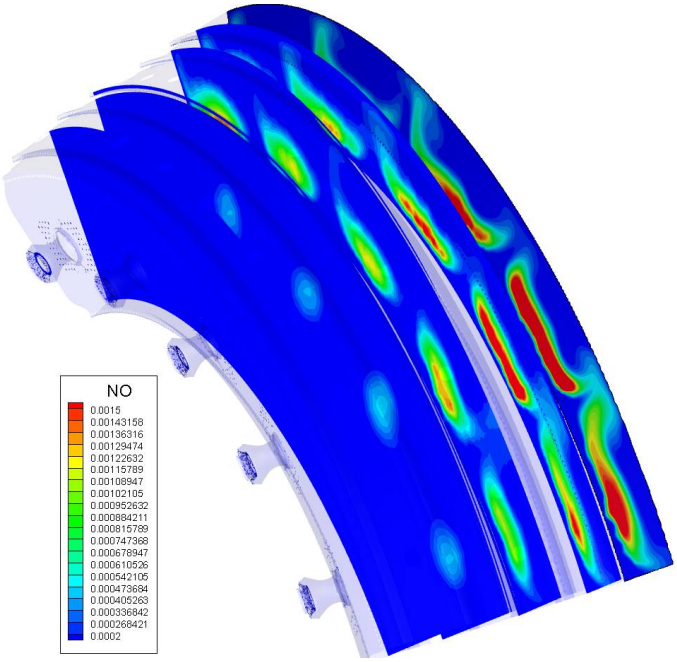

Figure 5.10: Contours of NO_x concentration [kg/kg], while burning *jatropha* biofuel at full power.

As explained in section 2.5, with a temperature increase it should be expected a reduction of both CO and UHC. However this behaviour was not verified in all of the fuels in study, as increasing the power resulted in an increase of CO and an irregular behaviour regarding UHC (figure 5.12). After noticing this problem, further investigation was held in order to figure out what was happening. The answer was discovered in a project from the European Commission [96]. Here it is concluded that empirical models such as the RSM used in this study, although being good for NO_x predictions with a relatively low CPU cost, they cannot capture consistent trades between NO_x and other pollutants such as CO and UHC, which make these models inappropriate for the combustor's operating conditions. Moreover, the effect of flow field simplification that comes from these models, affects the prediction of different pollutants, being CO and UHC more sensitive to turbulent mixing and fluid dynamics, then NO_x emissions. The quenching effect that thrives from the cooling air near the walls, that promotes CO oxidation reactions, cannot also be captured by these models; in fact the prediction of CO emissions from these models result from the primary zone, and which entrain among the combustor's cooling, where it fails to oxidize due to low temperatures; this can be seen in figure 5.11. This then explains why the CO predictions were erroneous, and why NO_x results obtained from this study are acceptable.

Nevertheless all of the fuels maximum CO EI predicted throughout the cycle did not differ that much with the maximum reference values, and as so, a comparison can be made between the fuels, which is in fact presented in figure 5.12(a). As can be seen, by increasing the power an increase of CO emissions is taking place; the prediction of CO emissions from the combustion of *jatropha* biofuel proved to be identical to Jet-A through the entire cycle; both *sunflower* and *algae* biofuel presented lower CO emissions, with *algae* presenting the lowest emissions until 85% power, followed by a big increase of these emissions from a 85 to 100% power setting. At full power, *sunflower* biofuel presented the lowest CO emissions.

Regarding $UHCs$, the predictions are also presented in figure 5.12(b), and only Jet-A presented the expected behaviour of a decrease in emissions with a increase in power. The erroneous

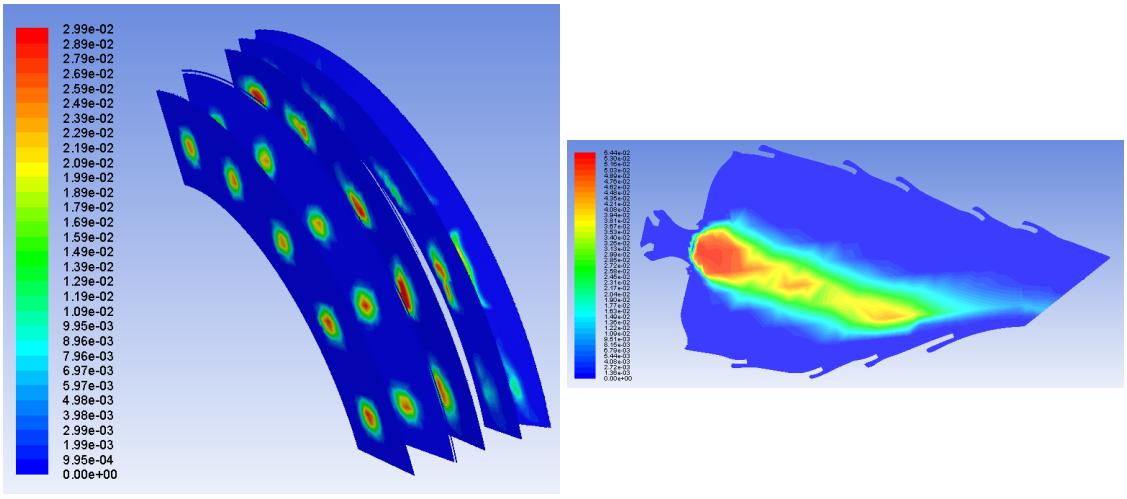

(a) (b)

Figure 5.11: Contours of CO concentration [kg/kg] at 85% power, while burning: (a) *jatropha* biofuel, and (b) *algae* biofuel.

behaviour predicted from the biofuels was verified from 7 to 30% and from 85 to 100%; from 30 to 85% the expected behaviour was correctly predicted. Overall, *sunflower* biofuel presented the lowest UHC emissions along with *algae* biofuel, until this last achieved the 85% power setting. Towards full power, the combustion of *algae* biofuel resulted in a similar increase of UHC emissions, as that verified with CO in the same power setting. Again, *jatropha* biofuel had the highest UHC emissions among the biofuels, and at which through great part of the cycle (30 to 100%), were superior than those of Jet-A. Overall, the biofuel that presented the best performance in both of these emissions was *sunflower* biofuel.

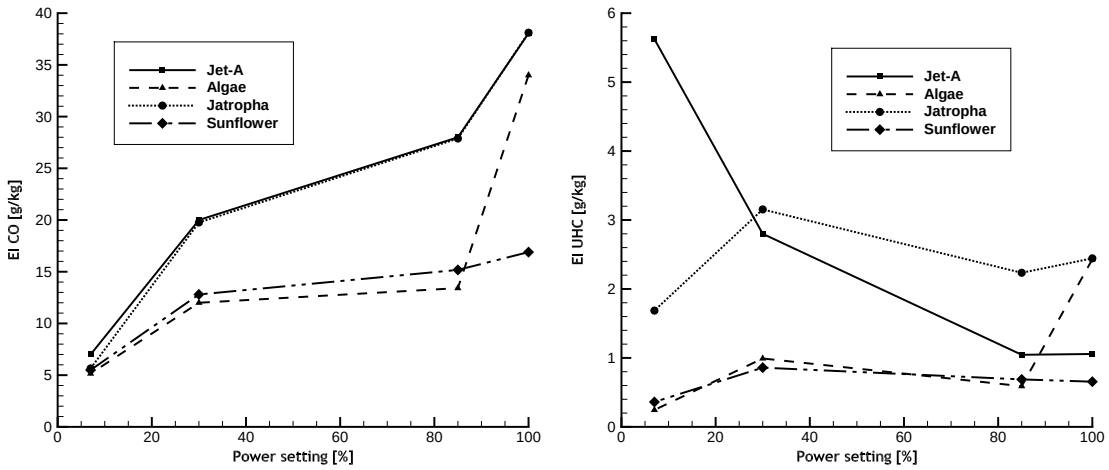

(a) (b)

Figure 5.12: EI results of (a) CO and (b) UHC, resultant from the combustion of Jet-A and the biofuels, throughout ICAO's LTO cycle.

5.5.3 Carbon dioxide

As said through this work, CO_2 is a GHG and is the major contributor for global warming, as it absorbs infrared radiation emitted by the atmosphere and earth surface, preventing it from being radiated into outer space [1]. CO_2 emissions are the result of complete combustion of fuels, and the only way of reducing these is to burn less fuel. By burning less fuel, a lower power output will be obtained, and as so the challenge for today's engineers is to design the GTE and combustor in a way that the same power output will be produced, when the $\dot{m}_f$ is reduced; this is the so called TSFC increase, and is generally achieved from improvements in engine thermal efficiency. However, as changes in aircraft structures take a long time to happen, and are very expensive to implement in the global scale, they do not occur at the required rate to create the so needed CO_2 reduction for global warming mitigation. Thus, the easiest way in reducing these emissions is to change the fuel, because different fuels produce different amounts of CO_2; among all of the fuels, biofuels should be the natural choice, because as stated in section 3.2, these are capable of reducing CO_2 emissions in up to 85%, and the results obtained in this study with the combustion of biofuels and CO_2, reveal in fact a significant decrease when compared to Jet-A.

The prediction of CO_2 emissions were not initially considered for this study, as no reference values from these were available. However after verifying the big differences between the CO_2 EI of biofuels versus Jet-A, it was considered important to analyse these emissions; the results are presented in figure 5.14. Before analysing these emissions, it is important to observe figure 5.13, in which it can be clearly noticed that CO_2 is formed mostly in the flame zone and extends to the post-flame zone, which is in agreement with Lieuwen et al. [64]. The emissions data presented in figure 5.14, indicate that the EI of CO_2 was the largest among the emissions considered; this is expected as CO_2 along with H_2O makes up great part of the exhaust gases. As can be seen from figure 5.14, all of the biofuels presented a reduction of CO_2, throughout all of ICAO's LTO cycle, when compared to Jet-A. This is curious because the biofuels are burning more fuel then Jet-A, at the same power setting, and nevertheless are producing less CO_2 emissions, which demonstrates the potentiality of biofuels in reducing the major contributor to global warming; moreover the expected increase of CO_2 emissions with the power increase (since more fuel is being burned), was predicted. Still in figure 5.14, it can be verified that *jatropha* biofuel presented the lowest CO_2 at idle, representing $\approx$ 45% difference from Jet-A emissions at the same power setting; at full power, *sunflower* biofuel had the less CO_2 emissions, presenting a $\approx$ 24% difference from Jet-A. Over all of ICAO's LTO cycle, the biofuel that presented the greatest reduction of CO_2 emissions was *jatropha* biofuel, which was predicted a 20% difference from Jet-A. This value is still not near from the stated difference of 85%, however taking into account that combustion inefficiency is occurring due to the non atomization of the fuel[7], these results are already good.

[7] Which would lead to a greater reduction of CO_2.

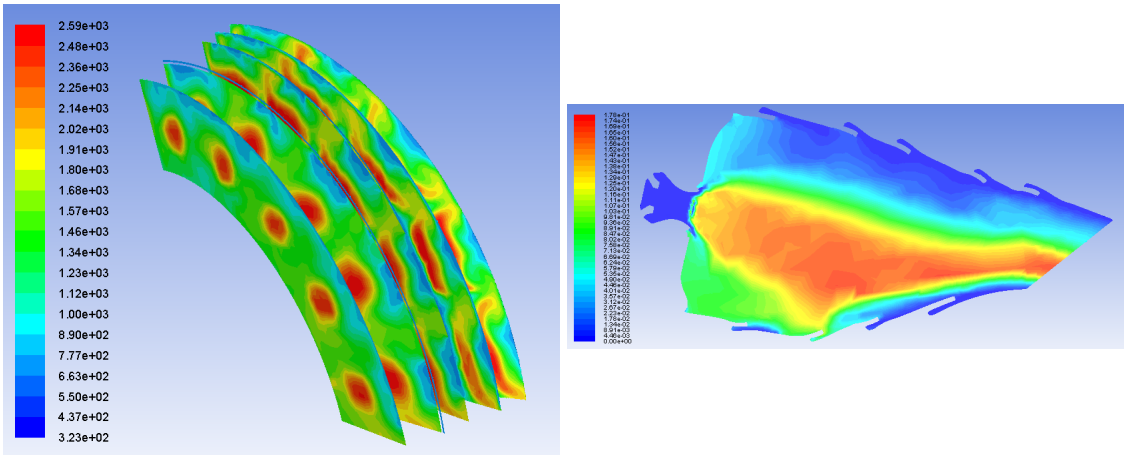

(a) (b)

Figure 5.13: Contours of CO_2 concentration [kg/kg] at 100% power, while burning: (a) *sunflower* biofuel, and (b) *jatropha* biofuel.

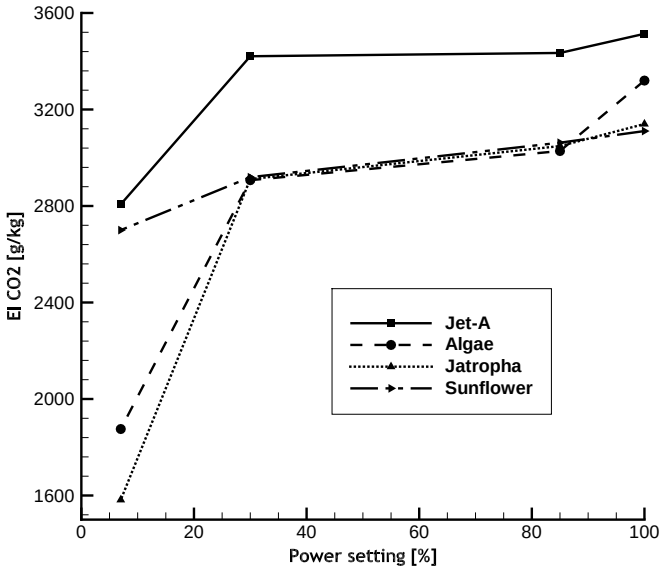

Figure 5.14: EI results of CO_2, resultant from the combustion of Jet-A and the biofuels, throughout ICAO's LTO cycle.

5.6 Conclusions

This study presents a numerical study of the combustion of Jet-A and biofuels in a CFM56-3 combustor, through specific power settings represented by ICAO's LTO cycle, and in which the CFD code used was *ANSYS Fluent 15.0*. The aim of this study was to analyse the emissions and the energy extracted, resultant from the combustion of biofuels from those of Jet-A; these emissions include NO_x, CO, CO_2 and $UHC's$. Additionally, after verifying the importance of cooling air and the combustor exit temperature, these were also included in the results analyses. As with any work of this kind, there are always numerous variables that must be taken into account, in order to correctly predict results that comply with experimental/measured data, but as each of these variables require a lot of work to develop, it is generally opted to stick with the most important. This study was no different, and as such there are some variables that were not

considered due to the existing complexity of this work. The present chapter explains some problems that appeared, what was done to solve them, and if these were unsolved, possible solutions. To conclude, results are discussed and future studies are presented.

Although this study concerns mostly the numerical study, the scanning/CAD phase was probably the phases in which most problems rose. The scanning process by itself was very challenging, and a lot of time/effort was spent in order to overcome some persistent problems. Most of these problems however, derives from the fact that the scanner used (*Artec Spider*) is not indicated for the model size, being *Artec Eva* more suitable. To give an idea why this scanner was not suitable, is as *Artec Spider* scanner took somewhat 40 scans to obtain a complete 3D model of the combustor, *Artec Eva* would only require around 5 scans. The most persisting problems was due to the fact that the scanner was always loosing track, which occurs because the scanner does not have sufficient reference elements from the previous scanned frames to continue; this was solved by adding a lot of texture markers and objects along the model. Importing this 3D model into the CAD software (*CATIA V5*) also presented some issues, as the normal procedure of importing STL files into *CATIA V5* is only capable of doing so with files of up a few KB, and the final STL model was in the order of 200MB; fortunately a new STL importing method was found within the *cloud import function*, which enabled the importation of the 3D model into *CATIA V5*. Finally the CAD process could be commenced and the end result was very good, resulting in a very accurate CAD representation of the CFM56-3 combustor, as all of the relevant parts which include the dome, walls, swirlers, fuel injectors and all of the cooling holes, could be represented. Overall, and accounting with all of the failed attempts, the scanning/CAD phase phase took more than half of the time invested in this study.

The complex geometry of the model combustor also means that most of the mesh generation software's would have a great deal in developing the required mesh for the present problem. The meshing capabilities of *HELYX-OS* were however overwhelming, as a very fine mesh was generated, while doing so in less then two hours, which is a very short time when compared to other meshing programs. The main problems that was occurring within the mesh generation, was due to layer creation on the walls; because the cooling lips present some complex curvatures, the layer creation in these zones resulted in them intersecting, which created errors. These were only overcome by refining to the maximum layer creation values that the machine could support, but nevertheless the mesh at this zone was still not refined enough, which resulted in relatively high skewness and y^+ values. These problems could be however overcome with a higher RAM available on the machine, but these would result in a higher computational cost, without it being necessary, when calculation the solution in *ANSYS Fluent*. In the end the required mesh for the problem was considered achieved, as a mesh independence test on the required results was carried out.

The boundary conditions calculated for this study was of paramount importance and were only possible through some information gathering presented in some literatures. With these boundary conditions all of the fuels could be successfully compared as they were subjected to the same conditions at a given power setting, i.e. the same AFR. Most of the diverging problems that occurred during the CFD analysis were due to high URF, and were only solved by decreasing most these values. Calculating the solution with first and second order also proved very important, as this last predicted far more better results, despite being more CPU expensive. Moreover, during the CFD analysis it was observed that when modelling the turbulence, the accuracy of

the simulation was significantly improved using the RSM, than using other models such as the Standard k-ε model.

As for the results obtained from the CFD analysis, these are acceptable due to a validation which was performed by analysing the emissions predicted with Jet-A, with those presented by ICAO, regarding the CFM56-3 engine through ICAO's LTO cycle. Initially it was already expected that the results would not be the same as those presented by ICAO, due to the fact that the atomization of the fuel is not considered, and which is of great importance for this type of study; nevertheless the validation results represented little margin of error from ICAO's reference values, and as so the prediction of the emissions resultant from the combustion of biofuels could now be commenced. The NO_x and some of the UHC predictions were very good, but CO predictions presented a erroneous behaviour; this is due to the incapability of empirical models such as the RSM to predict the correct formation of CO emissions. In order to improve the predicting capabilities of these models, it is necessary to couple detailed CFD calculation results to the emission models, by a direct transformation of the combustor's CFD results into a very accurate multi-reactor model. In this concept, a new numerical tool called KPPSMOKE has been developed to predict the correct formation of the pollutants considered for this study [96].

Overall, all of the biofuels presented a higher fuel consumption but this can be mitigated, by the fact that lower emissions were predicted from the biofuels, throughout all of the power cycle; all of the biofuels also presented lower combustor exit temperatures. Each of the biofuels considered presented better behaviour in some emissions than in others, and as so in the future it is necessary to weigh which would prove of more benefit. Thus, the biofuels in which were predicted a greater reduction of NO_x, CO, CO_2 and $UHC's$ emissions throughout the entire ICAO's LTO cycle, were respectively *algae* (48%), *sunflower* (46%), *jatropha* (19%) and *sunflower* (76%). This last difference is of great importance as it means that little amount of fuel is being wasted; moreover due to the fact that *sunflower* biofuel presented the best overall behaviour, it is concluded from this study that *sunflower* biofuel is the most suitable biofuel to replace Jet-A in a combustion point of view.

5.7 Future Studies

As stated throughout this work, there are many important variables and factors that were not considered, and with which the results could be much closer to the real values; thus, in the future this study can be continued involving the following factors:

- The fuel atomization along with the fuel injection angles, is of paramount importance if an exact prediction of the emissions resultant from the combustion of any fuel is intended. In fact this study has already been attributed in UBI, for a MSc project;
- Study the correct CO and UHC predictions, through more CPU expensive models like LES and DNS is of paramount importance as there is little research regarding these;
- The correct turbulent flow produced from the swirlers, has to be more deeply researched;
- A profound research on the biofuels properties, and their influence in the combustor performance is of great importance, as these already present some difficult challenges like altitude relight and high freezing points;

- A complete life cycle assessment, resultant from the production of the considered biofuels, has to be held to prove their advantages over petroleum fuels. These include social, economic and environmental factors.

Much more examples can be mentioned like improving the mesh near the walls, so that the heat transfer through these can be correctly studied. Most of these examples only prove the huge potential that CFD provide in offering solutions for problems, that if were carried out experimentally, would be much more expensive and less practical in some situations.

5.8 Authors note

This study appeared with the motivation to seek a biofuel which would provide an alternative to the environmental and non-renewable problems that conventional jet fuel present. It was proven through this study that biofuels are capable of supplying aviation's fuel demand, in an environmentally friendly manner. Biofuels however may not be a quick solution for the energy problems of the world, as many research on their properties and harvesting are required, and in short term these may even be more expensive than petroleum fuels; however to solve our dependency in petroleum fuels, it should not be expected that this can be accomplished in a cheap or easy way. Nevertheless the fact remains that biofuels are a reliable alternative energy resource, and with more research than that is already being held, it is possible to overcome the disadvantages of biofuels, and make them suitable for a wide variety of scenarios. Once these disadvantages are overcome, the world takes one step closer in not having to rely any more on petroleum, or other fossil fuel products to produce energy.

The reverse engineering adopted for this study, of bringing a service combustor into a CFD analysis proved to be challenging and very satisfying to accomplish. This hole process could never be performed without the combustor provided by TAP, and without the assistance of my supervisor, Dr. Francisco Brójo, whom I never tire of thanking, being forever grateful for everything you have done for me.

Bibliography

[1] E. Commission *et al.*, ``Climate change: commission proposes bringing air transport into EU emissions trading scheme." 1, 81

[2] R. Bleischwitz, K. Fuhrmann, and E. Huchler, ``The sustainability impact of the EU emissions trading system on the european industry," *Available at SSRN 1133515*, 2007. 1

[3] A. Runge, ``Aviation and emissions trading," ICAO Council Briefing, 29 Sep. 2011. 1

[4] ``British petroleum statistical review of world energy," *Providence, RI, USA*, p. 7, june 2015. 1

[5] ``Impact of fuel price increases on the aviation industry," United States Government Accountability Office, Tech. Rep. GAO-14-331, September 2014, report to Congressional Committees. 1

[6] F. Birol, ``Fossil fuel subsidies are "public enemy number one" – iea chief," Chief Economist said at the International Energy Agency at EWEA's Annual Event in Vienna on Monday, 2013. 1

[7] M. Grubb, C. Vrolijk, D. Brack, T. Forsyth, J. Lanchbery, and F. Missfeldt, *The Kyoto Protocol. A guide and assessment*. Royal Institute of International Affairs, 1999. 1

[8] Q. Schiermeier, ``Hot air," *Nature*, vol. 491, no. 7426, pp. 656--658, 2012. 1

[9] A. L. M. F. Basher, ``Optimum turbofan engine performance through variation of bypass ratio," *Journal of Engineering and Development*, vol. 17, no. 1, 2013. 2

[10] ``Alternative jet fuels," 2006, [A supplement to Chevron's Aviation Fuels Technical Review]. 2, 49, 50

[11] F. Wolters, R. Becker, and M. Schaefer, ``Impact of alternative fuels on engine performance and CO_2 emissions," in *28th International Congress of the Aeronautical Sciences, Brisbane, Australia*, 2012, pp. 23--28. 2, 16

[12] H. Conkle, E. Griesenbrock, H. Robota, R. Morris Jr, and E. Coppola, ``Production of unblended,"drop-in," renewable jet fuel," 2012. 2, 54

[13] A. Elbehri, A. Segerstedt, P. Liu *et al.*, *Biofuels and the sustainability challenge: a global assessment of sustainability issues, trends and policies for biofuels and related feedstocks*. Food and Agriculture Organization of the United Nations (FAO), 2013. 3

[14] A. H. Lefebvre and D. R. Ballal, *Gas turbine combustion*. CRC Press, 2010. 3, 6, 7, 8, 29, 31, 33, 36, 37, 48, 78

[15] H. I. H. Saravanamuttoo, G. F. C. Rogers, and H. Cohen, *Gas turbine theory*. Pearson Education, 2009. 3, 8, 10, 37, 39

[16] P. Maass, ``The breaking point," *New York Times Magazine*, vol. 21, p. 30, 2005. 3

[17] M. J. B. Davy, *Interpretive history of flight*. HM Stationery Off., 1948. 5

[18] *Death of Sir Hiram Maxim. A Famous Inventor, Automatic Guns And Aeronautics.* The Times, 1916. 5

[19] G. Jones, *The jet pioneers: the birth of jet-powered flight.* Methuen London, 1989. 5

[20] J. V. Casamassa and R. D. Bent, *Jet aircraft power systems.* Glencoe/McGraw-Hill School Publishing Company, 1965. 7, 8

[21] C. B. Meher-Homji, ``The development of the junkers jumo 004b: The world's first production turbojet," in *ASME 1996 International Gas Turbine and Aeroengine Congress and Exhibition*. American Society of Mechanical Engineers, 1996, pp. V002T02A012--V002T02A012. 7

[22] R. E. Stenger, ``Double annular combustor configuration," Mar. 25 1980, US Patent 4,194,358. 8

[23] C. International, ``CFM international's double annular combustor technology," 1999, last checked: 28.11.2015. [Online]. Available: http://www.cfmaeroengines.com/press/cfm-internationals-double-annular-combustor-technology/233 9

[24] R. Stickles, ``Taps II technology final report," Jun. 2013, this is report number DOT/FAA/AEE/2014-03 by the FAA's Office of Environment and Energy. 9

[25] M. Welch, ``Gas turbine fuel and fuel quality requirements for use in industrial gas turbine combustion," 2013. 10

[26] ``Offshore gas turbines and dry low NO_x burners; an analyses of the performance improvements limited database," Feb. 2015, oil and Gas UK, Technical note - [ENV002] Rev01. 11

[27] F. Güthe, J. Hellat, and P. Flohr, ``The reheat concept: the proven pathway to ultralow emissions and high efficiency and flexibility," *Journal of Engineering for Gas Turbines and Power*, vol. 131, no. 2, p. 021503, 2009. 11

[28] K. Syed, ``The reheat combustor of alstom's gt24/gt26 gas turbines," Gas Turbine Combustion, Cranfield University, short course, 2015. 11

[29] I. K. Reksowadojo, L. H. Duong, and D. N. Pham, ``Review of typical biofuel for aviation alternative fuel purposes," *Combustion Engines and Propulsion Systems Laboratory, Faculty of Mechanical and Aerospace Engineering*, 2014. 12, 54

[30] P. Lobo, D. E. Hagen, and P. D. Whitefield, ``Comparison of PM emissions from a commercial jet engine burning conventional, biomass, and fischer--tropsch fuels," *Environmental science & technology*, vol. 45, no. 24, pp. 10744--10749, 2011. 12

[31] P. Kumaran, M. Gopinathan, and S. Kantharrajan, ``Combustion characteristics of improved biodiesel in diffusion burner." *International Journal of Automotive & Mechanical Engineering*, vol. 10, 2014. 13

[32] M. Klassen, M. Ramotowski, L. Eskin, and R. Roby, ``Clean combustion of liquid biofuels in gas turbines for renewable power generation," *American institute of chemical engineers, LPP Combustion LLC, San Antonio*, pp. 1--6, 2010. 13

[33] E. Corporan, M. J. DeWitt, V. Belovich, R. Pawlik, A. C. Lynch, J. R. Gord, and T. R. Meyer, ``Emissions characteristics of a turbine engine and research combustor burning a fischer-tropsch jet fuel," *Energy & fuels*, vol. 21, no. 5, pp. 2615--2626, 2007. 14

[34] T. F. Rahmes, J. D. Kinder, T. M. Henry, G. Crenfeldt, G. F. LeDuc, G. P. Zombanakis, Y. Abe, D. M. Lambert, C. Lewis, J. A. Juenger *et al.*, ``Sustainable bio-derived synthetic paraffinic kerosene (bio-spk) jet fuel flights and engine tests program results," *Report No. AIAA*, vol. 7002, 2009. 14

[35] H. Bhimgade and S. Bhele, ``A review on use of computational fluid dynamics in gas turbine combustor analysis and its scope," *International Journal of Science and Research (IJSR), India Online ISSN*, pp. 2319--7064. 15

[36] I. Uryga-Bugajska, M. Pourkashanian, D. Borman, E. Catalanotti, L. Ma, and C. Wilson, ``Assessment of the performance of alternative aviation fuel in a modern air-spray combustor (MAC)," in *ASME 2008 International Mechanical Engineering Congress and Exposition*. American Society of Mechanical Engineers, 2008, pp. 61--69. 15

[37] A. Kyne, M. Pourkashanian, C. Wilson, and A. Williams, ``Validation of a flamelet approach to modelling 3-D turbulent combustion within an airspray combustor," in *ASME Turbo Expo 2002: Power for Land, Sea, and Air*. American Society of Mechanical Engineers, 2002, pp. 591--600. 16

[38] M. E. Mueller and H. Pitsch, ``Large eddy simulation of soot evolution in an aircraft combustor," *Physics of Fluids (1994-present)*, vol. 25, no. 11, p. 110812, 2013. 16

[39] M. E. Mueller, G. Blanquart, and H. Pitsch, ``A joint volume-surface model of soot aggregation with the method of moments," *Proceedings of the Combustion Institute*, vol. 32, no. 1, pp. 785--792, 2009. 16

[40] C. D. Pierce, ``Progress-variable approach for large-eddy simulation of turbulent combustion," Ph.D. dissertation, Citeseer, 2001. 16

[41] C.-M. Lee, K. Kundu, and B. Ghorashi, *Simplified jet-A kinetic mechanism for combustor application*. National Aeronautics and Space Administration, 1993. 17

[42] G. Dragone, B. D. Fernandes, A. A. Vicente, and J. A. Teixeira, ``Third generation biofuels from microalgae," 2010. 17

[43] Rolls-Royce, *The Jet Engine*, 5th ed. Technical Publications Department, Rolls-Royce plc, Derby, England, 1996. 20, 22, 26, 30, 36, 37, 39

[44] L. K. Loftin, *Quest for performance: The evolution of modern aircraft*. Scientific and Technical Information Branch, National Aeronautics and Space Administration, 1985, no. 468. 21

[45] Boeing, ``Propulsion : Jet engine basics." 22

[46] ICAO, ``ICAO engine exhaust emissions data bank," CFM56-3-B1, Tech. Rep., 2013. 22, 48

[47] R. Singh, ``Introduction to gas turbine combustion systems," Gas Turbine Combustion, Cranfield University, short course, 2015. 25, 26, 45, 46

[48] *CFM56-3 training manual*, CFM International, october 1995. 27

[49] B. Jones, ``Gas turbine combustor, design and development," Gas Turbine Combustion, Cranfield University, short course, 2015. 28, 38, 41, 66

[50] S. Samuelsen, ``Conventional type combustion," *Gas Turbine Handb*, 2006. 29

[51] V. Sethi, ``Introduction to design consideration and sizing methodologies in GTC's," Gas Turbine Combustion, Cranfield University, short course, 2015. 30, 32

[52] *The jet engine*. Rolls-Royce, 2005. 30, 36

[53] A. Lefebvre, *Atomization and sprays*. CRC press, 1988, vol. 1040, no. 2756. 34, 35

[54] S. J. Myers, ``Single circuit multiple spray cone pressure atomizers," Nov. 12 2013, US Patent 8,579,213. 34

[55] A. H. Lefebvre, ``A novel method of atomization with potential gas turbine applications," *Defence Science Journal*, vol. 38, no. 4, pp. 353--362, 2014. 35

[56] E. M. Goodger and S. O. Ogaji, *Fuels & Combustion in Heat Engines*. Cranfield University Press, 2011. 39

[57] S. R. Turns *et al.*, *An introduction to combustion*. McGraw-hill New York, 1996, vol. 287. 40, 43, 44, 56

[58] ``Class notes: Introduction to fuel and energy," Department of chemical and process engineering, University of Sheffield. 41

[59] R. C. Flagan and J. H. Seinfeld, *Fundamentals of air pollution engineering*. Courier Corporation, 2013. 42, 45

[60] I. A. Waitz, G. Gauba, and Y.-S. Tzeng, ``Combustors for micro-gas turbine engines," *Journal of Fluids Engineering*, vol. 120, no. 1, pp. 109--117, 1998. 44

[61] J. Bluestein, NO_x *Controls for Gas-fired Industrial Boilers and Combustion Equipment: A Survey of Current Practices, Topical Report*. Gas Research Institute, 1992. 45

[62] I. Glassman, R. A. Yetter, and N. G. Glumac, *Combustion*. Academic press, 2014. 45

[63] C. Meher-Homji, J. Zachary, and A. Bromley, ``Gas turbine fuels-system design, combustion and operability," in *Proceedings of the 39th Turbomachinery Symposium, George R. Brown Convention Center, Houston, Texas*, 2010, pp. 4--7. 46

[64] T. C. Lieuwen and V. Yang, *Gas turbine emissions*. Cambridge University Press, 2013, vol. 38. 46, 47, 81

[65] Y. B. Zeldovich, ``The oxidation of nitrogen in combustion and explosions," *Acta Physicochim. URSS*, vol. 21, no. 4, pp. 577--628, 1946. 46

[66] G. A. Lavoie, J. B. Heywood, and J. C. Keck, ``Experimental and theoretical study of nitric oxide formation in internal combustion engines," *Combustion science and technology*, vol. 1, no. 4, pp. 313--326, 1970. 46

[67] J. Kurzke, *GasTurb12, Design and Off-Design Performance of Gas Turbines*, Germany, 2012. 47

[68] J. A. Miller, M. J. Pilling, and J. Troe, ``Unravelling combustion mechanisms through a quantitative understanding of elementary reactions," *Proceedings of the Combustion Institute*, vol. 30, no. 1, pp. 43--88, 2005. 47

[69] H. Omidvarborna, A. Kumar, and D.-S. Kim, ``NO_x emissions from low-temperature combustion of biodiesel made of various feedstocks and blends," *Fuel Processing Technology*, vol. 140, pp. 113--118, 2015. 47

[70] D. Daggett, O. Hadaller, R. Hendricks, and R. Walther, ``Alternative fuels and their potential impact on aviation," *National Aeronautics and Space Administration, NASA/TM*, vol. 214365, no. 6, 2006. 49, 50, 51, 71

[71] M. Vera-Morales and A. Schäfer, ``Fuel-cycle assessment of alternative aviation fuels," *OMEGA Alternative Fuels Report (Draft), February*, 2009. 49

[72] Air Transport Action Group, ``Beginner's guide to aviation biofuels," Brochure, May 2009. 50, 51, 52, 53

[73] F. G. A. Fernández, C. González-López, J. F. Sevilla, and E. M. Grima, ``Conversion of CO_2 into biomass by micro-algae: how realistic a contribution may it be to significant CO_2 removal?" *Applied microbiology and biotechnology*, vol. 96, no. 3, pp. 577--586, 2012. 50

[74] R. on Sustainable Biofuels, ``Global principles and criteria for sustainable biofuels production version zero," 2008, preamble. 50

[75] S. D. Sanford, J. M. White, P. S. Shah, C. Wee, M. A. Valverde, and G. R. Meier, ``Feedstock and biodiesel characteristics report," *Renewable Energy Group*, vol. 416, pp. 1--136, 2009. 51, 101

[76] R. E. Bailis and J. E. Baka, ``Greenhouse gas emissions and land use change from jatropha curcas-based jet fuel in brazil," *Environmental science & technology*, vol. 44, no. 22, pp. 8684--8691, 2010. 51

[77] P. Goyal, M. Sharma, and S. Jain, ``Optimization of conversion of high free fatty acid jatropha curcas oil to biodiesel using response surface methodology," *ISRN Chemical Engineering*, vol. 2012, 2012. 51, 72, 101

[78] J. S. Requena, A. C. Guimaraes, S. Q. Alpera, E. R. Gangas, S. Hernandez-Navarro, L. N. Gracia, J. Martin-Gil, and H. F. Cuesta, ``Life cycle assessment (LCA) of the biofuel production process from sunflower oil, rapeseed oil and soybean oil," *Fuel Processing Technology*, vol. 92, no. 2, pp. 190--199, 2011. 52

[79] P. Schlagermann, G. Göttlicher, R. Dillschneider, R. Rosello-Sastre, and C. Posten, ``Composition of algal oil and its potential as biofuel," *Journal of Combustion*, vol. 2012, 2012. 52, 71

[80] H. Mongia, ``Comprehensive gas turbine combustion modelling methodology," *International Aerospace CFD conference*, 2007. 55

[81] P. Gauthier, ``Role of CFD in design and development: Combustion modelling," Gas Turbine Combustion, Cranfield University, short course, 2015. 55, 56, 71

[82] E. S. Oran and J. P. Boris, *Numerical simulation of reactive flow*. Cambridge University Press, 2005. 56

[83] M. Zedda, ``Introduction to CFD for combustion applications," Gas Turbine Combustion, Cranfield University, short course, 2015. 56, 57

[84] P. Chatterjee, ``A computational fluid dynamics investigation of thermoacoustic instabilities in premixed laminar and turbulent combustion systems," Ph.D. dissertation, Virginia Polytechnic Institute and State University, 2004. 57

[85] *Artec Studio 9 User Guide*, Artec Group. 58

[86] C. Fonte, ``Design of a Low Consumption Electric Car Prototype," Master's thesis, Universidade da Beira Interior, Portugal, 2015. 61, 63

[87] D. Combest, ``A concise introduction to pre-processing, meshing, and running OpenFoam® cases with HELYX-OS," *eighth OF Workshop*, June 2013. 61

[88] A. F. Ansys, ``Fluent meshing user's guide," *ANSYS inc*, 2013. 63

[89] A. Fluent, ``Fluent 6.3 documentation," *Fluent Inc., Lebanon, NH*, 2006. 63, 64, 65, 68, 70

[90] A. Burcat and B. Ruscic, ``Ideal gas thermodynamic data in polynomial form for combustion and air pollution use," 2007, last checked: 15.12.2015. [Online]. Available: http://garfield.chem.elte.hu/Burcat/THERM.DAT 64

[91] A. Burcat, *Third millenium ideal gas and condensed phase thermochemical database for combustion with updates from active thermochemical tables*. Argonne National Laboratory Argonne, IL, 2005. 64

[92] R. J. Kee, F. M. Rupley, and J. A. Miller, ``Chemkin-II: A fortran chemical kinetics package for the analysis of gas-phase chemical kinetics," Sandia National Labs., Livermore, CA (USA), Tech. Rep., 1989. 64

[93] B. Pereira, ``Numerical analysis of flow around a fan blade of a CFM56-3," Master's thesis, Universidade da Beira Interior, Portugal, 2015. 65

[94] P. Ribeiro, ``Análise de performance da Família de Motores de Avião CFM56," Master's thesis, Instituto Superior de Engenharia de Lisboa, Portugal, 2012. 65, 66, 73, 102

[95] M. Noor, A. P. Wandel, and T. Yusaf, ``Detail guide for CFD on the simulation of biogas combustion in bluff-body mild burner," in *Proceedings of the 2nd International Conference of Mechanical Engineering Research (ICMER 2013)*. Universiti Malaysia Pahang, 2013, pp. 1--25. 68

[96] The European Commission, ``Emicopter report summary," 2014, last checked: 12.01.2016. [Online]. Available: http://cordis.europa.eu/result/rcn/143538_en.html 79, 84

[97] E. Fleuti and J. Polymeris, ``Aircraft NO_x-emissions within the operational LTO cycle," *Unique (Flughafen Zrich AG) and Swiss Flight Data Services*, 2004. 93

Appendix A

Emissions data

A.1 ICAO reference LTO-cycle

Table A.1: ICAO gaseous emissions standards

Emission (g/kN)	Subsonic Turbojet/Turbofan Engines [1]	Supersonic Turbojet/Turbofan engines
HC	19.6	$140(0.92)^{\pi_{00}}$
CO	118.0	$4550(\pi)_{00}^{-1.03}$
NO_x	$32 + 1.6\pi_{00}$ $-1.04 + 2\pi_{00}(2007 + engines)$	$36 + 2.4\pi_{00}$

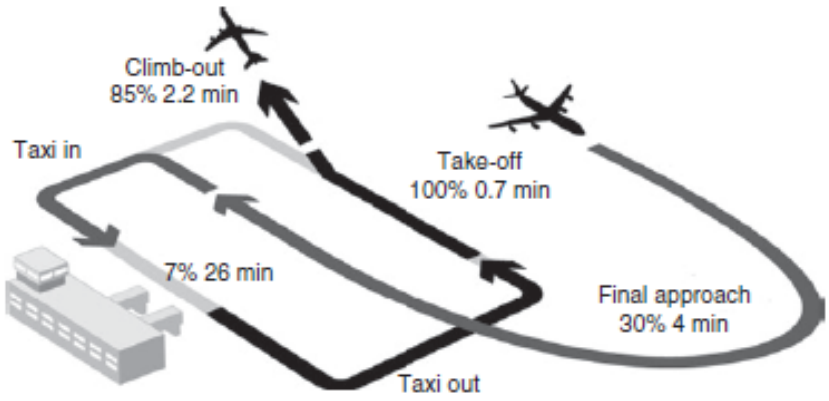

Figure A.1: ICAO reference LTO-cycle [97].

A.2 Pollutant effects and their limitation strategy

Table A.2 has been created by the author in order to summarize the pollution effects of emissions and their limitation strategies, through an information gathering of several works.

[1] Newly manufactured engines with rated take-off thrust greater then 26.7 kN.

Table A.2: Pollutant effects and their limitation strategy

Pollutant	Effect	Limitation strategy
CO_2	Global warming	Increase thermodynamic efficiency of GTE
SO_2	Toxic, Corrosive	Remove sulphur from fuel
CO	Toxic	Increase combustion efficiency/residence time
UHC	Toxic	Sufficient local oxygen concentration
$Smoke\ soot$	Visible	Prevent fuel-rich pockets of fuel, by injecting more air in the PZ
NO_x	Toxic	Lower the reaction temperature
	Depletion of ozone within stratosphere	Eliminate hot spots from the reaction zone
	Ozone increases at ground level	Time formation of NO_x should be kept to a minimum

Appendix B

Images from the Scanning and CAD phase

B.1 CFM56-3 combustor picture

Figure B.1: CFM56-3 combustor photograph. Here it can be seen the tape/markers added to aid the scanning process.

B.2 Final scanned images from the 3D model combustor

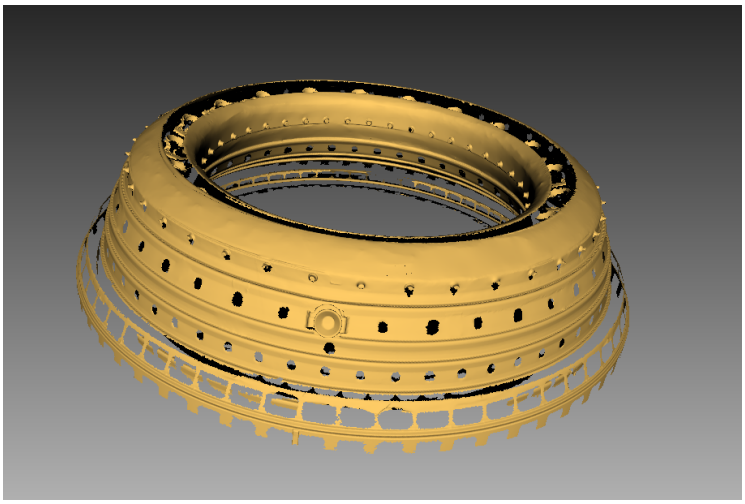

Figure B.2: 3D model combustor, obtained from the post-processing step in Artec Studio 9.2.

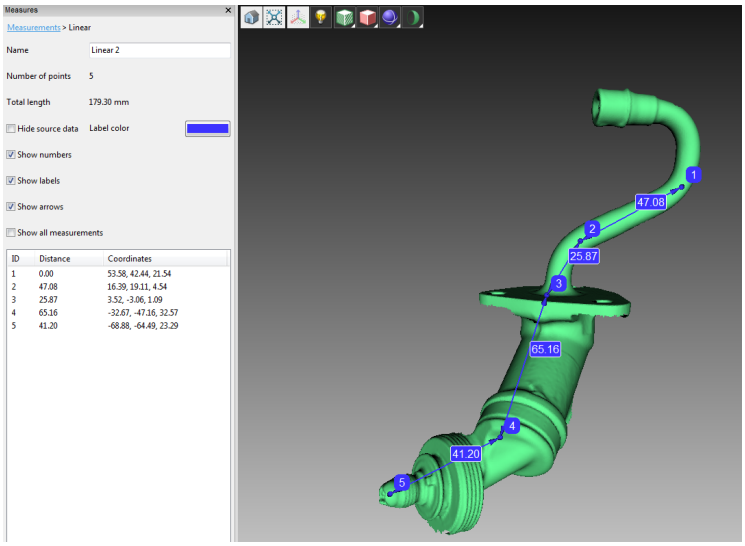

Figure B.3: Measurement methodology that can be used in Artec Studio 9.2.

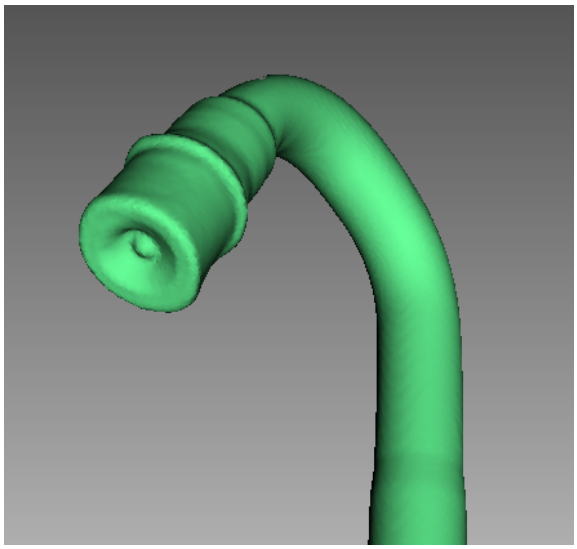

Figure B.4: Close up on the tip of the scanned fuel injector.

B.3 CAD illustrations

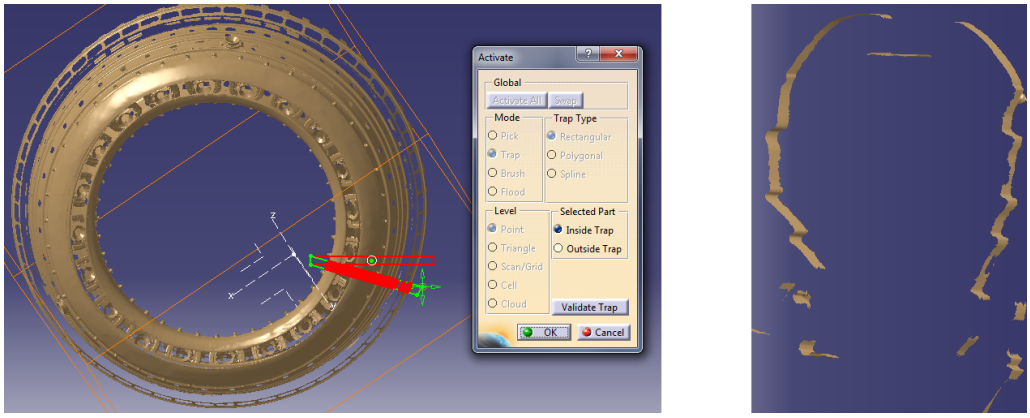

Figure B.5: Activation of a selected section of the STL 3D model. On the left it is selected the section which is desired to work with, and on the right it can be seen the result of this selection.

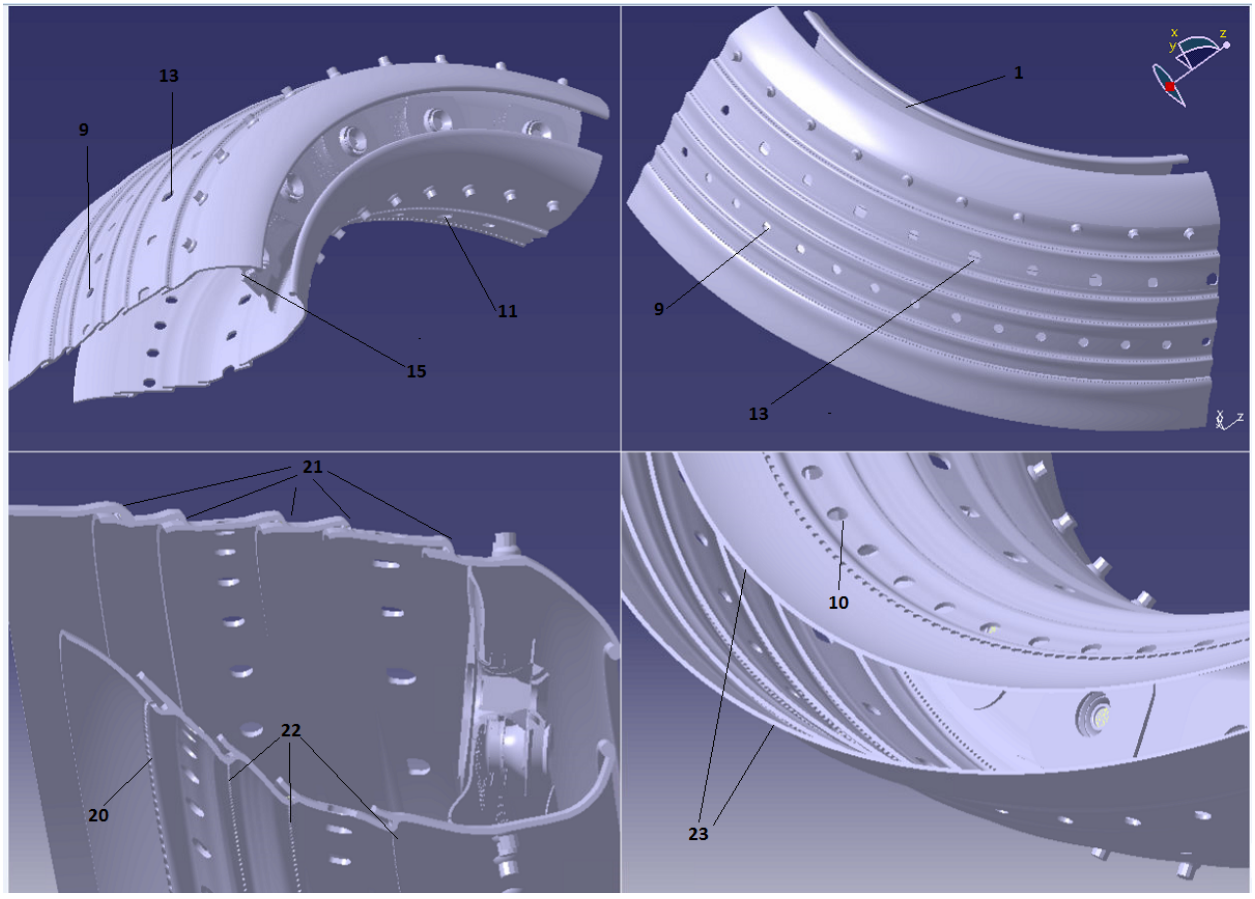

Figure B.6: Views of the CAD combustor model section used in the simulations[1].

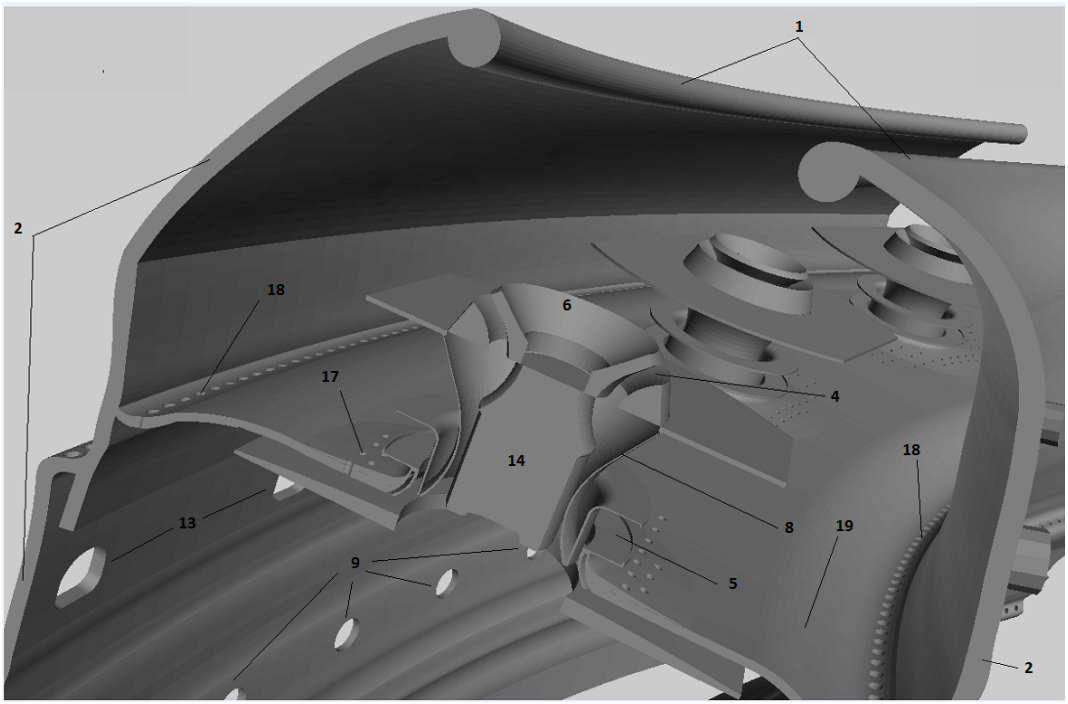

Figure B.7: Close up on the primary and secondary swirlers, along with the placement of the fuel injector[1].

[1]The numbered selections are named in table C.1, presented in App. C.

Appendix C

Mesh

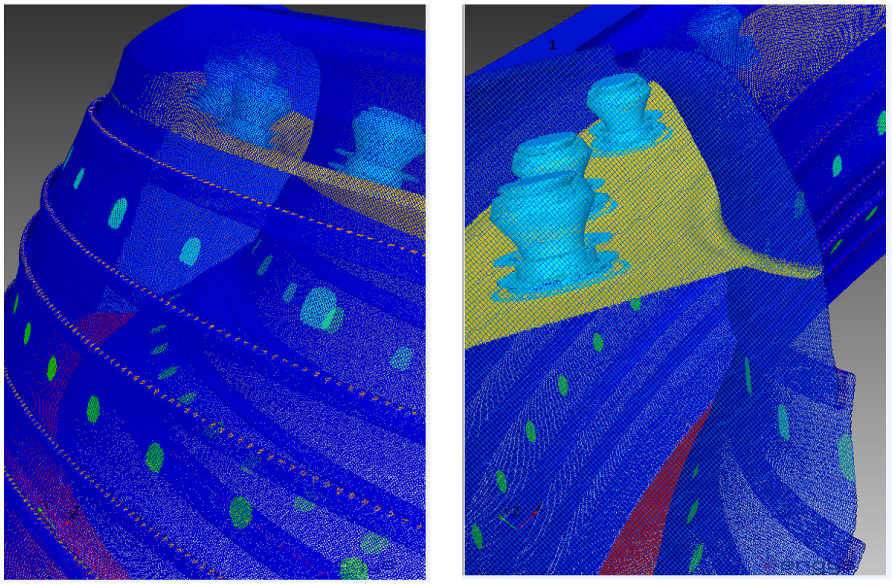

Figure C.1: Mesh of the model combustor before the upper volume of the dome being removed.

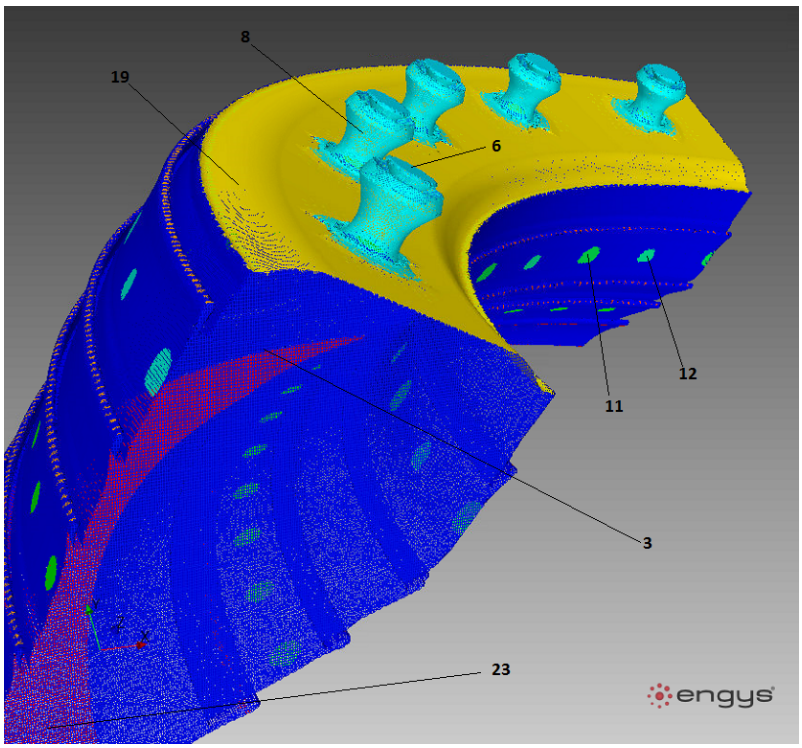

Figure C.2: Mesh of the model combustor after the upper volume of the dome being removed[1].

[2]The numbered selections are named in table C.1.

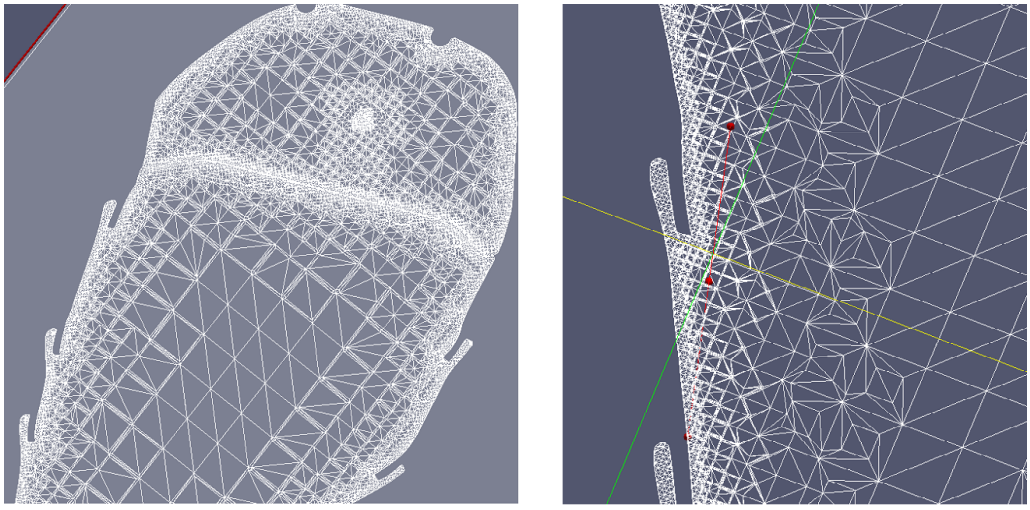

Figure C.3: Close up of the layers creation, with a sectional cut of the model, using *Paraview*.

C.1 Combustor model boundary names

Table C.1: Combustor model boundary names/type

Numbered selection names	Correspondent figure	Boundary type
1	Top	B.6 • B.7 • C.1	- - -
2	Walls	B.7	Wall
3	Symmetry	C.2	Symmetry
4	Swirler 1	B.7	Mass-flow inlet
5	Swirler 2	B.7	Mass-flow inlet
6	Swirl cone inlet	B.7 • C.2	Wall
8	Swirl cone	B.7 • C.2	Wall
9	Mix	B.6 • B.7	Mass-flow inlet
10	Mix2	B.6	Mass-flow inlet
11	Mix3.1	B.6 • C.2	Mass-flow inlet
12	Mix3.2	C.2	Mass-flow inlet
13	Mix4	B.6 • B.7	Mass-flow inlet
14	Fuel inj	B.7	Mass-flow inlet (fuel)
15	Fuel inj rich	B.6	Mass-flow inlet (fuel)
17	Dome holes	B.7	Wall
18	Dome holes 1	B.7	Mass-flow inlet
19	Dome	B.7 • C.2	Wall
20	Dil 1.1	B.6	Mass-flow inlet
21	Dil 2	B.6	Mass-flow inlet
22	Dil 2.1	B.6	Mass-flow inlet
23	Bottom	B.6 • C.2	Pressure-outlet

Appendix D

Problem setup inputs

Table D.1: Fuel Stoichiometric ratios obtained with CEA; flash point and LHV for the fuels in study

	Jet-A	**Biofuel**		
		$Jatropha$	$Algae$	$Sunflower$
Stoichiometric ratio (AFR)	14.7	13.3	13.5	13.5
Stoichiometric ratio (FAR)	0.0680	0.0751	0.0743	0.0741
FSRFL	0.0748	0.08261	0.0817	0.0815
Flash Point (K)	312	445	433	450
LHV (MJ/kg)	43.1	39.5	30.0	38.4

Table D.2: Jatropha [77], Algae and Sunflower [75], biofuel fatty acid composition

Fatty acid	**Carbon number**	**Formula**	**Biofuel composition** $(\%)$		
			$Jatropha$	$Algae$	$Sunflower$
Mystric	C14:0	$C_{14}H_{28}O_2$	- - -	0.6	- - -
Palmitic	C16:0	$C_{16}H_{32}O_2$	16.2	6.9	4.2
Palmitoleic	C16:1	$C_{16}H_{30}O_2$	- - -	0.2	- - -
Stearic	C18:0	$C_{18}H_{36}O_2$	8.2	3	3.3
Oleic	C18:1	$C_{18}H_{34}O_2$	38.4	75.2	63.6
Linoleic	C18:2	$C_{18}H_{32}O_2$	36.8	12.4	27.6
Linolenic	C18:3	$C_{18}H_{30}O_2$	0.4	1.2	0.2
Arachidic	C20:0	$C_{20}H_{40}O_2$	- - -	0.4	- - -
Behenic	C22:0	$C_{22}H_{44}O_2$	- - -	0.1	0.7
Lignoceric	C24:0	$C_{24}H_{48}O_2$	- - -	- - -	0.4
Total	- - -	- - -	100	100	100

Table D.3: Oxidizer and temperature species model inputs values

Power (%)	100	85	30	7
Oxidizer temperature (K)	743.91	674.25	418.82	311.15
Operating pressure (kPa)	2343.346	1981.730	655.804	101.325

Table D.4: Relevant data for the CFM56-3, obtained from Pedro's work [94]

Station	$\dot{m}_{total}\ kg/s)$	$\dot{m}_{1/4}\ (kg/s)$	**Temperature (K)**	**Pressure (kPa)**
Fan	314.82	- - -	288.15	101.325
HPC exit	51.52	12.86	743.91	2343.346
Combustor entry	41.51	10.36	743.91	2343.346
Combustor exit	42.58	10.64	1649.94	2226.179
HPT entry	45.727	11.432	1593.23	2226.179

Table D.5: Solution control parameters for flow Courant number, ERF and URF

Parameters	Original value	New value
Flow Courant Number	200	80
ERF: Momentum	0.75	0.3
ERF: Pressure	0.75	0.3
Under relaxation factors (URF)		
Density	1.0	0.3
Body Force	1.0	0.5
Turbulent Kinetic Energy	0.8	0.5
Turbulent Dissipation Rate	0.8	0.5
Turbulent Viscosity	1.0	0.6
Pollutant NO	0.9	0.9
Energy	1.0	0.9
Temperature	1.0	0.8
Discrete Ordinates	1.0	1.0
Mean Mixture Fraction	1.0	0.9
Mean Fraction Variance	0.9	0.9

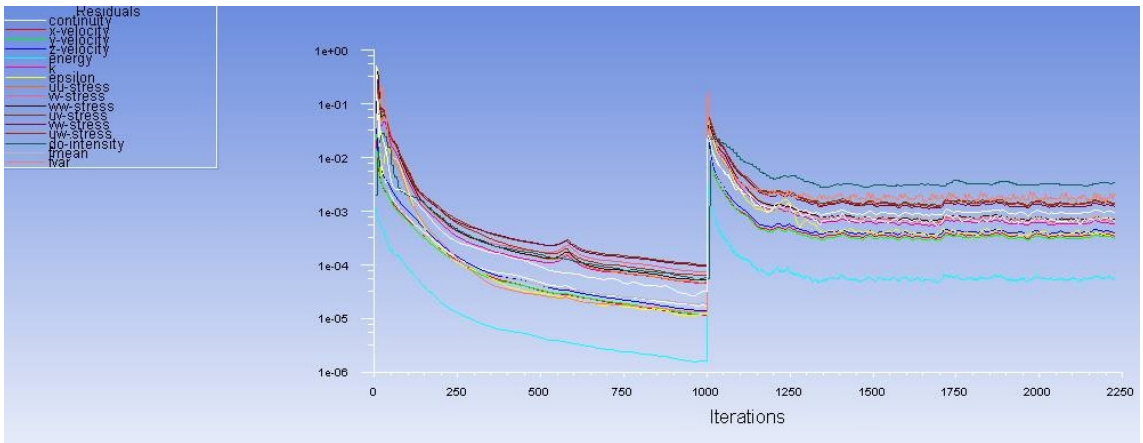

Figure D.1: Converged solution for second order method.

Table D.6: Air mass flow (kg/s) inputs for each boundary, at its respective power setting, while burning the biofuels

Fuel	**Jatropha**				**Algae**				**Sunflower**				**Cooling air flow**
Power (%)	100	85	30	7	100	85	30	7	100	85	30	7	%
Dome holes 1	0.0142	0.01462	0.0101	0.0028	0.0186	0.0191	0.0132	0.0037	0.0145	0.0149	0.0103	0.0029	0.1851
Dil 1.1	1.6835	1.7337	1.1955	0.3374	2.2019	2.2703	1.5697	0.4431	1.7203	1.7737	1.2263	0.3462	21.9534
Dil 2	3.3670	3.4675	2.3909	0.6747	4.4039	4.5407	3.1393	0.8862	3.4406	3.5474	2.4526	0.6923	43.9068
Dil 2.1	1.9079	1.9649	1.3548	0.3824	2.4956	2.5731	1.7789	0.5022	1.9497	2.0102	1.3898	0.3923	24.8805
Mix	0.3367	0.3468	0.2390	0.0675	0.4404	0.4541	0.3139	0.0886	0.3441	0.3547	0.2453	0.0692	4.3907
Mix 2	0.3367	0.3468	0.2390	0.0675	0.4404	0.4541	0.3139	0.0886	0.3441	0.3547	0.2453	0.0692	4.3907
Mix 3.1	0.0056	0.0058	0.0040	0.0011	0.0073	0.0076	0.0052	0.0015	0.0057	0.0059	0.0041	0.0012	0.0732
Mix 3.2	0.0056	0.0058	0.0040	0.0011	0.0073	0.0076	0.0052	0.0015	0.0057	0.0059	0.0041	0.0012	0.0732
Mix 4	0.0116	0.0116	0.0080	0.0022	0.0147	0.0151	0.0105	0.0029	0.0115	0.0118	0.0082	0.2461	0.1464
Swirler 1	1.6805	1.4310	0.5051	0.1179	2.2500	1.9125	0.6750	0.1575	1.7578	1.4942	0.5274	0.12305	- - -
Swirler 2	1.6805	1.4310	0.5051	0.1179	2.2500	1.9125	0.6750	0.1575	1.7578	1.4942	0.5274	0.12305	- - -
Total cooling $\dot{m}_a$	7.9419	8.1299	5.5276	1.5559	10.0302	10.3417	7.1500	2.0183	7.8361	8.0794	5.5859	1.5768	$\approx$ 100
Total $\dot{m}_a$	11.0356	10.7595	6.4557	1.7725	14.5302	14.1667	8.5000	2.3333	11.3517	11.0677	6.6406	1.8229	
Fuel flow $(\dot{m}_f)$	0.2532	0.2152	0.0759	0.0177	0.3333	0.2833	0.1000	0.0233	0.2604	0.2214	0.0781	0.0182	
Overall AFR	43.6	50	85	100	43.6	50	85	100	43.6	50	85	100	
PZ AFR	13.3				13.5				13.5				

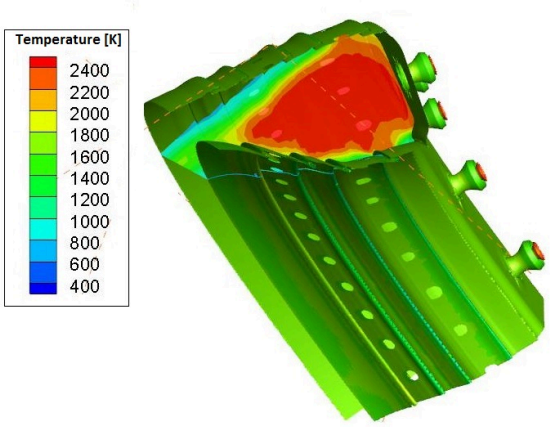

Figure D.2: Temperature contours, with the introduction of a cone angle of 60^{o}.

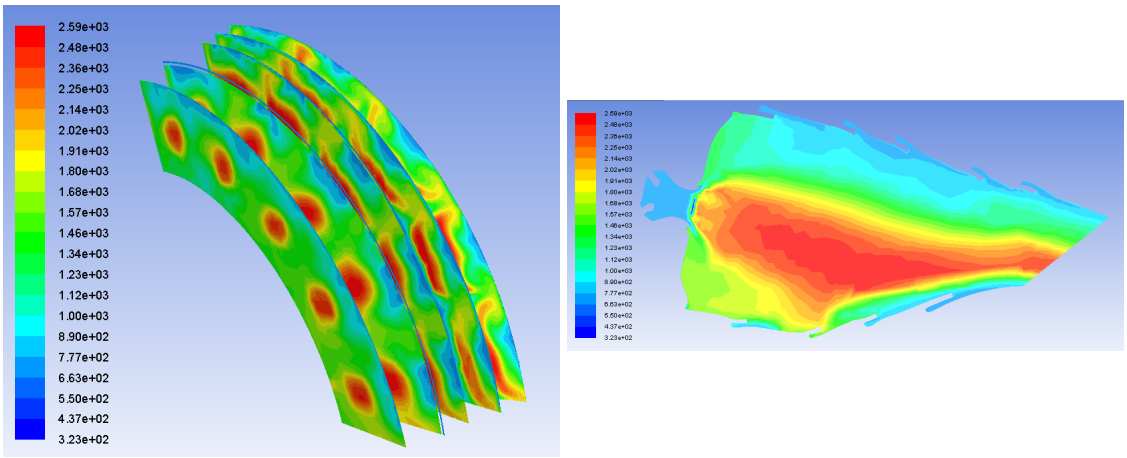

(a) (b)

Figure D.3: Contours of static temperature [K], while burning jet-A at full power through: (a) a quarter section view, and (b) a cross section of the combustor.

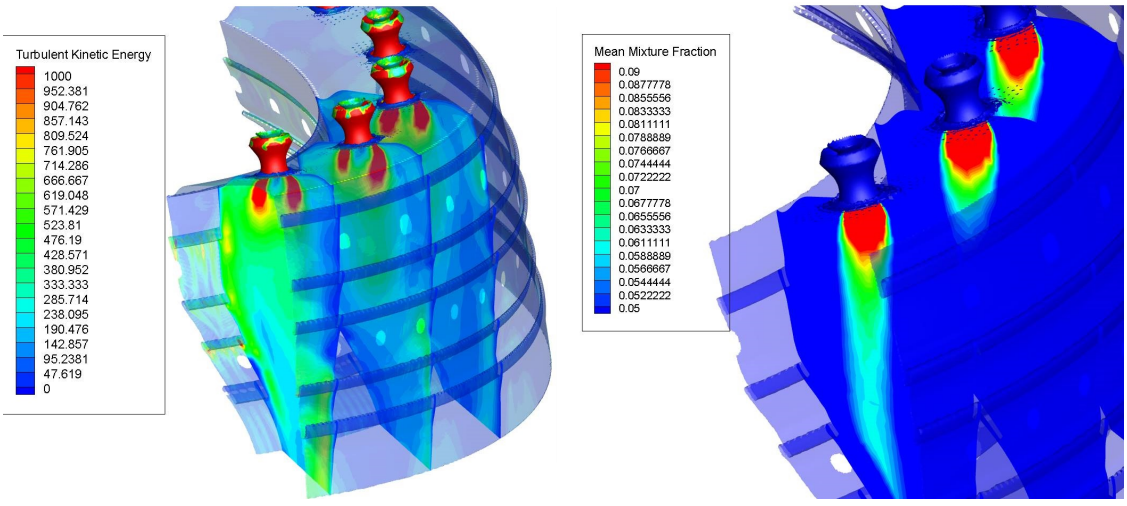

(a) (b)

Figure D.4: Additional combustor contours: (a) turbulent kinetic energy and (b) mean mixture fraction